Characterization of adaptor proteins involved in protein translation in Apicomplexa

Swati Gupta

Structural parasitology, Molecular medicine

Swati Gupta

Signature of Student

Swati Gupta

Amit P. Sharma

Signature of Supervisor

Dr. Amit Sharma

RECOMMENDATION FORM FOR EVALUATION BY THE EXAMINER/S

CERTIFICATE

This is to certify that the dissertation/thesis titled……**Characterisation of adaptor proteins involved in protein translation in Apicomplexa**…submitted by Mr/Ms…**Swati Gupta**…in partial fulfillment of the requirements for award of degree of M.Phil/M.Tech/M.Ph.D of Jawaharlal Nehru University, New Delhi, has not been previously submitted in part or in full for any other degree of this university or any other university institution.

We recommend this thesis/dissertation be placed before the examiners for evaluation for the award of the degree of M.Phil/M.Tech/M.Ph.D.

Dr. Amit Sharma
Project-In-Charge
Structural Parasitology
ICGEB, New Delhi

Signature of Supervisor

Date: 10/12/21

Director

15/12/2021

Signature of Director/Chairperson

Date:

Acknowledgement

It always seems impossible until it's done.

The submission of my thesis gives me immense pleasure, satisfaction and a unique sense of accomplishment despite many difficulties and troubles that came in its way. This journey was a beautiful and an adventurous roller coaster ride just like climbing a high peak step by step accompanied with encouragement, hardships, trust, and frustration; which would not have been a memorable experience without some people. This thesis is the result of five years of hard work at ICGEB and the PhD journey seemed pretty long, but on the whole, an interesting and exciting one. On this moment of submission of my PhD thesis, I would like to thank all the people who have contributed and inspired me during my doctoral study. I take this opportunity to express my gratitude towards those, whose unconditional support and encouragement made this dream come true. The time spent at ICGEB has given me some of the best and enduring years of my life and has shaped me into the person I am today.

First and foremost, I pay my sincerest regards to my supervisor and mentor **Dr. Amit Sharma**, under whose expert guidance I was able to finish my thesis work. I'm thankful to him for providing me access to all resources, for showing faith in my scientific ability and giving me an exceptional opportunity to work under his guidance. His scientific criticisms, patient hearing, constant support and encouragement, valuable suggestions and thought-provoking ideas all through these years directed me to perform better day by day. The freedom given by him right from the start of the work was exceptional. His ever-enthusiastic approach towards science has greatly inspired me to work hard until success is achieved and never be disheartened by the failures. Right from the first year of my PhD, this journey with him has been trulyamazing. Besides being a great scientist, he is also a wonderful human and has been the true

guiding light. His all-round guidance has immensely helped me to accomplish this work.

I am grateful to the Director of ICGEB, New Delhi, Dr. Dinakar M. Salunke, for presenting the opportunity to pursue a Ph.D. from ICGEB as well as for providing and preserving a stimulating, comfortable and harmonious working environment within the campus. I have debt of gratitude for Dr. Yogavel and Dr. Jyoti for their continuous guidance & overcoming the problems of crystallographic data processing essentially required for the accomplishment of my thesis work. I would also like to thank my research advisory committee members Dr. Anmol Chandele and Dr. Ranjan Nanda for their valuable suggestions during my presentations. I thank Dr. Sam for organizing the Schrödinger drug discovery workshop and helping us with research related queries. Great colleagues make a great workplace and with positive energy in the working environment it was easier to work and get things done. A helping hand was always there in form of second mentor which helped me enjoy the curves of this journey and provide laboratory training required for scientific experimentation and critical analysis of results. They helped me overcome the day-today failures by sharing the joy of high and low spirits and be resilient to rise again. **There are friends, there is family, and then there are friends that become family**. I will always be grateful to my friends Palak and Rini to be with me throughout my journey, support and encourage all my endeavours. My most sincere thanks to my friends and batchmates Prakhar, Pooja, Ramesh, Wajahat, Ankit, Priya, Priyanshu, Omair, Gokul, Shobhan, Akanksha, Mamta for the laughs and jokes cracked at adversity and the innumerable celebrations and elaborate scientific discussions. My sincere and heartfelt gratitude to Rahul and Navneet for their unconditional support throughout these years that gave me strength to cope up personally as well as professionally.

Research isan effort of not an individual's glory but contribution of many involved in its various stages. At this moment of accomplishment, I am also grateful to **Dr. Kailash Pandey and Dr. Vandana** (NIMR) for working with me on their collaborative projects.

My sincere thanks to the entire technical staff of ICGEB, who have helped me to the best of their capabilities. I'm grateful to **Purnima mam** for helping me with the confocal microscope with an ever- consistent smile and patience. I would like to thank the animal house staff members **Ashok ji**, **Rakesh ji**, **Munna ji** and **Patra ji** for their efforts andhelping me in handling mice. May God forgive me for sacrificingthe life of all those animals. I am gratefulto the financial, academic and technical support of the ICGEB. The supportand concern of **Pratibha mam**, **Sachin sir**, and **Mayank sir** during all these years at ICGEB have been indispensable

I would like to thank all the present and past members of SPG group: Vitul Sir, Abhishek Sir, Preeti, Sunny, Vivek, Sid, Payal, Nachi Sir for their support and lively work atmosphere. Special thanks to Rajan for arranging all our research related requirements and ensuring smooth operation of lab.

I'm highly indebted to my lab mates and friends for everything starting from workcooperation to being problem solvers in every aspect of my life. I was extremely lucky to be in a lab filled with cheerful and helping co-mates which brought smiles even during the strenuous hours of research. My special thanks goes to Dr. Ekta Saini (my ex-roommate) who is always there to love and teach me, may that be lab lessons or life lessons.

I owe a lot to The Almighty for blessing me with a loving family. I am indebted to my **Mumma and Papa** whose blessings helped me to pursue research despite all odds. I take this platform as a special opportunity to thank mymother and father for their unconditional love and care, for always being there as apillar of strength during this whole time. I address my whole family for the selflesslove, care, pain and sacrifice you did to

shape my life. It's only because of their constant support, immense faith in me and their uncountable prayers for me that I have been able to achieve this.

I thank **CSIR**, for granting me the CSIR-JRF Fellowship to carry out my PhD work at ICGEB. The financial support provided by **CSIR**, Govt. of India in the form of JRF and SRF is duly acknowledged. I also acknowledge **EMBO** for travel support for attending international conference during my PhD.

At the end, I would like to apologize to all those whom I could not accommodate in this note, but I would like to express my heartfelt gratitude to all those who went unmentioned in this note of acknowledgement.

"People are capable, at any time in their lives, of doing what they dream of"– Paulo Coelho

Swati

Characterization of adaptor protein p43 involved in protein translation in Apicomplexan malaria parasite

Table of Contents

Abbreviations

%	**Percentage**
Å	**Angstrom**
aaRS	**Aminoacyl-tRNA synthetase**
Ab	**Antibody**
APS	**Ammonium persulfate**
ASU	**Asymmetric unit**
bps	**Base pairs**
BSA	**Bovine serum albumin**
C ter	**Carboxy terminal**
CQ	**Chloroquine**
DAB	**Diaminobenzidine**
DAPI	**4', 6-Diamidino-2-phenylindole**
DRS	**Aspartyl tRNA synthetase**
DTT	**Dithiothreitol**
E.coli	***Escherichia coli***
EDTA	**Ethylene diamine tetra acetate**
IFA	**Immnofluorescence assay**
gm	**Gram**
hrs	**Hours**
HRP	**Horseradish peroxidase**
IPTG	**Isopropyl thiogalactoside**

iRBC	**Infected RBC**
Kan	**Kanamycin**
kDa	**Kilo Dalton**
kbp	**Kilo basepair**
LB	**Luria bertini**
M	**Molar**
MS	**Mass spectrometry**
MARS	**Multi aminoacyl tRNA synthetase complex**
MSC	**Multisynthetase complex**
min	**Minute**
mg	**Milligram**
mg/ml	**Milligram per millilitre**
mM	**Millimolar**
N ter	**Amino terminal**
Ni-NTA	**Nickel nitriloacetate**
Nm	**Nanometre**
°C	**Degree Celsius**
OD	**Optical density**
PAGE	**Polyacrylamide gel electrophoresis**
PBS	**Phosphate buffer saline**
PBST	**Phosphate buffer saline with Tween 20**
PCR	**Polymerase chain reaction**
Pf	***Plasmodium falciparum***
PMSF	**Phenyl methyl sulfonyl fluoride**
RBC	**Red blood corpuscle**

RPM	**Revolutions per minute**
RMSD	**Root mean square deviation**
SD	**Standard deviation**
SDS	**Sodium dodecyl sulphate**
SDS-PAGE	**Sodium dodecyl sulphate- Polyacrylamide gel electrophoresis**
TE	**Tris-EDTA**
TEMED	**N, N, N', N'-Tetramethylethylenediamine**
tRNA	**Transfer ribonucleic acid**
TSA	**Thermal shift assay**
WHO	**World health organisation**
βMe	**Beta mercaptoethanol**
µg	**Microgram**
µl	**Microlitre**
µM	**Micromolar**

Chapter 1

Introduction

History of malaria

Malaria occupies a major place in history throughout ages affecting neolithic dwellers, ancient Chinese and Greeks. Being one of the most ubiquitous diseases, the early origin of malaria has been testified by its around 125 different species which afflict mammals, birds and reptiles. In the 20th century malaria claimed around 200 to 300 million lives (1). Most of the convalescents belong to the Sub Saharan Africa, Asia and the Amazon basin. By propriety of climate, ecology and poverty, 80-90% cases of malaria and deaths exist in Africa. Stronger evidence of the ancient prevalence of malaria in Africa is affirmated with the occurrence of the sickle cell trait where individuals with one copy of the gene have a selective advantage over malaria by virtue of the sickle shaped RBCs containing needle shaped cluster of haemoglobin (2). The remarkable prevalence of malaria exemplifying to 20-40% were recorded in certain Mediterranean populations, African tribes and Indian aboriginal groups. The coexistence of the sickle cell trait (SCT) and malarial endemicity ushered A.C. Allison to conclude with the conjecture that the heterozygous sickle cell trait bestows a selective advantage against malaria (3). .Long reign of malaria has been illustrated through ancient writings which also include those from the Indian Vedic period (1500 to 800 BC), the Chinese *Nei Chin* (270 BC), clay tablets with cuneiform script from Mesopotamia etc (4), ancient Egyptian writings (1550 BC) and Greek scripts (413 BC). In the 21st century in Africa, Malaria arose as a zoonotic disease in primates. Since the time these parasites were discovered, research has been focussed on the parasite as well as vector biology of mosquitoes which transmit the parasites. It was ascertained by a French army doctor named Charles Laveran (1845-1922), that malaria was also rampant in the temperate zones apart

from the tropical areas. Though malaria had been associated with marshes and swamps giving rise to the Roman terminology as “bad air”, Laveran discerned that these many diseases linked to bad vapors were actually caused by microbes (Jarcho, 1984). On October 20, 1988, while looking through the blood of a delirious soldier, Laveran found out crescent shaped transparent bodies containing a dot. Later hemozoin (byproduct of haemoglobin digestion) in the blood and spleen of malaria patients was detected by Meckel, Virchow and Frerichs. Soon Laveran identified the four diverse stages of asexual malarial parasite as female and male gametocytes, trophozoite and schizont stages (5). That the recurrence of fever on 3rd and 4th days in case of *P. vivax* and *P. falciparum* and is linked to the parasite release or outburst from schizonts was established by Camillo Golgi. The Italian scientists Raimondo Filetti and Giovanni Batista Grassi characterised *P. vivax* and *P. malariae in 1890.* In 1897, William H Welch coined the term *P. falciparum* for the lethal human tertiary parasite. *John William Watson Stephens* characterised *P. Ovale in 1922*. *P. knowlesi* which first infested human in 1965 was peculiarized by Brij Mohan Dasgupta and Robert Knowles in the year 1931. Ronald Ross, in 1895 undertook the investigation to resolve if mosquitoes played role as the vectors in transmission of human malaria. The *Plasmodium* life cycle involves two hosts- a definite/primary host which is the mosquito and the secondary or intermediate host- the human. Exflagellation of microgametocytes (sexual stages) of *Plasmodium vivax* occurs in the mosquito and barely appears in human peripheral blood. Sir Ronald Ross noticed flagellation of *Plasmodium* in the blood meal of mosquitoes which was further investigated by McCallum in the year 1897 (6) In July 1897, after rearing mosquitoes from larvae He investigated the gametocyte stage derived from the infected patient blood. The mosquitoes feeding on this bloodstage were sacrificed to observe the “exflagellation” (male gametocyte production) (6) Ross had concluded that mosquitoes take up the gametocytes while feeding from an infected host which later developed into sporozoites for infecting the new host (7, 8).

Chemoprevention and Drug Resistance

Throughout ages, traditional herbal remedies have been have been useful in treating malaria. (9). The history of modern antimalarial therapy started with methylene blue, (one of the three magic bullets invented by Paul Ehrlich) which was the world's first synthetic drug against malaria patients in 1890s (10). Following arrival, Spanish missionaries learnt from Indian tribes the use of a medicinal bark for treating fevers. The countess of Chinchon was treated of her illness with the bark of this tree. The bark of tree by this means was acknowledged as the Peruvian bark and the tree was entitled as Cinchona. Quinine having antimalarial properties is thus extracted from the bark. Besides spasmodic cognition of quinine resistance , it remains the favoured treatment of choice till date (11). Depending on the recurrence of drug resistance, different species of *Plasmodium* are cured by different lines of antimalarials. Chloroquine remains choice of drug in treating non-*P. falciparum* malaria, while newer drugs are required against *P. falciparum*. The only drug targetting hypnozoites of *P. ovale* and *P. vivax* (dormant liver stage responsible for relapse of infection), after clearance of infection is primaquine. Pyrimidine derivative Proguanil also emerged from the pipeline and paved way for the unravelling of Pyrimethamine (12). Sulfones and sulphonamides were used in combination with Proguanil or pyrimethamine for preventing resistance against monotherapies. Sulfadoxine and sulfamethoxypyridazine based antimalarial drugs inhibit the dihydropteroate synthetase to kill parasite (13). Atovaquone targets the cytochrome bc1 complex belonging to the electron transport chain taking place in parasite mitochondria. Pyrimethamine and Proguanil kill the parasite by inhibiting the enzyme dihydrofolate reductase (DHFR) (14). Antibiotics like Tetracycline, Clindamycin, and Doxycycline have also been used to treat malarial parasites as mono or combination therapy (15). Progress of malaria control in endemic regions is vulnerable due to the emergence of sulfadoxine–pyrimethamine as well as chloroquine-resistant *Plasmodium* parasites, majority

being *P. falciparum* strains. The resistance developed by the parasite to this line of treatment, threatened the efficacy of these drugs and raised a concern in their design. This resulted in the use of combinations of these drugs and development of novel drugs and identification of new targets. Artemisinin from *Artemisia annua* (sweet wormwood) was extracted by Chinese scientists in 1972 which proved as an efficient antimalarial like Quinine and Chloroquine. Artemisinin combination therapy with associated drugs having higher shelf lives increased efficacy of Artemisinin and also helped to combat resistance (16). In response to the resistance against various antimalarials - chloroquine, pyrimethamine and sulfadoxine, combination therapies with artemisinin (ACTs) are approved nowadays for treating uncomplicated malaria, and their practice is effective in decreasing global malaria burden remarkably. Though, there are reports of declining sensitivity towards derivatives of ART in *P. falciparu*m patients from Cambodia, Southeast Asia and greater Mekong subregion, after monotherapy, which poses a potential threat for partner drug resistance as well (17). Such an observation threatens the continued efficacy of ACTs to contain and abolish resistance to artemisinin. Current treatment recommended for curing uncomplicated *P. falciparum* malaria involves ACTs, which involves combination of artemisinin derivative with a quinine derivative (WHO 2015). Semisynthetic water-soluble derivatives of artemisinin are used in combination therapies namely, DHA, artesunate or artemether. Studies conducted between the period of 2010 and 2017 have shown ACTs to be efficiently successful in global malaria control (WHO 2018). It is speculated that the emerging resistance against ACTs has risen largely due to faulty medical practice, including profound mono-therapeutic usage of artemisinin derivatives.

Development of Novel Antimalarials

Medicines for Malaria Venture (MMV) is a composed library of 400 exclusive compounds, termed as the Malaria Box (Spangenberg, Burrows et al. 2013), which displayed antimalarial activity against the blood stage parasite. The MMV library was compiled from the 13,533

compounds available from the GlaxoSmithKline's chemical library- Tres Cantos antimalarial set (TCAMS) for inhibitors of P. falciparum (18). MMV collaborated with researchers and the pharmaceutical industry to screen these lead compounds in order to build novel antimalarials (19)(Promising compounds have been identified using three different approaches: development of alternatives to already marketed compounds (ozonides); target-based screening of inhibitors [for e.g. *P. falciparum* dihydroorotate dehydrogenase (PfDHODH)]; and phenotypic screens.

Global distribution of malaria

Malaria is a public health concern of immense degree predominantly in the developing countries. As per the latest estimates, 219 million malaria cases were reported all over the world in 2017 as compared to 239 million cases in 2010 and 217 million in 2016. 92% cases were reported in the WHO African Region. India and Sub-Saharan Africa were having around 80% of the global burden of malaria. In 2017, deaths from malaria globally counted to around 4,35,000. *Plasmodium falciparum* is rampantly prevalent in Africa, responsible for 99.7% of cases in 2017, while *P. vivax* represents the key parasite in WHO Region of America, in lieu of 74.1% of malaria cases (WHO 2018). As per the latest released world malaria report, there are 229 million malaria cases in 2019 and the assessed death rate counted to 409000. The WHO African Region shares the highest stake globally. The region had 94% malaria deaths and cases in the year 2019 and 6 countries were bearing half of the burden globally- Nigeria (23%), United Republic of Tanzania (5%), the Democratic Republic of the Congo (11%), Burkina Faso (4%), Niger and Mozambique (4% each). Children below 5 years of age are worst affected with malaria.

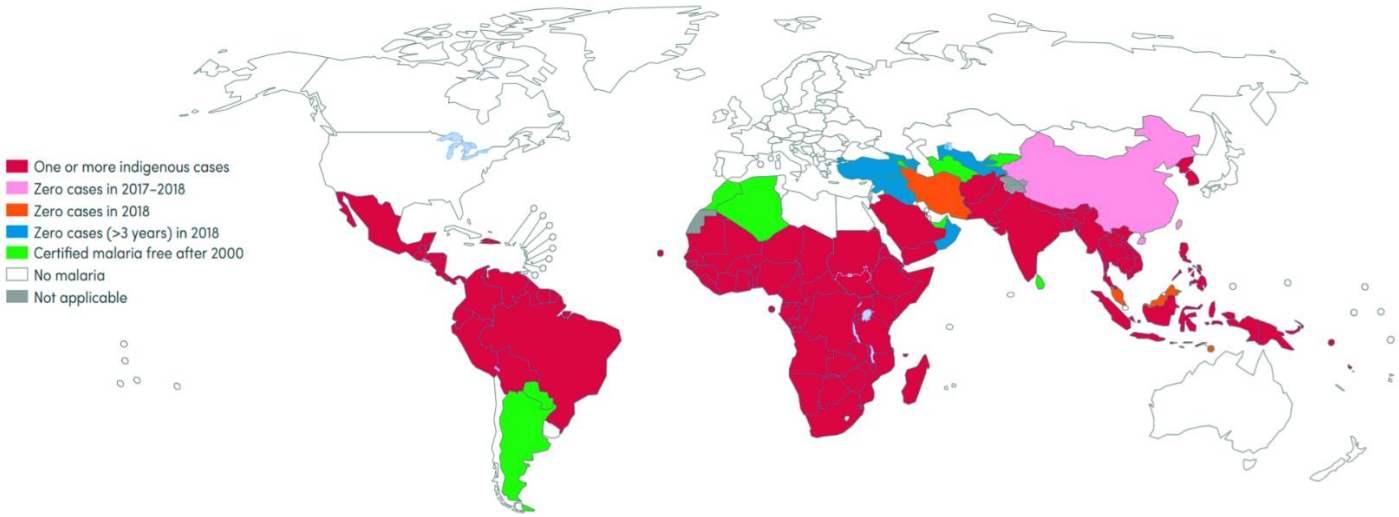

Figure 1: Indigenous cases of malaria status-2019 (Adapted from WHO malaria map)

Malaria incidence in India

Malaria has jeopardised India from ancient times and this is relevant from Vedic Indian literature as well. Around one fourth of India was disease stricken with the advent of the twentieth century specially Bengal and Punjab (20). According to WHO 2017, India is one of the 15 countries to have the highest cases and deaths in malaria. India along with other Sub Saharan countries accounts for 80% of the world's cases and deaths. In 1947, about 75 million out of 330 million people were affected with malaria annually and the approximated deaths were around 0.8 million every year (21). As per the World malaria report (WMR) released in the year 2020 by WHO, India has considerably reduced its malaria load. India reported a decline of 17.6% in a span of one year from 2018 to 2019. Region wide cases have also reduced from 20 million to round 6 million.

The cases and mortalities have reduced encouragingly by 21.27% and 20% in 2019 (77 deaths, 3,38,494 cases) in comparison to 2018 (96 deaths ,4,29,928 cases). The over-all malaria cases as testified up till October 2020 have also reduced by 45 % from 2019.

Efforts for malaria elimination after beginning in 2015, strengthened in 2016 after the launch of National Framework for Malaria elimination (NFME).

Chhattisgarh, Meghalaya, Orissa, Madhya Pradesh, Jharkhand, Meghalaya and Madhya Pradesh reported for around 45.47 percent (1,53,909 cases within 3,38,494 cases) and 70.54 % (1,10,708 cases out of 1,56,940) of *P.falciparum* cases in 2019.

"High Burden to High Impact (HBHI)" as implemented by WHO in 11 countries entailing India has reignited the progress in malaria reduction. This initiative is applied in 4 states of India as of now in July 2019- Madhya Pradesh, Chattisgarh, West Bengal and Jharkhand.

Malaria has been made notifiable in 31 states/UTs (Andhra Pradesh, Arunachal Pradesh, Gujarat, Chhattisgarh, Assam, Jammu & Kashmir, Goa, Haryana, Himachal Pradesh, Kerala, Jharkhand, Madhya Pradesh, Manipur, Karnataka, Nagaland, Mizoram, Odisha, Sikkim, Punjab, Tamil Nadu, Rajasthan, Tripura, Telangana, Uttarakhand, Uttar Pradesh, West Bengal, Chandigarh, Pudducherry, D&N Haveli, Daman & Diu, and Lakshadweep) and cases have also declined in the highly endemic states. Trend of decline in 2019 in comparison to 2018 is as suveyed: Meghalaya- 59.10%, Odisha – 40.35%, Madhya Pradesh –36.50% Jharkhand – 34.96%, and Chhattisgarh –23.20%. Hence these figures and implications within previous two decades displays the essential decrease in malaria.

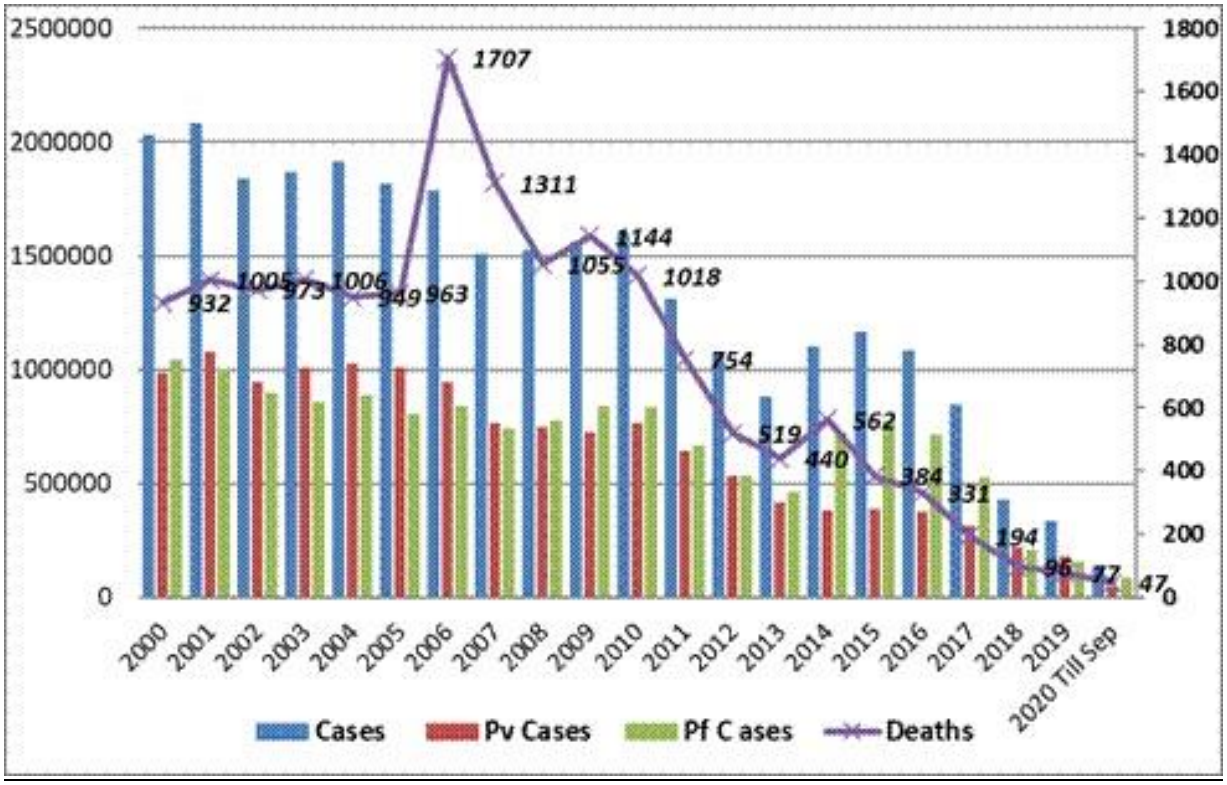

Figure 2: Epidemiology trend of Malaria in India (2000-2019) Pv; Plasmodium Vivax & pf; Plasmodium Falciparum (Adapted from the WHO world malaria report 2020)

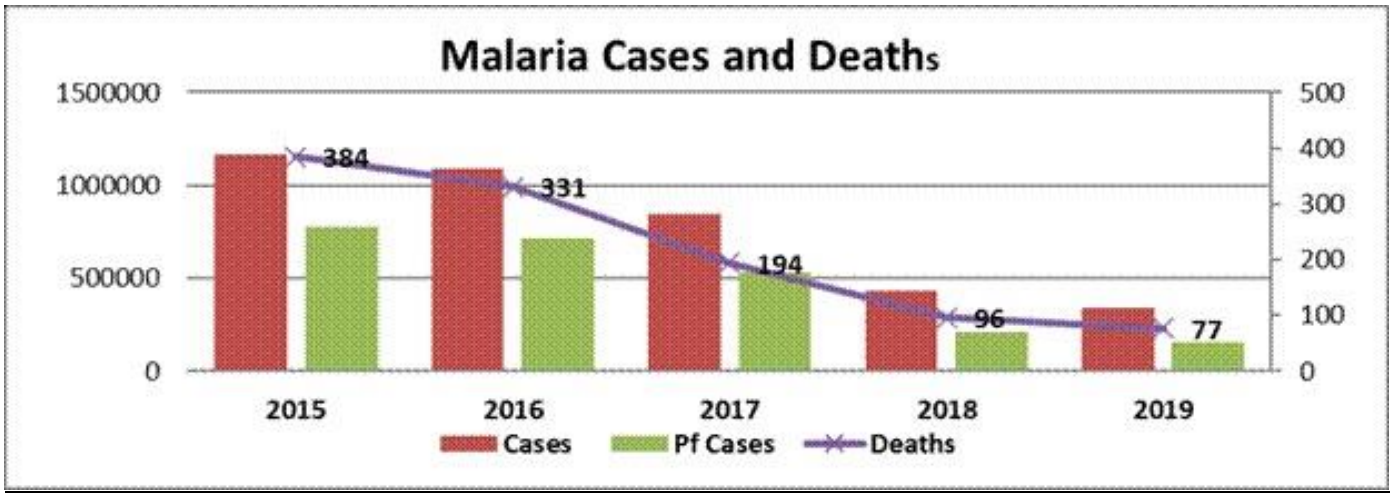

Figure 3: Current epidemiology in India (2015 – 2019)

Life cycle of *Plasmodium*

The five known human malaria species known till date are *P. falciparum, P. vivax, P. malariae, P. ovale,* and *P.knowlesi*. The recent one to vitiate individuals was perceived by WHO as the fifth species in 2008- *P.knowlesi*. The main mode of transmission implicates an infested female *Anopheles* (during blood meal) which stings and inoculates the infectious stage into a healthy individual (22). Malaria infects diverse genres of organisms including various reptiles, birds and mammals. Among more than 100 species belonging to *Plasmodium*, 5 species infect humans and around 29 species are infective to non-human primates, rodents, bats, squirrels and porcupines (23). Further ways of transmission entail transplantation, diseased blood transfusion, infected needles, and also from a pregnant mother to her foetus (congenital malaria) (CDC). The life cycle of *Plasmodium* constitutes the following stages- the sporozoite stage infective to human, the asexual and sexual stages in the RBCs.

The infectious stage for human is the sporozoite stage which is injected into the bloodstream via an infected *Anopheles* mosquito. Thereby the asexual reproduction in human proceeds through the liver stage and erythrocytic schizogony. In a period of one hour of sporozoites' administration, they enter the liver through the bloodstream. The sporozoites after entering the hepatocytes start proliferating into schizonts within a week(24). The schizonts propagate into thousands of merozoites which entering into bloodstream initiate the erythrocytic schizogony.

P. ovale and P. vivax and not *P. falciparum* liver sporozoites often remain dormant in the hepatocytes(25). These hypnozoites later recommence reproduction and begin infection as merozoites reinvading the bloodstream after infinite time (26). The clinical symptoms generally appear 7–10 days after the mosquito bite i.e., exoerythrocytic phase lasts for up to 10 days. These merozoites as released into the bloodstream target the RBCs and begin the erythrocytic schizogony. The cycle initiates with a dormant signet ring which develops into the feeding trophozoite. The trophozoite cannot digest heme so converts it to hemozoin via heme polymerase

and utilizes the globin as source of amino acids to assist their replication. Schizonts enact in the subsequent stages bursting into numerous merozoites. These merozoites on being released in bloodstream attack other red blood cells accompanied by clinical symptoms of fever chills and enhanced parasitemia. Unlike the erythroschizogony of liver stage, this phenomenon happens in multiple cycles. A second form in the RBCs is the differentiation of parasite into the dormant gametocytes (male and female). After a gametocyte is committed for sexual differentiation, it takes ~11 days for them to develop into mature infectious gametocytes. During this developmental phase, they remain sequestered within bone marrow so as to evade splenic clearance until they appear in the peripheral circulation for uptake by a feeding mosquito (27). Once ingested by a mosquito, gametocytes develop to form extracellular female and male gametes in midgut. After fusing of micro- and macrogamete, the resultant zygote elongates into an ookinete over an interval of 24 h, which travels across midgut epithelium and encysts to form oocyst wherein asexual sporogenic replication takes place. Following the oocyst rupture, motile sporozoites come out to the hemocoel, which then pass on to the mosquito salivary glands to be injected to next human host (28, 29).

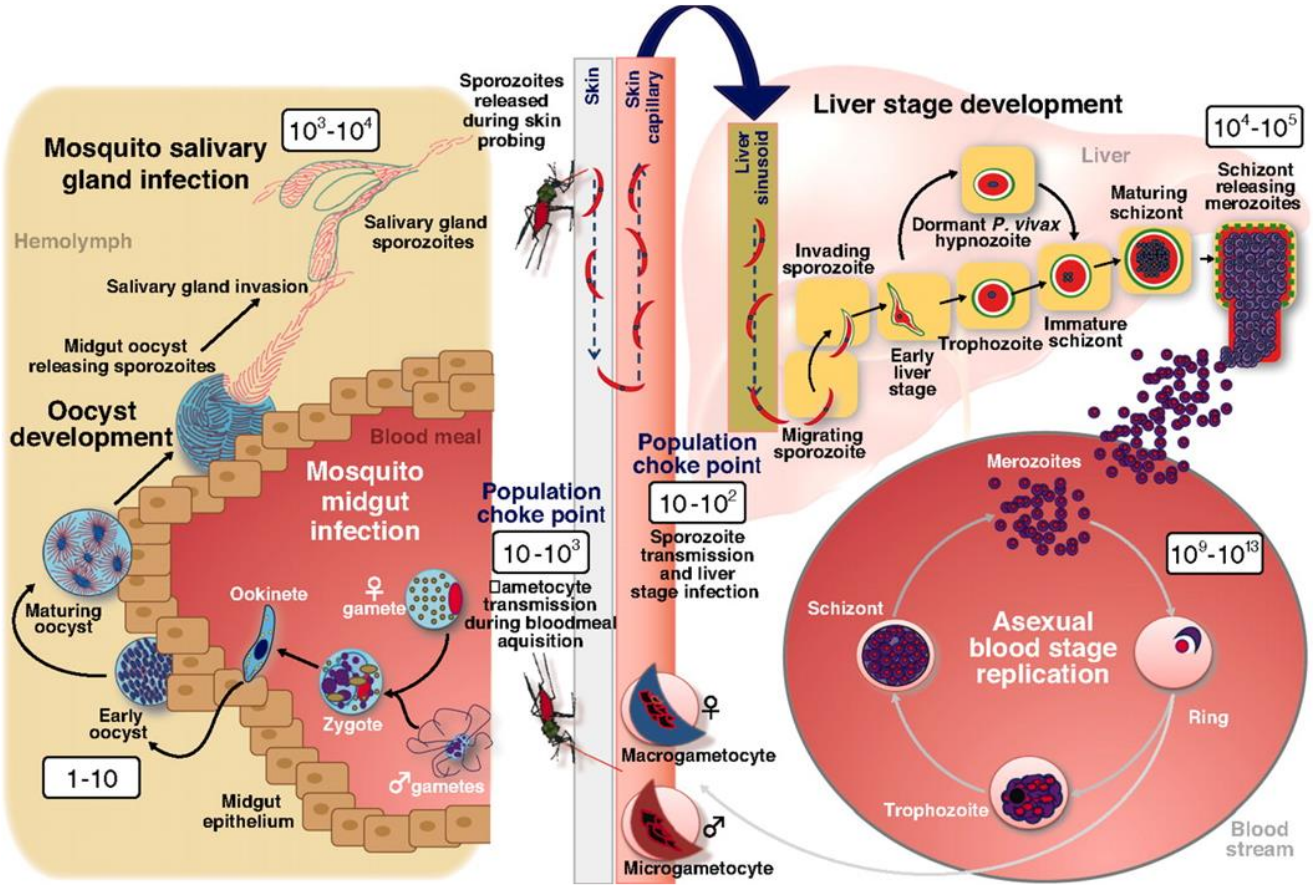

Figure 4: Schematic representation of Life cycle of human malaria parasite. (Adapted from Kappe et al., 2010 (30)

6. Malaria symptoms and diagnosis

Clinical indications of malaria are accredited to asexual stage of parasite owing to lysis of parasite infected RBCs. Following haemolysis, symptomatic malaria occurs in response to the release of parasites and malaria endotoxins (hemozoin in association with parasite DNA) in the blood stream, that triggers Toll-like receptor 9 (TLR9), which in turn induces production of tumour necrosis factor (TNF) (31). Symptoms include mild fever, chills, arthralgia (joint pain) & vomiting. These symptoms typically appear between 10 to 15 days post mosquito bite, and progress to the sweats and high temperature fever. The delayed treatments for malaria may cause severe complications include severe anemia, hemoglobinuria, acute kidney failure, hypoglycemia, abnormalities in blood coagulation and acute respiratory distress syndrome. *P.*

falciparum may cause periodic fever every 36-48 hours or almost continuous fever. Severe malaria can often be fatal due to underlying anaemia and displays microvascular obstruction leading to multi-organ damage.

Rapid and active diagnosis of malaria mitigates suffering and reduces community transmission (32). The usual laboratory techniques are conventional Giemsa staining of peripheral blood smears (33), concentration methods like quantitative buffy coat (QBC) (34), fast diagnostic tests like OptiMAL (35), SD Bioline (36) as well as molecular diagnosis methods as polymerase chain reaction (PCR) (37).

Malaria prevention

Since the causal agent of malaria is *Plasmodium* and vector is female *Anopheles* mosquito spreading it to the mammalian host (humans), the control measures are very inclusive of the three genera and hence daunting. Moral education of humans is very important for controlling malaria since they can be educated and thus take part in controlling the disease. Inspite of the diverse vaccine candidates tested against the malarial parasite, their complicated life cycle and genetic heterogeneity variations have rendered it unintelligible to develop a plausible vaccine against malaria (38). Many prophylactic drugs for treating malaria including primaquine, chloroquine, doxycycline, mefloquine, pyrimethamine and atovaquone. Antibiotics like Tetracycline, Clindamycin, and Doxycycline have also been used to treat malarial parasites as mono or combination therapy (15). However, the extensive use of these antimalarials over past several years has led to drug resistance' development. Currently, artemisinin (derived from Artemisia annua) and derivatives are in use for effective malaria treatment (16, 39). Artemisinins are administered orally in uncomplicated malaria whereas intramuscular and intravenous routes are preferred for severe malaria. Artemisinin derivatives (artesunate, dihydroartemisin,

artemether and arteether) are developed for improving the artemisinin bioavailability and to improve the effectiveness of antimalarial therapy. Uncomplicated *P. falciparum* malaria is treated by one of the following recommended ACTs:

- lumefantrine + artemether
- amodiaquine + artesunate
- mefloquine + artesunate
- Piperaquine + dihydroartemisinin
- sulfadoxine–pyrimethamine (SP)+ artesunate

ACT treatment involves 3 days' treatment with an artemisinin derivative.

P. falciparum malaria sufferers should be treated with utmost care and in view of possibility of resistance to antimalarials. Primaquine is also used as a gametocytocidal drug to avert spread. In case of merged infections blood schizonticides are endorsed against *P. falciparum* and Primaquine is recommended for treating *P. vivax*. In case of suppressive treatment, falciparum malaria can be abolished by eliminating the erythrocytic stages which is achieved through the administration of schizonticidal drugs.

Primaquine, by virtue of its tissue schizonticidal activity eradicates the liver forms thus curing *P. vivax*/ *P. ovale* malaria in about 2 weeks and also inhibits recurrence. Primaquine is gametocidal in case of *P. falciparum* malaria thus preventing transmission in the primary host mosquito. Since *P. vivax* is not supposed to be chloroquine resistant unlike falciparum, chloroquine is the drug of choice for treatment (www.cdc.gov). More recently the malarial parasite has started showing resistance against Artemisinin too. The need of higher artemisinin

dose for antimalarial therapy in Thailand, Myanmar, Cambodia and Vietnam is cause for deep concern (40, 41).

Treatment for *Pf* and *Pv* malaria in India

Initial diagnosis and treatment of malaria aims at aims at the stoppage of the advancement from uncomplicated malaria to the severe state. Hence this reduces spreading of resistant parasites. Treatment of uncomplicated malaria after diagnosis by microscopy/RDT must be attended promptly (42).

A. Treatment of P. vivax cases: The *P.vivax* cases are cured with chloroquine at a dosage of 25mg/kg throughout 3 days. *P. vivax* malaria also relapses by virtue of hypnozoites in the liver. For inhibition, primaquine is administered at dosage of 0.25 mg/kg regularly upto 14 days. On the other hand, Primaquine is not advisable in pregnant women, infants, as well as G6PD deficient patients. Primaquine might lead to hemolysis in G6PD deficiency (42).
B. Treatment of P. falciparum cases: Artemisinin Combination Therapy (ACT) is administered in drug resistant areas and chloroquine is advisable in drug susceptible areas after confirmation by RDT/microscopy.

ACT comprises of the artemisinin derivative in conjugation with lengthy acting antimalarial (amodiaquine, mefloquine, lumefantrine, or sulfadoxine-pyrimethamine). The ACT used in India is artesunate + sulfadoxine-pyrimethamine (SP). Also, Artemether + Lumefantrine fixed dosage combination as well as blister pack of artesunate + mefloquine are also available. According to the current WHO guidelines, ACTs are administered in 2nd and 3rd trimester of pregnancy. The endorsed treatment in 1st trimester is quinine (42).

In severe malaria cases, quinine or artemisinin derivatives are given. Specific antimalarial treatment of severe malaria should be given promptly.

• Artesunate: At the dosage of 2.4 mg/kg intramuscularly/intravenously (i.m/i.v) diluted in 5 % $NaHCO_3$ at time=0 and then at 12 and 24 hours respectively is given.

• Quinine: 20 mg quinine salt/kg is administered intravenousy in infusion of 5% dextrose saline/dextrose throughout 4 hours. This is followed by a dosage of 10mg/kg for 8 hours regularly. In case this parenteral therapy continues past 2 days, the dosage should be decreased to 7mg/kg for 8 hours.

• Artemether: This is administered at the dosage of 3.2 mg/kg intramuscularly at day=0 of admission and then this is reduced to 1.6mg/kg per day.

• αβ Arteether: This is not recommended for children. Hence this is administered to adults only at the dosage of 150 mg (i.m) consecutively for 3 days (42).

Plasmodium falciparum genome

A detailed investigation of the genomic sequence belonging to *Plasmodium falciparum*-3D7 clone reveals a nuclear genome of 23 megabase. The genome of *P. falciparum* is nearly double the size of *Schizosaccharomyces pombe* genome. Asexual blood stage *Pf* in total involves 14 chromosomes, encoding around 5300 genes. *Pf* genome is the most abundant (A+T) rich genome, around 80.6% with only 17-19 % of (G+C) which has been sequenced till date (43, 44). In 1995, the "Malaria genome project" was started for sequencing the *P. falciparum genome*. Gene sequence of chromosome 2 was released first in 1998 followed by chromosome 3 sequence in 1999. The entire sequence of *P. falciparum* gene was released in 2002 (44). The genome of parasite mitochondria (45) and apicoplast (46) was earlier reported separately in 1991 and 1996

respectively. The genes responsible for causing the antigenic variations are positioned in subtelomeric sections of the chromosomes. Though the genome of *Plasmodium* encodes for few transporters and enzymes, a greater chunk of genes is dedicated to host-parasite interplay. The nuclear-encoded proteins target the apicoplast which takes part in isoprenoid and fatty acid metabolism. Transcriptome analysis using ribosome profiling has established that transcription and translation in the infected cell are tightly coupled for 90% of the genes (47) Exception to this transcription pattern are translationally upregulated genes encoding cell surface proteins associated with merozoite egress and invasion. Till now over 5,300 Plasmodium genes have been described and annotated in PlasmoDB, GeneDB and UCSC Malaria Genome Browser. The genome sequence delivers the basis for upcoming studies of this organism, and hence is being exploited in search of novel vaccines and drugs in order to combat malaria.

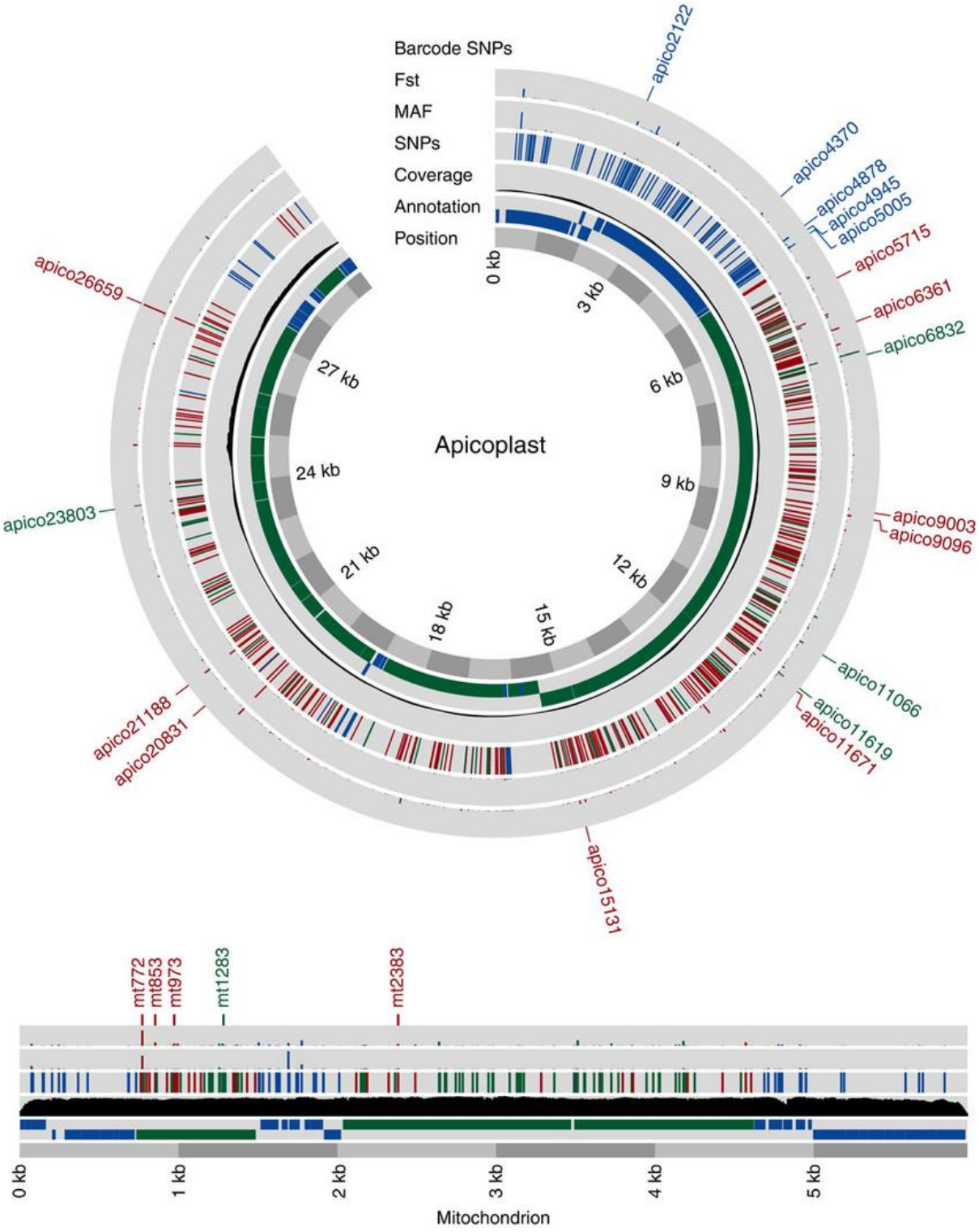

Figure 5: Nucleotide sequence of the densely packed P. falciparum mitochondrion (mt) and apicoplast (apico) genomes. Protein-coding (green) and non-translated RNA (blue) regions in the 'annotation' ring are transcribed from either strand (inner, negative strand; outer, positive strand). (Adapted from Preston et al., 2014) (48)

Malarial translational machinery

Aminoacyl tRNA synthetases (aaRS) and Aminoacyl tRNA synthetase interacting multifunctional proteins (AIMPs)

Aminoacyl-tRNA synthetases append the requisite amino acids to their tRNAs. The reaction of aminoacylation which annexes the appropriate aminoacyl group to 3' CCA terminal of tRNA takes place in two-steps as shown in Fig 6. With the energising of the amino acid with ATP, it produces an aminoacyladenylate intermediate. This further relocates to 3' terminal end of the analogous tRNA for processing during translation. Basic architecture of their active sites divides aaRS into two classes. Eleven amino acids constitute the Class I *aaRS* and are inclusive of Tyr, Trp, Val, Met, Lys, Leu, Ile, Cys, Gln and Glu. Class II *aaRS*s encompasses ten amino acids namely Pro, Ser and Thr, Asp, Ala, Asn, His, Phe. Gly, Lys, Class I enzymes possess a pivotal domain namely Rossman fold which embodies β sheets and α-helices. The domain is downright convoluted in binding ATP and has two conserved motifs ('KMSKS' and 'HIGH'). Class II enzymes house a catalytic site which displays a solitary fold having a cardinal core comprising of anti-parallel β sheets encircled by α helices (49). The two classes of aaRS also demonstrate contrasting approaches of aminoacylation - class I enzymes aminoacylating the 2'OH end of the cognate tRNA and class II enzymes that of the 3'OH end. (exception *PheRS*) (50).

Plasmodium falciparum constitutes of 36 synthetases which fall under 20 varieties and an entire forum of tRNAs (51). Duplicate copies of synthetases are due to active translating compartments as apicoplast and mitochondria which being of bacterial origin are potent targets of antimalarials. The synthetases in congruence with other auxiliary protein factors accomplish many non-canonical tasks apart from translation. Though mostly found in eukaryotes, many of these multisynthetase complexes have also been discovered in bacteria and archaea where they accomplish various functions of transcriptional and translational regulation with apoptosis and splicing as well. (52). A section of aaRS embodies the multiaminoacyl tRNA synthetase complex

(MARS/MSC) in advanced eukaryotes. The MSC is composed of 9 aaRS embracing glutaminyl (QRS), lysyl (KRS), , aspartyl (DRS), isoleucyl (IRS), arginyl (RRS), methionyl (MRS), leucyl (LRS), and bifunctional glutamyl-prolyl aminoacyl-tRNA synthetase (ERS,PRS) in the higher eukaryotes ranging all over from arthropods to vertebrates. These synthetases are found in a consortium with three other auxiliary proteins namely p38 (AIMP2), p18(AIMP3) and p43(AIMP1) (53)(54). MSC might play a role in accentuating protein synthesis by separating activated tRNAs from biological pool and augmenting the plethora of tRNA in the vicinity of protein synthesis (51). These MSC have been recognized in both archaea and bacteria (52). Eukaryotic complexes are larger and function multifariously beyond translation. In the lofty eukaryotic cell, the synthetases continue to remain amalgamated into a well-organized tRNA transport machinery and are thus in approximation with the protein synthesis machinery (55). The minor complex of aminoacyl-tRNA synthetase enzymes entailing ERS and MRS synthetases with the protein ARC1p have been recognised in yeast (56). The C-terminal ARC1p docks a tRNA-binding domain (TRBD), well sustained in p43 and additional proteins (57, 58). These proteins interact through their N terminal domains. ARC1p houses an EMAPII-like domain at the C-terminal portion, which encompasses the oligonucleotide-binding (OB) fold. These bestow ARC1p with equity of binding tRNA (52, 59, 60).

An alpha helical glutathione-S-transferase C-terminal-like domain trailed by the EMAPII–like domain comprises *Tg*-p43 protein. (MRS, QRS, ERS, and YRS) constitute the interactive proteome of the *Tg*-p43 protein in *Toxoplasma* mutisynthetase complex (53). *Aquifex aeolicus* consists of the tRNA-binding protein (Trbp111) which shares sequence based connexions with human p43 C terminal domain (accessory protein of the mammalian MSC) & ARC1p (61). These tRNA binding motifs are also shared by metazoan AIMP1 and Tgp43 proteins (62). Although bound to the multisynthetase complex, p43 is cleaved into EMAPII (endothelial

monocyte activating protein) under hypoxic conditions and turns into a proinflammatory cytokine on diverse targets like dendrites, fibroblasts, endothelial cells, pancreatic a cells ,monocyte/macrophage etc (63–65). Of the three nonsynthetase proteins in the MARS assembly, p18 interacts with EF-1γ thus facilitating tRNA transfers to the ribosome (66). p38 functions in assemblage of the multifaceted complex (67) and p43 being a cytokine precursor has tRNA binding properties , modulates aminoacylation activity and plays role in integration of MSC (68, 69). In higher eukaryotes, new interactions have been reported which ascertain that AIMP1 binds to both EPRS and AIMP3 in addition to AIMP2. Thus the three auxiliary proteins form the core of the MSC (70). The organisation of the tRNA binding domain of p43 has been deciphered, exemplifying the chief part of it to be an OB fold or oligonucleotide binding fold (71).

The N terminal domain of *Plasmodium* p43 is homologous to GST domain and C terminus displays an OB fold with tRNA binding domain. The sequence identity between *Plasmodium* p43 and human counter parts of p18 and p38 is < 20% for N-terminal GST like domain and C terminal tRNA binding domain shares 30 % identity with that of the human p43 (53).

Lately apicomplexa specific *P. falciparum* (*Pf)*AIMP1/p43 has been annotated and characterized for its tRNA-binding capability and termed tRNA import protein (tRIP) (72). In addition, it was advocated that *Plasmodium* N-terminal GST-like domain encloses a transmembrane domain that permits this protein to accept tRNA in malaria parasite sporozoites (72).

In order to address the structural features of *Plasmodium* p43, we undertook the production of recombinant full-length, N-terminal GST-like as well as C-terminal OB-fold domain in the heterologous bacterial system (*E. coli*) and purified it to homogeneity. Our structural analyses of these domains sheds light on their overall oligomeric structure, and reveal several notable features which suggest that *Plasmodium* p43 is likely to be a soluble, cytosolic protein. The

structural analysis of these proteins forms the basis of elucidation of the MARS complex in *Plasmodium*.

Aminoacyl tRNA synthetases as drug targets

Over the past decades, studies have focused on protein synthesis machinery, with an aim to identify druggable targets (73, 74). Protein translation is an essential process accomplished by codon-anticodon recognition by aminoacyl-tRNA synthetases (aaRSs) (75, 76). Inhibitors of bacterial synthetases are utilized in parasites and current inhibitors of bacterial synthetases have been utilized in parasites and the unique ones have been established to combat parasite enzymes. Aminoacyl tRNA synthetases are targeted by compounds which may hence develop as antiparasitic drugs (77). The synthetases are multi-domain proteins with - an anticodon, a catalytic and the editing domains. The translational fidelity is dependent on aaRSs that safeguard appropriate charging of amino acids to respective tRNA. Many binding sites on aaRS proteins like that for amino acid, tRNA or ATP might be examined for druggability.

Various natural compounds with their derivatives as well are presently being concentrated on for drugging malarial synthetases. We have previously shown and established three cytosolic aaRSs – phenylalanyl, prolyl or lysyl tRNA synthetases as advanced antimalarial drug targets that are being pursued currently against the leads – cladosporin, halofuginone and bicyclic azetidine derivatives, respectively (73)(78–84) . Borrelidin (fungal metabolite) acts as a noncompetitive inhibitor against some bacterial and eukaryotic ThrRS. Recently a few of its derivatives also potent inhibitors of Pf ThrRS. Again muciprocin from fungus also blocks the interaction of Ile-AMP thus inhibiting PfIleRS (85).

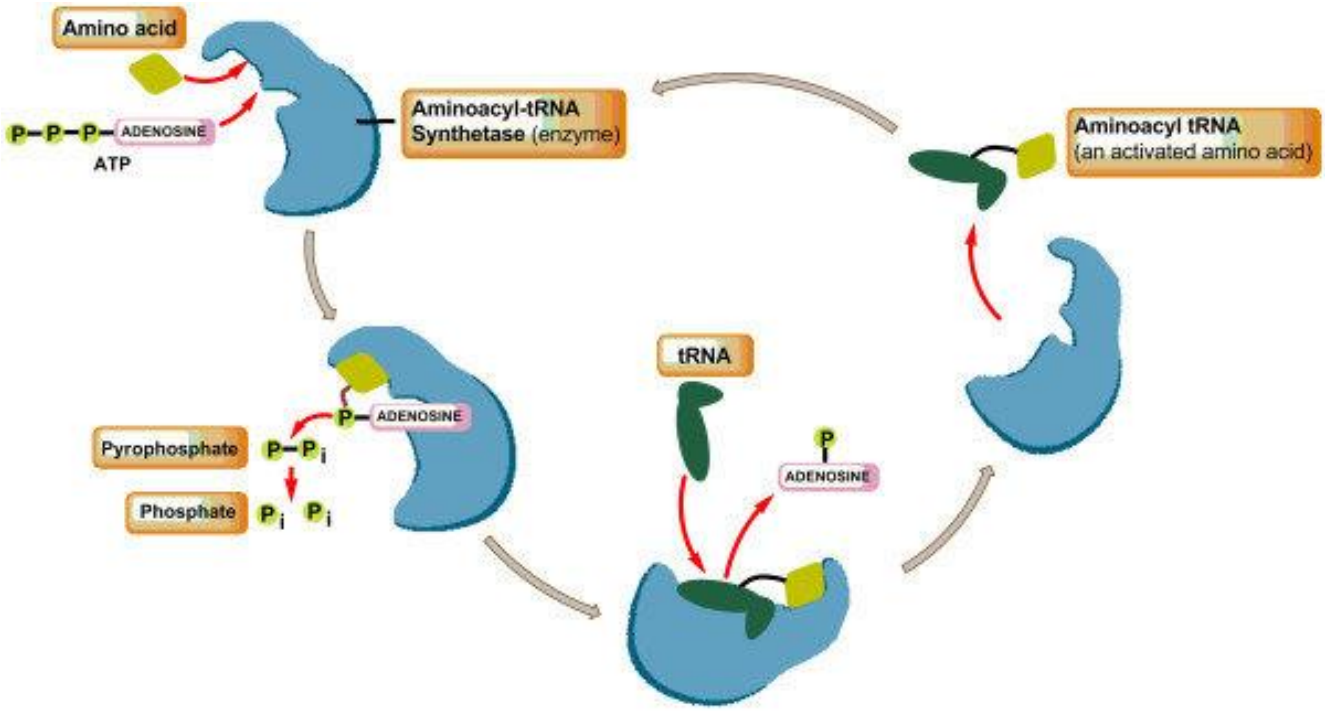

Figure 6:Role of (aaRS) in translation by triggering addition of amino acids to cognate tRNAs (Adapted from Singh et al., 2013)(86)

Chapter-2

Structural characterization of the two domains of *Plasmodium vivax* p43 protein

Introduction

Aminoacyl-tRNA synthetases (aaRSs) are ubiquitous enzymes that are key players in protein translation (75). In complex eukaryotes, some aaRSs form a larger multi-aaRS (MARS) complex collected of a mixture of class I and class II aaRSs alongside with three non-aaRS scaffolding proteins known as aaRS-interacting multifunctional proteins (AIMP1/p43), (AIMP2/p38) and (AIMP3/p18) (54). The protein-protein interaction studies divulge that a significant role of the AIMPs is to initiate congregating of MARS complexes (69).

Lately, the structure of the tRNA binding domain of p43 has been unravelled, displaying that portion of it resumes the OB fold, an oligonucleotide-binding structural motif (71, 87).

Structural and biochemical studies imply that the GST domains of p38 and p43 are responsible for associations in the MARS complex (56, 60, 70, 88). Subjecting upon the cellular localization and cooperating partners, AIMP1/p43 displays miscellaneous tasks. For example, the splitting of p43 into EMAPII supports in angiogenesis and induction of apoptosis (53, 89). The EMAP II domain is homologous to the bacterial tRNA-binding protein but has an extra domain with no homology to known proteins (71). The EMAP II domains are monomers, whereas the corresponding bacterial tRNA-binding domains are dimers and bind one tRNA per dimer (57, 61, 71).

In addition to driving the assembly of MARS complexes, the AIMPs are involved in various biological functions and signalling pathways (64, 69, 90–95). The AIMPs contain an N-terminal glutathione S-transferase (GST)-like module and a C-terminal oligonucleotide/oligosaccharide-binding (OB) fold containing a tRNA-binding domain (TRBD) (53). Structural and biochemical studies have suggested that the N-terminal GST like domain of the AIMPs is responsible for their association with the MARS complex (56, 88, 96). For instance, the interaction and complex formation of AIMP2/p38 and AIMP3/p18 with glutamylprolyl-tRNA synthetase (EPRS; PDB entries 5a34 and 5bmu, respectively; (96) and that of AIMP3/p18 with methionyl-tRNA synthetase (MRS; PDB entry 4bvx) via the AIMP2/p38 GST-like domain have been reported (53, 56, 70). Furthermore, in yeast, a smaller aaRS complex consisting of MRS and glutamyl-tRNA synthetase (ERS) as well as the ARC1p protein (the yeast homologue of p43) has been identified both in vivo and in vitro (56). Experimental evidence shows that the catalytic efficiencies of the in vitro-reconstituted complexes of MRS or ERS with ARC1p are substantially increased compared with those of the uncomplexed aaRSs (56). Further, the C-terminus of ARC1p harbours a TRBD that is conserved in p43 as well as in other AIMPs (97, 98). However, the biological role of AIMPs in MARS complexes remains poorly understood. Depending upon its cellular localization and collaborating partners, p43 displays diverse functions; the cleavage of p43 into endothelial monocyte activating polypeptide II (EMAP II) aids in the induction of apoptosis and angiogenesis (53, 89). More recently, the tRNA-binding ability of the apicomplexan-specific Plasmodium falciparum p43 (Pfp43) has been characterized and it has been termed a tRNA-import protein (tRIP; (62). These authors suggested membrane association of Pfp43 via a transmembrane-helix motif within the p43 sequence and therefore Pfp43-aided transport of tRNAs (62). In the absence of Pfp43, the fitness of P. falciparum in its asexual stages was compromised, suggesting that the parasite requires Pfp43 for the import of tRNA

from the host (62). In order to address the structural features of wild type, full length *Pv* p43 (PVX_118375), we produced the protein recombinantly in bacteria and purified it to homogenity. The full length *Pv* p43 failed to crystallise. Subsequently, the NTDs and CTDs of *Pv* p43 were separately cloned, purified and crystallized. Here, we describe the crystal structures of the N terminal GST like domain (NTD) and C terminal tRNA-binding domain (CTD) of *Pv* p43 protein. Our structural analyses of these domains sheds light on their overall oligomeric structure, and reveals several notable features which suggest that *Pv* p43 is likely to be a soluble, cytosolic protein.

Materials and methods

Gene cloning and protein purification

Protein sequences for PfP43 (PF3D7_1442300) and PvP43 (PVX_118375) were accessed from *Plasmodium* database PlasmoDB (www.PlasmoDB.org). Full-length *Pv*p43 (1-405 amino aicds) Pfp43 (1-402 amino acids) were synthesized and purchased from GeneArt, and the shorter constructs corresponding to the N and C-terminal domains (NTD and CTD) of *Pv*p43 encoding residues 1-180 and 206-405 respectively were synthesised for optimum expression in *E.coli*). The NTD retained the GST domain and the CTD corresponded to the oligonucleotide binding fold. Primers used for cloning are -5'-GGGCCCATGGCAATGTGTGTTCTGACCCTG-3'and 5'-CCCGGCCGGTACCTTATTATTCCAGGCTATCACGAAC-3' for NTD and 5'-GCGGGGCCATGGCAGATAAAAACGCCAAAAATGAG-3 and 5'-GGGGGTACCTTATTAGCTAATGGTGCCCTGTTCCAG-3'for CTD of *Pv* p43. The N and C terminal constructs were cloned into pETM11 vector having protease cleavable His_6 tag using NcoI and KpnI restriction sites. Expression of protein was induced by adding 0.8 mM IPTG to cells grown at 37° upto OD_{600} 0.8. The bacterial culture pellets of these short constructs were harvested 18-20 hours post induction at 18 degree Celsius. The cell pellets were resuspended in lysis buffer constituting of 50 m*M* Tris–HCl pH 8.0, 300 m*M* NaCl, 2 m*M* β-me and 10 percent glycerol with 0.1 mg ml^{-1} lysozyme and 1 m*M* PMSF. The bacterial cells were thus lysed by sonication and cleared by centrifugation at 20,000 g for 45 minutes. Recombinant proteins were affinity captured applying supernatant to Ni-NTA agarose beads (Qiagen) followed by cleavage at 20° C overnight by TEV protease in the presence of 1 mM DTT and 0.5 mM EDTA for the removal of 6X-His tag. TEV protease was added at a mass ratio of 1:40. After another round of buffer exchange to 50 m*M* Tris–HCl pH 8.0 and 200 m*M* NaCl, the proteins were passed through nickel-nitrilotriacetic acid (His-Trap FF; GE Healthcare) column to get liberated of the TEV

protease. The cleaved N and C terminal Pvp43 were concentrated using 10 kDa cutoff Centricon centrifugal device (Millipore) and further purified to homogeneity by gel filtration chromatography on Superdex 200 column 16/60 GL (GE Healthcare) equilibrated with 50 m*M* Tris–HCl pH 8.0, 200 m*M* NaCl and 10 m*M* β-Me. The pure fractions were analyzed through SDS PAGE, pooled and concentrated to 20 mg ml^{-1}, 15 mg ml^{-1} for NTD/CTD of *Pv* p43 respectively. These were stored at -80°C for further crystallization. The full-length p43 was purified similarly with an additional step of heparin chromatography (GE Healthcare) after TEV cleavage using NaCl gradients with buffer A and B containing 50 m*M* Tris–HCl pH 8.0 each and 80 m*M* NaCl and 1.5 *M* NaCl respectively in buffer A and B. The protein was eluted at 20 % of buffer B. We observed degradation of full length *Pv* p43 at even 4°C during the purification process. We made several attempts to obtain crystallized full length *Pv* p43 protein, but were unsuccessful. Hence we proceeded with NTD/CTD of *Pv* p43.

Analytical size-exclusion chromatography

The oligomerization of Pvp43 was examined by sizeexclusion chromatography (SEC) using an A¨ KTAexplorer system (GE Healthcare) equipped with a Superdex 200 HR 10/300 column (GE Healthcare) in 50 mM Tris–HCl pH 8, 200 mM NaCl, 5 mM -Me. A total of 500 ml full-length Pvp43 protein at a concentration of 4 mg ml1 was applied to the column; 100 ml Pvp43 NTD and Pvp43 CTD at a concentration of 2 mg ml1 were separately injected into the column. The molecular-weight standards used are indicated in Fig. 7(b). A standard curve was generated of partition coefficient (Kav) against log10 (molecular weight) (log10 MW) for each standard marker. The curve was fitted to a linear equation and apparent molecular weights were deduced from the Kav values for the respective proteins.

Crystallization and data collection

The purified full-length Pvp43 and Pvp43 NTD and CTD proteins were used for crystallization by the hanging-drop vapour-diffusion method at 293 K using commercially available crystallization

screens (Index, JCSG-plus, Morpheus, PACT premier, PGA, Crystal Screen, PEG/Ion and ProPlex; Hampton Research and Molecular Dimensions). Initial screening was performed in 96-well plates using a nanodropdispensing Mosquito robot (TTP Labtech). Three different drop ratios were used for the crystallization trials by mixing 75, 100 or 50 nl purified protein solution with 75, 50 or 100 nl reservoir solution, respectively (i.e. 1:1, 2:1 and 1:2 drop ratios). Each of the drops was equilibrated against 100 ml of the corresponding reservoir solution. The full-length Pvp43 protein (crystal form 1) crystallized in 20% PEG 3350, 0.2 M sodium bromide, 5% ethyl acetate. Pvp43 NTD crystallized in several conditions and crystals of unliganded Pvp43 NTD (crystal form 2) were obtained from condition B8 of the JCSG-plus crystallization screen (Table 1). The crystals of Pvp43 NTD in complex with GSH (crystal form 3) were obtained from condition F5 of the PACT premier crystallization screen (Table 1). Crystals of forms 1 and 2 of Pvp43 CTD were obtained from condition H4 of the Morpheus crystallization screen (Table 1). All crystals were mounted in nylon loops (Hampton Research) or litho loops (Molecular Dimensions) after being soaked for 10–30 s in a cryoprotectant containing the corresponding crystallization mother liquor with 20%(v/v) glycerol. The crystals were subsequently flash-cooled in liquid nitrogen (Fig. 14). Preliminary data sets were collected at 100 K using in-house Cu K radiation = 1.54 A˚) generated by a Rigaku MicroMax-007 HF rotating-anode X-ray generator operated at 40 kV and 20 mA with Osmic mirrors, and the diffraction images were recorded using a MAR345dtb image-plate detector. The full-length Pvp43 protein crystals were soaked in cryoprotectant containing 200 mM CoCl2 for 30 s and several Co SAD data sets were collected on beamline I02 at Diamond Light Source (DLS), United Kingdom at a wavelength of 1.59 A˚. The data sets for unliganded (form 2) and GSH-complexed (form 3) Pvp43 NTD and for form 2 Pvp43 CTD were collected on beamline I03 at DLS. The data set for form 1 Pvp43 CTD was collected on the PROXIMA2 beamline at SOLEIL, France. The in-house data sets were processed using HKL-2000. The data collected on the DLS beamlines were processed by the xia2 auto-processing pipeline (99) using DIALS (100)

for integration. The data set collected on the PROXIMA2 beamline at SOLEIL was integrated using XDS (101). Data were scaled with AIMLESS (102) and processing statistics are shown in Table 2.

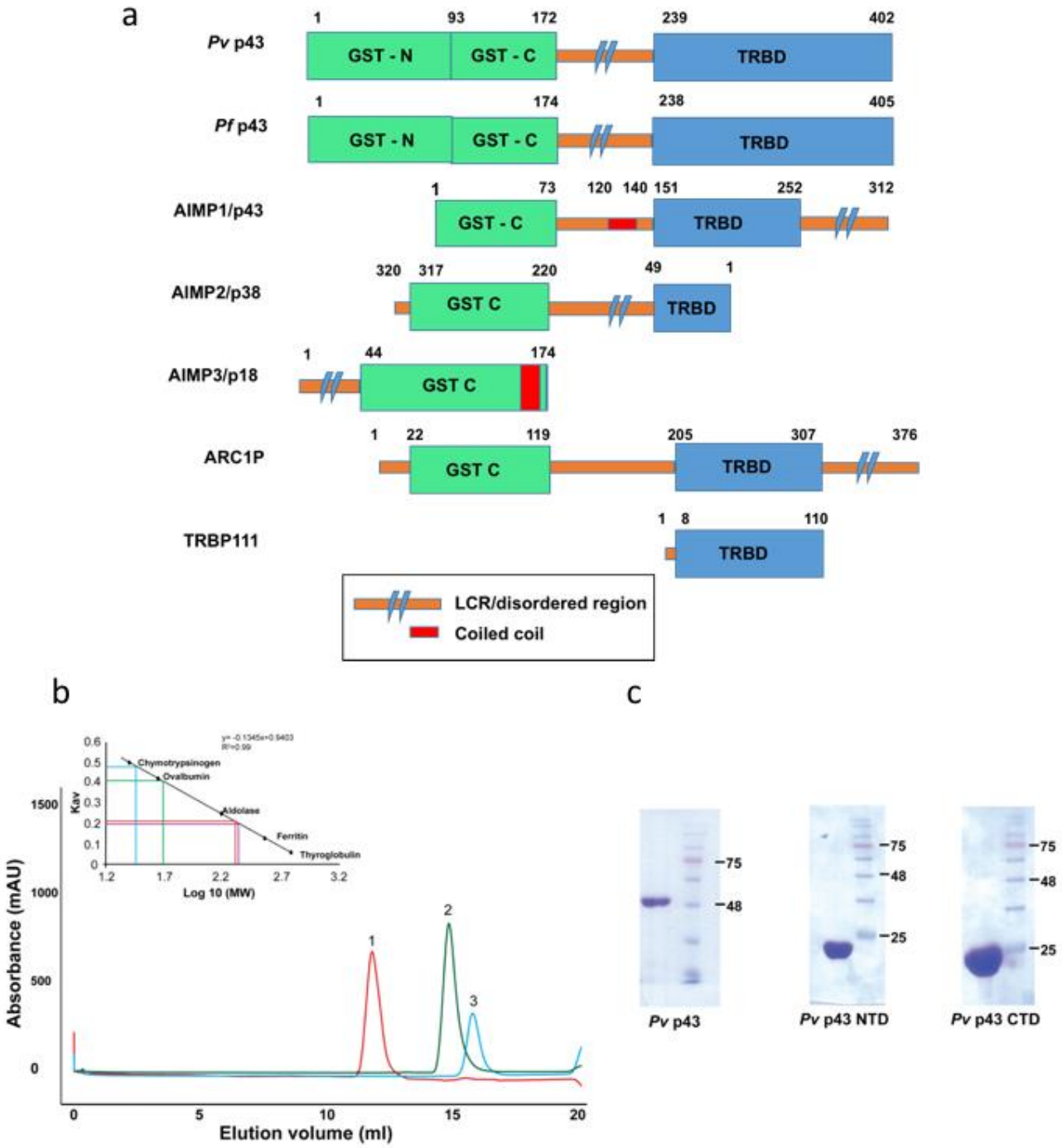

Figure 7:The overall assembly of p43 proteins. (a) The domain architectures of P. vivax p43 (Pvp43), P. falciparum p43 (Pfp43), aminoacyl-tRNA synthetase (aaRS)-interacting multifunctional proteins (AIMP) AIMP1/p43, AIMP2/p38, AIMP3/p18, ARC1p and tRNA-binding protein 111 (TRBP111) are shown. The boundaries of the N-terminal glutathione S-

transferase (GST)-like domain are shown [the N-terminal thioredoxin domain (GST-N) and Cterminal helical domain (GST-C) are shown in purple and blue, respectively]. The C-terminal tRNA-binding domain (TRBD) is shown in light brown and the linker region is shown in orange. (b) Size-exclusion chromatography (SEC) profiles for full-length Pvp43 protein (residues 1–402), the GST-like N-terminal domain (NTD; residues 1–180) and the C-terminal domain (CTD; residues 239–402). Kav = Ve-Vo/Vt-Vo, where Ve is the elution volume of the native proteins from the SEC column, Vo is the void volume of the column and Vt is the total volume of the column. Log10 (MW) is the logarithm of the molecular weight in kDa. (c) SDS–PAGE gels of full-length Pvp43 (pink), Pvp43 NTD (green) and Pvp43 CTD (blue).

Table 1: Crystallization conditions for full-length Pvp43, Pvp43 NTD and Pvp43 CTD

Protein	PDB code	Space group	Well solution
Pvp43 (NTD)	**6jre (form 1)**	**P41212**	**Polyethylene glycol (PEG) 3350, 0.2 M sodium bromide, 5% ethyl acetate**
NTD (unliganded)	**5zkf (form 2)**	**P21**	**0.2 M magnesium chloride_6H2O, 0.1 M Tris pH 7, 10%(w/v) PEG 8000**
NTD	**5zke (form 3)**	**P212121**	**0.2 M sodium nitrate, 0.1 M bis-tris propane pH 6.5, 20%(w/v) PEG 3350**
CTD	**5zkg (form 1)**	**P43**	**12.5%(w/v) PEG 1000, 12.5%(w/v) PEG 3350, 12.5%(v/v) 2-methyl-2,4-pentanediol (MPD), 0.02 M**

			sodium l-glutamate, 0.02 M dl-alanine, 0.02 M glycine, 0.02 dl-lysine–HCl, 0.02 M dl-serine, 0.1 M 2-(N-morpholino)ethanesulfonic acid (MES) buffer
6ipa	**(form 2)**	**P212121**	**12.5%(w/v) PEG 1000, 12.5%(w/v) PEG 3350, 12.5%(v/v) MPD, 0.02 M sodium l-glutamate, 0.02 M dl-alanine, 0.02 M glycine, 0.02 M dl-lysine–HCl, 0.02 M dl-serine, 0.1 M MES buffer**

Structure determination and refinement

The structure of the crystallized fragment of the full-length protein Pvp43 was determined using Co SAD data. SHELXC and SHELXD from the SHELX suite (103) and phenix.xtriage (104), Phaser (105), AutoSol and AutoBuild (106) from the Phenix package (107, 108) were used for anomalous signal analysis, heavy-atom location, phasing and density modification as well as for model building. The ARP/wARP web server (109) and the automated model-building platform Auto-Rickshaw (110) were also used for phasing and model building. Structure refinements were performed using REFMAC5 (111) in the CCP4 package and phenix. refine (112, 113). After each

refinement step, the models generated were inspected and manually rebuilt in Coot (114). During refinement, water molecules were manually added and included in the refinement based on positive peaks in difference Fourier maps. The structures of forms 2 and 3 of Pvp43 NTD were determined by the molecular-replacement (MR) method using Phaser (105) with form 1 of Pvp43 NTD as the template. Forms 1 and 2 of Pvp43 CTD were solved by MR using Phaser (105) with an EMAP II-like domain (PDB entry 1ntg; (115) as the template. Form 2 (space group P21) of Pvp43 NTD has four molecules in the asymmetric unit. Form 1 (space group P43) and form 2 (space group P212121) of Pvp43 CTD have two and four molecules in the asymmetric unit, respectively. The different copies of a molecule in the asymmetric unit have different overall displacements and these can be accounted for by refining translation–libration–screw (TLS) parameters for each molecule. Therefore, TLS refinement was carried out as implemented in phenix.refine (112, 113) or REFMAC5 (111), and systematic comparisons of the inclusion or the absence of TLS parameterization were performed by monitoring any decrease in the R factors (particularly of >1–2% in Rfree). An improvement was indeed confirmed for the Pvp43 NTD and CTD models. Hence, TLS groups were maintained in the final refinement cycle. Full anisotropic refinement was carried out for the Pvp43 NTD data at 1.49 A˚ resolution (form 3; Table 2). The occupancies of alternate side-chain conformations and water molecules were also refined. Prior to the deposition of atomic coordinates, validation and final corrections were completed using MolProbity (116). The rotameric conformations of the modelled side chains were validated using the PDBREDO server (117). Final refinement statistics are shown in Table 2. The stereochemical quality of each model was assessed using MolProbity (116). All figures were generated using UCSF Chimera (118) and PyMOL v.2.0 (Schrodinger; http:// www.pymol.org).

Results

Domains and recombinant production of P. vivax p43

The domain boundaries were assessed using several web servers, including InterPro (119), SMART (120) and PROSITE (121), and the NCBI CDD (122) and Pfam (123) databases. Low-complexity regions were predicted for residues 181–190 and 215–226 using the Pfam protein domain database, along with a tRNA-binding domain for residues 242–344. The boundaries of the GST-like Pvp43 NTD were predicted using the Pfam protein domain database to include residues 93–163. However, based on analyses of crystal structures of AIMP3/p18 (PDB entry 4bvx), AIMP2/p43 (96) II-like domain (PDB entry 1ntg; (115) and the crystal structures of Pvp43 NTD and Pvp43 CTD reported in this work, we suggest that the GST-like Pvp43 NTD includes residues 1–180 (Fig. 7a). The oligomeric states of the full-length Pvp43 and the Pvp43 NTD and CTD proteins were analyzed using SEC. Single bands for the purified full-length Pvp43 (48 kDa) and the Pvp43 NTD/CTD (22 kDa) proteins were observed on SDS–PAGE (Fig. 7b). The full-length Pvp43 protein eluted at a position similar to aldolase, indicating it to be a tetramer of 204 kDa. The Pvp43 NTD protein eluted with ovalbumin, suggesting a dimer of 46 kDa, while the Pvp43 CTD protein eluted near chymotrypsinogen, indicating it to be a monomer of 29 kDa (Fig. 7b).

Table 2: Summary of data collection and refinement statistics. Values in parentheses are for the highest resolution shell.

	*Pv*p43-NTD form 1 (Co-SAD)	*Pv*p43-NTD form 2	*Pv*p43-NTD form 3	*Pv*p43-CTD form 1	*Pv*p43-CTD form 2
PDB code	**6JRE**	**5ZKF**	**5ZKE**	**5ZKG**	**6IPA**

Data collection					
Beam line	**DLS I02**	**DLS I03**	**DLS I03**	**SOLEIL PROXIMA 2**	**DLS I03**
Wavelength(Å)	**1.59**	**0.9763**	**0.9763**	**0.980**	**0.9763**
Detector type	**DECTRIS PILATUS 6MF**	**DECTRIS PILATUS3 6M**	**DECTRIS PILATUS3 6M**	**DECTRIS EIGER X 9M**	**DECTRIS PILATUS3 6M**
Crystal-to-detector distance (mm)	**625**	**600**	**238**	**317**	**514**
Oscillation (°)	**0.1**	**0.1**	**0.1**	**0.2**	**0.1**
Exposure (s)	**0.050**	**0.010**	**0.010**	**0.010**	**0.010**
Beam size (μm) (elliptical)	**100 x 20**	**80 x 20**	**80 x 20**	**5 x 5**	**80 x 20**
Flux (photons s^{-1})	**6.54×10^{10}**	**1.28×10^{12}**	**1.28×10^{12}**	**1.0×10^{13}**	**4.6×10^{11}**
Transmission (%)	**3.0**	**100**	**100**	**50**	**40**
Number of images	**9900**	**3600**	**3600**	**3600**	**3600**
Software used for data processing	**XIA2 (Winter *et al.*, 2013)**	**XIA2 (Winter *et al.*, 2013)**	**XIA2 (Winter *et al.*, 2013)**	**XDS (Kabsch, 2010)**	**XIA2 (Winter *et al.*, 2013)**
Cell dimensions *a, b, c* (Å) *α, β, γ* (°)	**87.40, 87.40, 53.41; 90.0, 90.0, 90.0**	**53.18, 86.96, 78.41; 90.0, 91.81, 90.0**	**59.15, 74.62, 77.45; 90.0, 90.0, 90.0**	**105.20, 105.20, 36.97; 90.0, 90.0, 90.0**	**37.17, 146.90, 146.93; 90.0, 90.0, 90.0**

Space group	***P*4$_1$2$_1$2**	***P*2$_1$**	***P*2$_1$2$_1$2$_1$**	***P*4$_3$**	***P*2$_1$2$_1$2$_1$**
Resolution (Å)	**61.80-2.59 (2.63-2.59)**	**45.35-2.75 (2.80-2.75)**	**77.45-1.49 (1.52-1.49)**	**47.05-3.30 (3.50-3.30)**	**40.75-2.47 (2.51-2.47)**
R_{meas} (%)	**0.081 (3.353)**	**0.063 (1.964)**	**0.045 (1.162)**		**0.174 (1.806)**
$\langle I/\sigma(I)\rangle$	**27.1 (1.2)**	**5.4 (0.9)**	**18.9 (2.2)**	**5.92 (0.98)**	**12.0 (1.2)**
Completeness (%)	**95.8 (71.8)**	**99.5 (89.8)**	**99.8 (98.5)**	**99.8 (98.8)**	**99.98 (100)**
Average redundancy	**58.1 (28.3)**	**6.4 (5.3)**	**13.0 (13.3)**	**12.8 (10.3)**	**12.8 (11.4)**
$CC_{1/2}$	**1.0 (0.70)**	**1.0 (0.40)**	**1.0 (0.80)**	**0.99 (0.44)**	**0.99 (0.56)**
Number of unique reflections	**6539 (242)**	**18633 (844)**	**56387 (2772)**	**6367 (993)**	**29902 (1455)**
Refinement					
Resolution (Å)	**61.51-2.59 (2.66-2.59)**	**43.36-2.75 (2.89-2.75)**	**37.31-1.49 (1.52-1.49)**	**47.05-3.30 (3.50-3.30)**	**36.73-2.47 (2.53-2.57)**
No. of reflections in Work set/test set	**5177/623**	**18182/952**	**56319/2752**	**6347/318**	**25848/1995**
R_{work}/R_{free} (%)	**22.0/27.4**	**22.1/27.9**	**14.6/17.1**	**21.7/27.8**	**22.6/27.8**
Number of atoms					
Protein/Water/Ions	**1381/0/2 (Co^{2+})**	**5748/30**	**2975/201**	**2344/0**	**4978/32**
Average *B* factor (Å^2)					
Protein/water/ion	**113.9/103.5**	**58.3/46.8**	**30.1/40.8**	**85.4**	**47.3/46.5**

RMSD from ideal geometry					
Bond length (Å)	**0.010**	**0.008**	**0.009**	**0.003**	**0.014**
Bond angle (°)	**1.470**	**1.160**	**1.020**	**0.799**	**1.830**
Ramachandran plot favored/allowed (%)	**92.0 (8.0)**	**96.0/4.0**	**97.0/3.0**	**98.0/2.0**	**92.0 (7.0)**

Structure determination of the Pvp43 N-terminal domain (NTD)

The crystals obtained from the full-length Pvp43 protein diffracted to between 3.0 and 3.5 A˚ resolution at an in-house X-ray source. Our preliminary analysis of the data indicated that these crystals belonged to the tetragonal system and the data sets consistently processed in point group P422. However, the asymmetric unit volume was too small for the full-length Pvp43 protein. Further analysis of the crystallized protein via SDS–PAGE revealed the molecular weight of the crystallized protein fragment to be 22 kDa (Fig.16). This indicated that only a fragment of Pvp43 had crystallized, i.e. either Pvp43 NTD or CTD. Attempts were made to solve the structure by the molecular-replacement method using GST-like or EMAP II-like tRNA-binding domains as templates. The sequence identity between the available templates for Pvp43 NTD and Pvp43 CTD are 10–20 and 20–40%, respectively. Structure solution of this crystallized fragment of Pvp43 was unsuccessful using MR methods. This was attributed to the low sequence identity between the GST-like domains or possibly because the fragment was indeed not the tRNA-binding domain. Therefore, we concurrently attempted heavy-atom derivatization for phase determination. Thus, crystals obtained from full-length Pvp43 protein were soaked in cryoprotectant solution containing 200 mM CoCl2 for 30 s and several Co SAD data sets were collected at a wavelength of 1.59 A˚ (Table 3). The Co SAD data sets were collected using ten different crystals and multiple data sets

were also collected from each crystal at a different region within the crystal. The data sets with an anomalous signal-to-noise ratio [hF/(F)i] of >1.0 are listed in Supplementary Table S1. We selected two data sets, x10_3 (where x10 is the crystal number and the number after the underscore refers to the number of the data set) and a merged data set (x3_2, x3_4, x7_2, x10_3 and x10_6) with an anomalous signal-to-noise ratio [hF/(F)i] of >1.5 for structure solution (Table 3). The substructure was determined using SHELXD (124) and AutoSol (107) and the top two located sites were found to be identical using either program. The phasing and density modification produced an interpretable map in space group P41212 (Fig. 15). The figure of merit (FOM) before/after density modification (0.19/0.64), the overall score (BAYES CC, 30±15) and the map skew (0.07) were moderate for Co SAD data set x10_3 and these data alone were sufficient to solve the structure. However, improved phasing parameters (FOM before/after density modification, 0.28/0.67; BAYES CC, 37±14; map skew, 0.09) were observed for the merged data set (Fig. 15). Three rounds of iterative model building resulted in the fitting of 103 amino acids within nine fragments with an Rwork and Rfree of 38.9% amd 45.0%, respectively. The traced model had five helices and thus the crystallized fragment of the Pvp43 protein was identified as the N-terminal GST-like NTD (Fig. 17). The remaining residues were manually traced using Coot (Emsley et al., 2010). The final model consists of 173 N-terminal residues of Pvp43. The asymmetric unit of form 2 (space group P21) of Pvp43 NTD contains two dimers (four molecules per asymmetric unit). TLS refinement was used and resulted in a 2% decrease in Rwork and Rfree. In the final refinement step, isotropic riding H atoms were introduced into the model, followed by individual anisotropic B factors for the highresolution (1.49 A˚) form 3 (space group P212121) of Pvp43 NTD. Several attempts were made to crystallize Pvp43 NTD (form 3) in the presence of 5 mM glutathione (GSH). However, no electron density for a GSH molecule was observed.

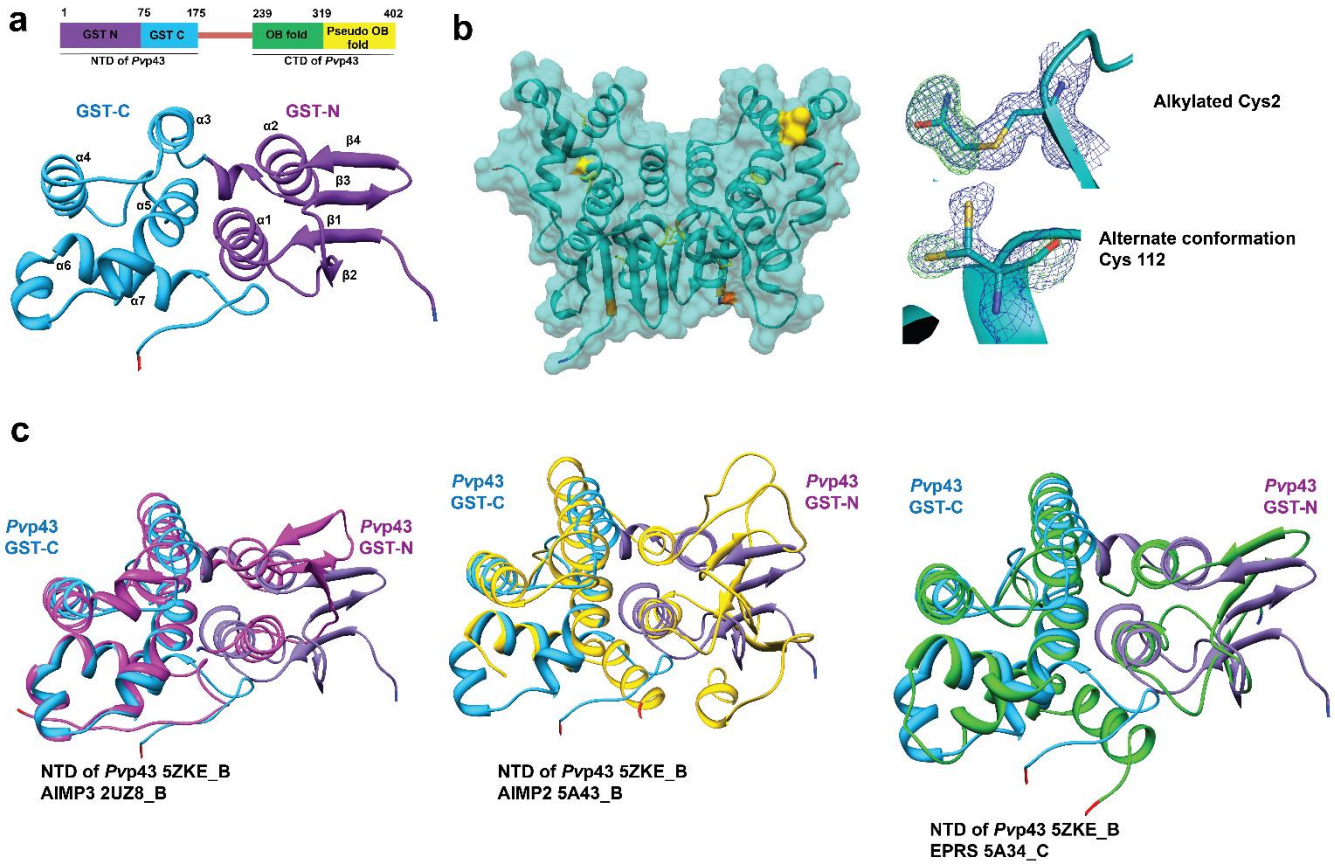

Figure 8: The crystal structure of Pvp43 NTD. (a) The monomeric structure of the Pvp43 N-terminal GST-like domain with the canonical four-stranded _-sheet (PDB entry 5zke chain A). (b) A molecular-surface representation highlighting the solvent-exposed cysteine residues (yellow) is shown. Cys2 and Cys112 are exposed to the surface. Cys2 has been modified as S-(2-amino-2-oxoethyl)-l-cysteine or cysteine-S-acetamide (YCM) during protein production; see the main text. The difference Fourier electron-density map (Fo_ Fc) was generated without the coordinates of the carboxamido group of the modified Cys2, as was the alternate conformation of Cys112. The Fo_ Fc (green) and 2Fo _ Fc maps (blue) are contoured at the 4_ and 1_ levels, respectively. (c) Structural superposition of the Pvp43 GST-like domain (GST-N and GST-C are in purple and blue, respectively) with other GST-like domains from AIMP3 (PDB entry 2uz8 chain B, magenta), AIMP2 (PDB entry 5a34 chain B, yellow) and EPRSGST (PDB entry 5a34 chain C, green).

Crystal structure of the Pvp43 N-terminal domain (NTD)

The overall fold of Pvp43 NTD is similar to GST family proteins, with two domains: an N-terminal sandwich thioredoxin domain (GST-N) and a C-terminal all--helical domain (GST-C) (Fig. 8a). The asymmetric unit of the orthorhombic space group P212121 contained one dimer (chains A and B) and that of the monoclinic space group P21 contained four copies, chains A to D, that associated into two dimers AC and BD. Clear electron density was observed for four additional residues (GAMA) at the N-terminus of chain B in the orthorhombic form (Fig. 13).

These residues were part of the vector pETM-11 containing the NcoI restriction-enzyme site that was used during the cloning of Pvp43 NTD. The superposition of molecules in the asymmetric units of the tetragonal, monoclinic and orthorhombic forms yielded a root-mean-square deviation (r.m.s.d.) value of 0.6 A˚ for 171 C atoms. Superposition of the monoclinic dimers onto the orthorhombic dimers yielded r.m.s.d. values of 1.6 A˚, which was owing to small structural differences that were distributed throughout the two monomers. Hereafter, we will discuss the high-resolution (1.49 A˚) orthorhombic form of the Pvp43 NTD dimer AB. Pvp43 NTD has five cysteine residues per molecule, of which three are buried and two (Cys2 and Cys112) are surface-exposed (Fig. 8b). None of these five cysteine residues form internal disulfide bonds. The residue Cys2 in Plasmodium spp. is unique when compared with p43 proteins from other organisms. The covalent modification of the surface-exposed Cys2 was apparent in the electron-density maps (Fig. 8b). Based on the electron density and the surrounding environment, this covalent modification was modelled as S-(2-amino-2-oxoethyl)-l-cysteine or cysteine-Sacetamide. It is probable that Cys2 of Pvp43 was covalently modified during protein expression in E. coli, during protein purification or by the crystallization buffer. However, additional experiments such as mass spectrometry are needed to confirm the Cys2 modification of Pvp43 (125–127). Further, the second surface-exposed Cys112 in chain A of the orthorhombic crystal form was found to adopt two different conformations (Fig. 8b). A search against the 25% redundant Protein Data Bank (PDB25) using DALI (Holm & Sander, 1993) yielded several proteins that were structurally similar to Pvp43 NTD, including GSTs and other proteins with a GST fold (Fig. 8c and Table 5). Several GST family proteins showed Z-scores ranging from 9 to 15, although with low sequence homology (9–19%). The structure of Pvp43 NTD was compared with the EPRSGST domain that contains a canonical four-stranded -sheet and with AIMP3 and AIMP2, which have three-stranded and five-stranded -sheets, respectively (Fig. 8c). The assembly of Pvp43 NTD is a dimer of 48 kDa as observed in SEC experiments (Figs. 7c and 9a). The buried

surface area per monomer is 867 A˚ 2. The dimer is stabilized via hydrophobic interactions, seven hydrogen bonds and three salt bridges. The central core of the dimer interface is composed of five aromatic residues (Phe58, Phe90, Tyr54, Tyr62 and Tyr71) that are conserved only in Plasmodium p43 proteins. The aromatic ring of Phe58 in one monomer (chain A) is at a face-to-face stacking distance of 4.0 A˚ from the aromatic ring of Phe90 of its partner (chain B). The complementary interaction is not observed (left panel of Fig. 9b), thereby establishing a nonsymmetric dimer contact. In the monoclinic form 2, Phe90 of one monomer (chain B) is at a face-to-face stacking distance of 4.3 A˚ from Phe90 of its partner (chain D; right panel of Fig. 9b). Similar asymmetric interactions were observed for hydrogen bonds and salt bridges (Figs. 3c, 3d and 3e). In Pvp43 NTD helices 2 and 3 of one monomer pack against helices 20 and 30 of its partner (2 against 20 and 3 against 30; Fig. 10a). In the canonical GST dimeric association, helices 2 and 3 of one monomer pack against helices 30 and 20 of its partner (2 against 30 and 3 against 20; Fig. 10b). Thus, the dimerization assembly of Pvp43 NTD is different when compared with other GSTs. In addition, the dimerization helices (2 and 3) of one monomer are perpendicular to its partner helices (20 and 30; Fig. 10c). In contrast, in the canonical GST assembly the helices of one monomer are aligned parallel to the other monomer (Fig. 10c). An alternate dimer formation has also been observed in the fungal-specific class A1 GSTs from Phanerochaete chrysosporium (PcGSTFuA1 or GST5118) and the -esterase enzymes LigE and LigF from Sphingobium sp. strain SYK-6 (128, 129). In these, helix 4 of one subunit packs in the groove between helices 4 and 5 of the other protomer (128); thus, the entire dimer interface is contained within the -helical domain. The additional -hairpin prevents the packing of the 4 and 5 helices of one monomer against the N-terminal domain of its partner. Thus, the GST dimer formation displays differences in the assembly modes, and Pvp43 NTD here presents another example of this. Further experiments are required to determine the biological relevance and function of these observations.

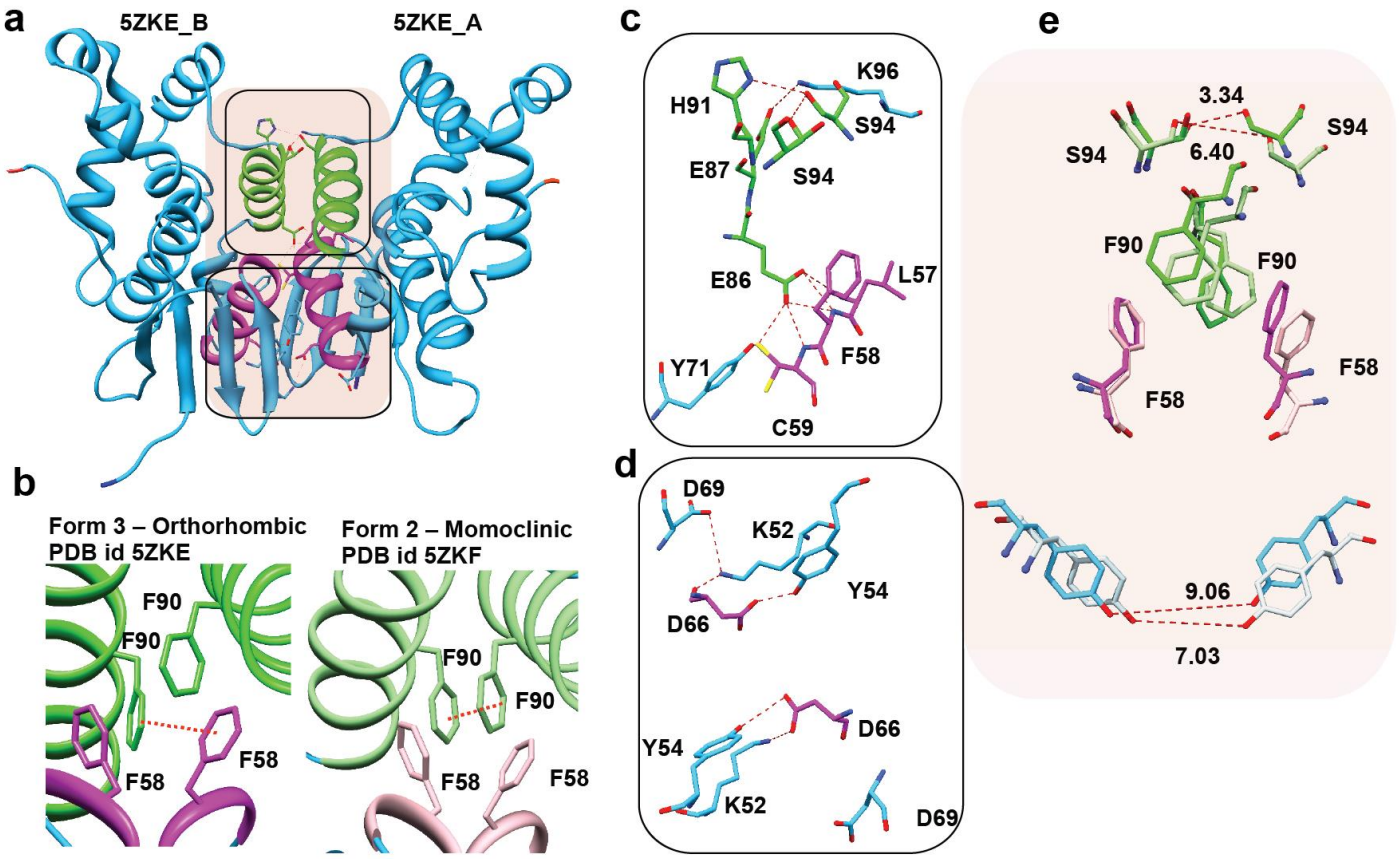

Figure 9:Conformational asymmetry at the Pvp43 NTD dimer interface. (a) The Pvp43 NTD dimer is shown. The helix involved in the dimer interface is highlighted in magenta and green. (b) The aromatic stacking interaction at the dimer interface in crystal forms 2 and 3 of Pvp43 NTD is shown. In the orthorhombic form Phe58 of one monomer stacks against Phe90 of its partner, and in the monoclinic form Phe90 of one monomer stacks against Phe90 of its partner. (c, d) Hydrogen bonds and salt bridges observed in the high-resolution structure of NTD at the dimer interface. The marked hydrogen-bond lengths are in the range 2.5–3.6 A. (e) Comparison of the monoclinic and orthorhombic forms of Pvp43 NTD reveals the asymmetric chain–chain contacts (black dashed lines) at the dimer interface.

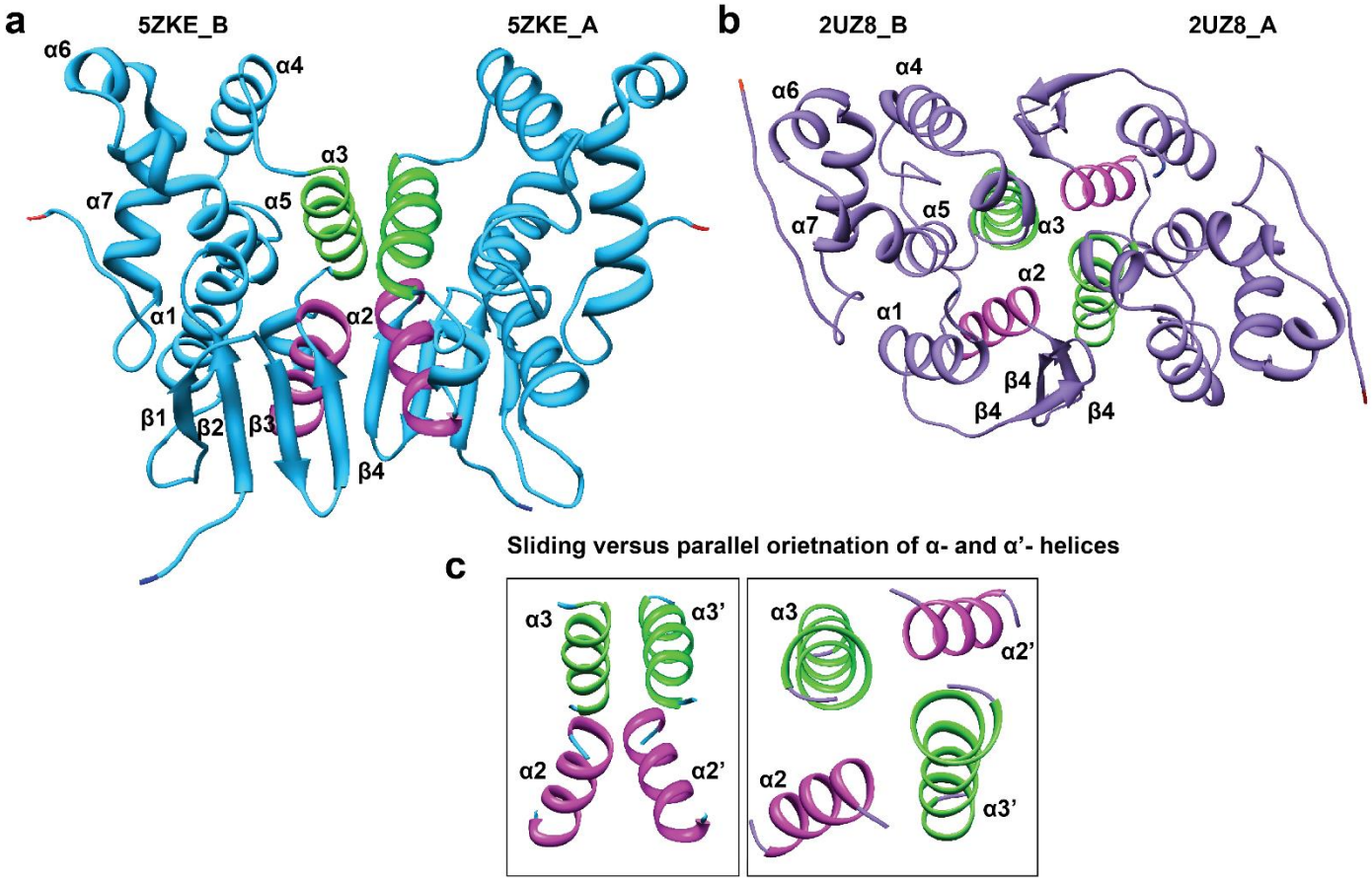

Figure 10 :Dimeric Pvp43 NTD versus canonical GST dimers. (a) The dimeric Pvp43 NTD association is shown. The last helix (α2, magenta) of the N-terminal thioredoxin domain (GST-N) and the first helix (α3, green) of the C-terminal helical domain (GST-C) are involved in oligomerization. Helices α2 and α3 of one monomer pack against helices α20 and α30 of its partner (α2 against α20 and α3 against α30). (b) The canonical GST dimeric association observed in AIMP3 (PDB entry 2uz8) and other GSTs, where α2 and α3 of one monomer pack against α30 and α20 of a partner (α2 against α30 and α3 against α20). (c) A representation of the helix orientations in canonical and noncanonical GST assemblies is shown. Helices α2 and α3 of one monomer in Pvp43 NTD are perpendicular to those in their partner molecule (left panel). The same helices are parallel to each other in other canonical GST assemblies (right panel).

Structure determination of the Pvp43 C-terminal domain (CTD)

The Pvp43 CTD protein crystallized in the tetragonal space group P43 in two different crystal forms (form 1, unit-cell parameters a = b = 105.2, c = 36.97 A˚; form 2, unit-cell parameters a = b = 146.99, c = 37.18 A˚). The twin fraction was estimated using phenix.xtriage (Britton analysis, H-test and maximum-likelihood method values for form 1 are 0.04, 0.07 and 0.02, respectively, and those for form 2 are 0.45, 0.46 and 0.46, respectively). The structures of both forms were solved by the MR method using Phaser (105) with an EMAP II-like domain (PDB entry 1ntg;

(115) as the search model. The MR solutions obtained for Pvp43 CTD (form 2) belonged to space groups P43 (LLG 1850 and TFZ 16) and P43212 (LLG 215 and TFZ 12). However, the refinements did not converge in either space group, since the Rwork and Rfree for refined Pvp43 CTD (form 2) models were 37% and 44%, respectively, in space group P43 and 46% and 50%, respectively, in space group P43212. Therefore, the Pvp43 CTD (form 2) data were reprocessed in the orthorhombic space group P212121, with unit-cell parameters a = 37.17, b = 146.90, c = 146.93 A˚. The data were pseudomerohedrally twinned and the suggested operator was h, k, l. The twin fraction was estimated using phenix.xtriage (104); the calculated twin fraction was 0.35, 0.37 and 0.33 using Britton analysis, the H-test and the maximum-likelihood method, respectively). There are four Pvp43 CTD molecules in the asymmetric unit in space group P212121 and the LLG and TFZ scores were 7124 and 34, respectively, for the obtained MR solution. Twin refinement resulted in decreases in Rwork and Rfree of 3.7% and 4.5%, respectively, and we observed dramatic improvements in the connectivity of the electrondensity map. The refined twin fraction was 0.35 with the pseudomerohedral twinning operator h, k, l. The final structure refinement converged to an Rwork and Rfree of 20.2% and 26.1%, respectively. The statistics for data collection and structure refinement for both forms 1 and 2 of Pvp43 CTD are listed in Table 2.

Crystal structure of the Pvp43 C-terminal domain (CTD)

The Pvp43 CTD protein (residues 241–405) along with the linker region (residues 204–240) was recombinantly expressed. Purified protein (202 amino acids, molecular mass 22 kDa; Fig. 7c) was used for crystallization and its structure was solved. The final model of Pvp43 CTD includes 165 residues (Leu241–Ser405). No electron density was observed for the low-complexity linker region (204-KDDKNAKNE NGDNEKGKKKNNAQNKNAQKKKVEEPKN-240). The asymmetric units of forms 1 and 2 contain two and four molecules, respectively. The superimposition of independent chains gave an r.m.s.d. of 0.4 A˚ for C atoms, suggesting that

their conformations were similar. The Pvp43 CTD protein can be divided into two subdomains (CTD-N and CTD-C; Fig. 11a). The first subdomain, CTD-N, is a -barrel (Leu24–Val319) that resembles an OB-fold. This domain consists of seven -strands, i.e. OB strands 1–5 and linker strands 0 1 and 0 2, as well as two short 310-helices at the N-terminus and between strands 3 and 4. The -sheets (1–2–3 and 1–4–5) share the twisted 1 strand and interact at almost a right angle with each other (Fig. 11a). The second subdomain, CTD-C, is from Leu320 to Ser405 (Fig. 11) and consists of two -sheets (8–11–12 and the curved 6–7–13–9–10), with a long loop between 8 and 9 that joins the two sheets (Fig. 11a). The OB-fold is commonly found in RNA-binding proteins and in several other proteins unrelated to oligonucleotide binding (130, 131). A search against all entries in the 25% redundant Protein Data Bank (PDB25) using DALI (132) yielded models of low homology similar to Pvp43 CTD (Table 4). The sequence identity between these proteins is in the range 23–38% (Supplementary Table S4). While Pvp43 CTD is a monomeric protein and is similar to the EMAP II-like tRNA-binding protein (71, 133), other bacterial tRNA-binding OB-fold proteins are dimers (57, 61). The dimerization interface of the OB-fold in Pvp43 CTD is masked by an additionally present pseudo OB-fold subdomain when compared with dimeric TRBP111 (PDB entry 1pyb; Fig. 11b; (61).

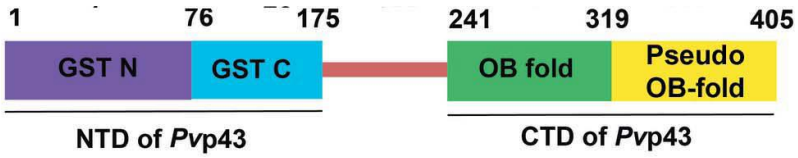
1
76
175
241
319
405
GST N
GST C
OB fold
Pseudo OB-fold
NTD of Pvp43
CTD of Pvp43

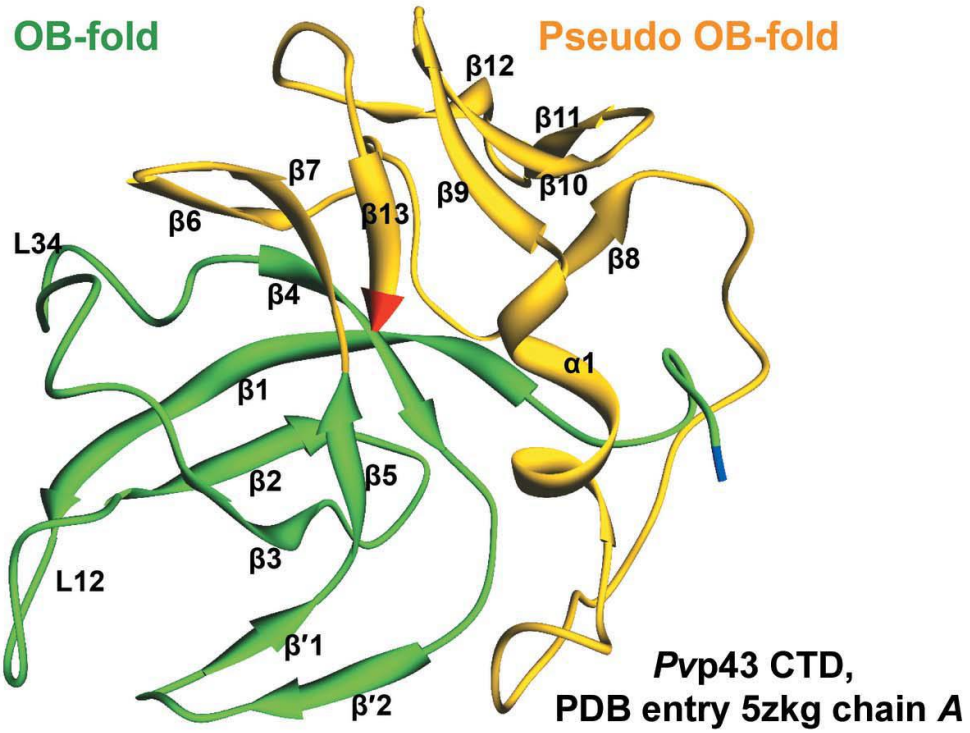
OB-fold
Pseudo OB-fold
β12
β11
β7
β9
β10
β6
β13
L34
β8
β4
α1
β1
β2
β5
β3
L12
β′1
β′2
Pvp43 CTD,
PDB entry 5zkg chain A

(*a*)

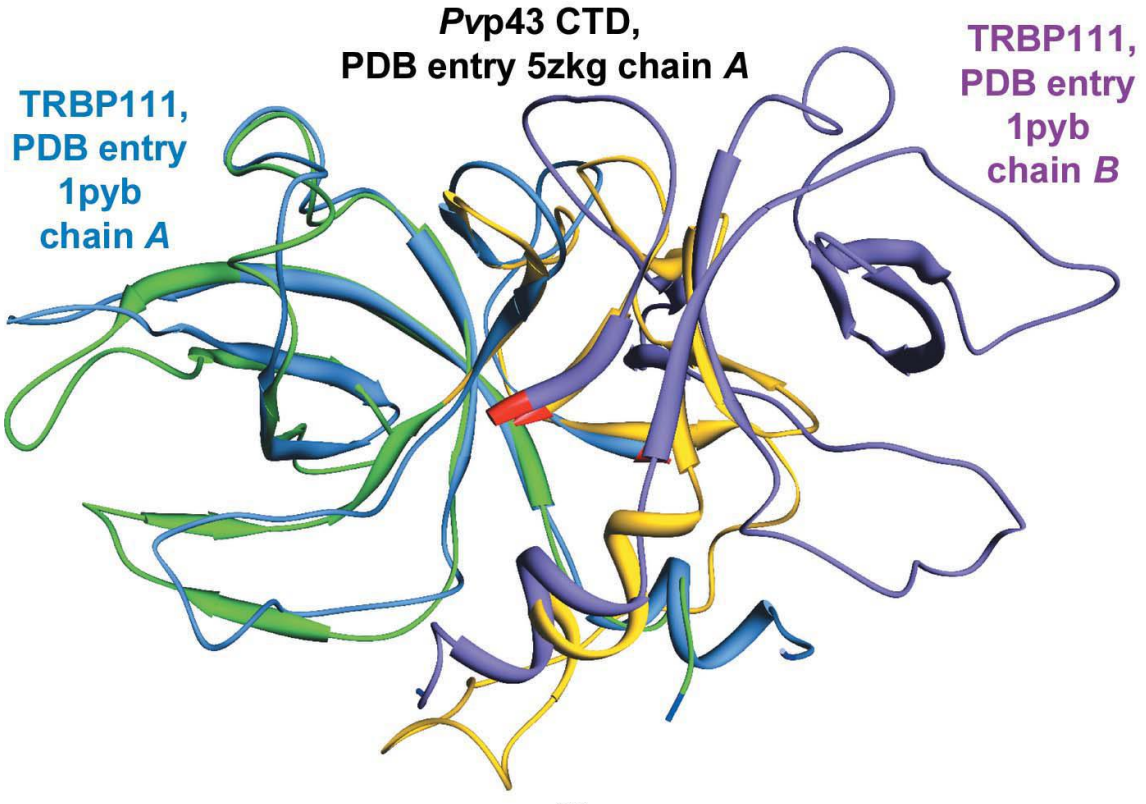
Pvp43 CTD,
PDB entry 5zkg chain A
TRBP111,
PDB entry
1pyb
chain A
TRBP111,
PDB entry
1pyb
chain B

(*b*)

Figure 11:Pvp43 CTD in comparison to bacterial dimeric tRNA-binding domains. (a) The structure of Pvp43 CTD with its EMAP II-like domain is shown. The OB-fold (green) and pseudo OB-fold (orange) subdomains are highlighted. (b) Superposition of monomeric CTD on dimeric bacterial TRBP111 (PDB entry 1pyb). Chains A (cornflower blue) and B (purple) of TRBP111 are colored differently.

a

***Pv*p43 NTD** LCEKSYIVSNRHASIVDIFYFCSVYKPLSEMPAKERVEISHIYRWFLHIQETLVG

LCEKSYI+SN+HASIVDIFYFC+++K L EM KER+E S+IYRW+LHIQETL+

***Pf*p43 NTD** LCEKSYIISNKHASIVDIFYFCAIHKLLDEMAVKERIEFSYIYRWYLHIQETLLA

b

Figure12:The transmembrane domain predicted by Bour et al. (2016) in p43 versus the Pvp43 NTD structure. (a) The predicted transmembrane domain as per Bour et al. (2016) is highlighted in the P. falciparum and P. vivax sequences (orange box). (b) The crystal structure of Pvp43 NTD (PDB entry 5zke) reveals the protein core/buried nature of the predicted transmembrane domain (in orange) within the GST fold. This therefore suggests that p43 is likely to be a soluble protein.

Discussion and conclusion

A previous study has suggested that Pfp43, termed tRIP (tRNA-import protein), is a membrane-anchored protein with an N-terminal GST-like domain and a C-terminal tRNAbinding domain along with a predicted transmembrane domain such that tRIP directs the import of exogenous tRNAs (62). This membrane association of Pfp43 was established by Bour et al. (2016) using detergent (Triton X-100)-based extraction of membrane proteins from blood stages of P. falciparum. However, our crystal structures of Pvp43 NTD and CTD show that these are soluble proteins that contain GST-like and tRNA-binding modules, respectively. Further, the transmembrane motif (residues 121- RHASIVDIFYFCSVYKPLS-139) predicted by Bour et al. (2016) is in fact fully buried within the GST fold of Pvp43 NTD and residues 123–139 form an -helix in the protein core (Figs. 12a and 12b). Therefore, the crystal structure of Pvp43 NTD makes it unlikely that the transmembrane motif predicted by Bour and coworkers is a structural feature that will allow membrane association. It is feasible, however, that Plasmodium p43s may associate with membranes via binding to authentic membrane proteins. Therefore, further experiments are required to assess alternative modes of membrane association, if any, for the Plasmodium p43 proteins. Size-exclusion chromatography and crystal structures reveal a dimeric assembly of Pvp43 NTD (Figs. 7b and 10b). This is unique when compared with the known canonical GST assembly (Fig. 10b). This special feature of Pvp43 NTD as a dimer is consistent in the structures determined here from different crystal forms. Size-exclusion chromatography of the full-length Pvp43 protein suggests the formation of a tetrameric assembly. We made several attempts to crystallize the full-length Pvp43 protein but were unsuccessful. However, based on analyses of the data at hand, we propose a tetrameric assembly for Pvp43 possibly via a linker (residues 181–240). This work therefore provides a platform for further analysis of p43 and its orthologs in the

context of their roles in the assembly of multi-protein MARS complexes in eukaryotes, especially in apicomplexans (53).

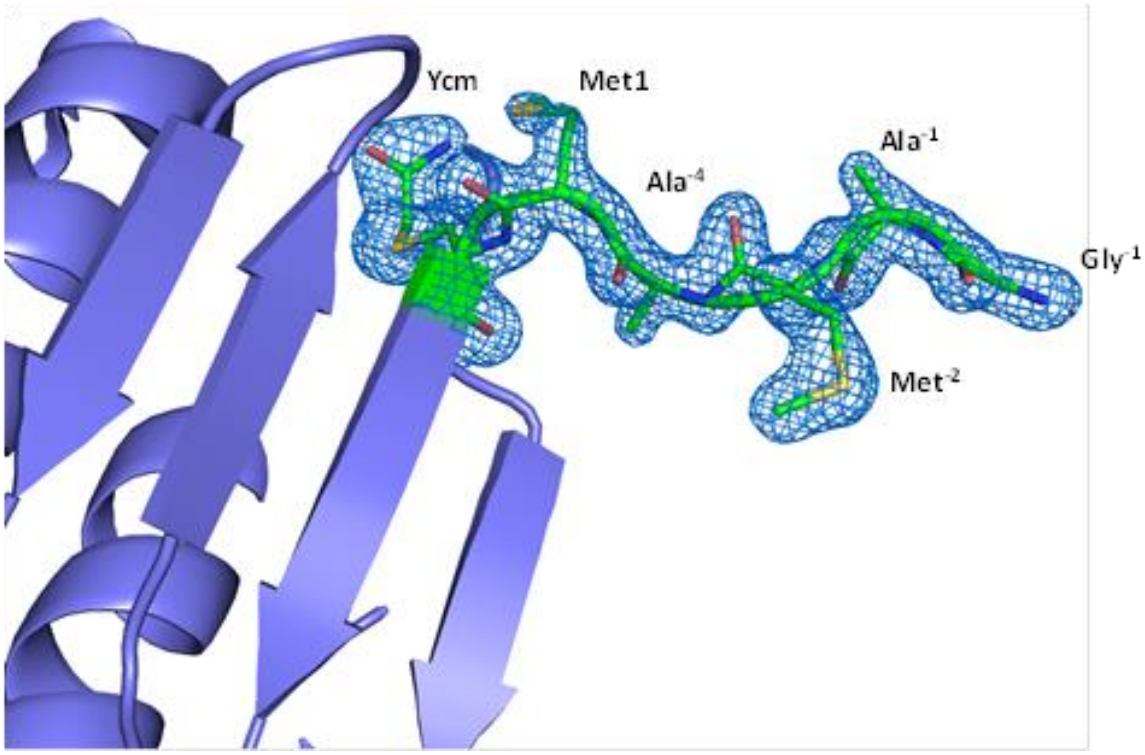

Figure 13:The ordered linker residues (GAMA) between the 6X-His tag and the Pvp43 NTD (orthorhombic form, PDB ID: 5ZKE_B). The final $2F_o$-F_c map was contoured at 1.0 σ level. The N-terminal tag residues are: MKHHHHHHPMSDYDIPTTENLYFEGAMA-Pvp43 NTD.

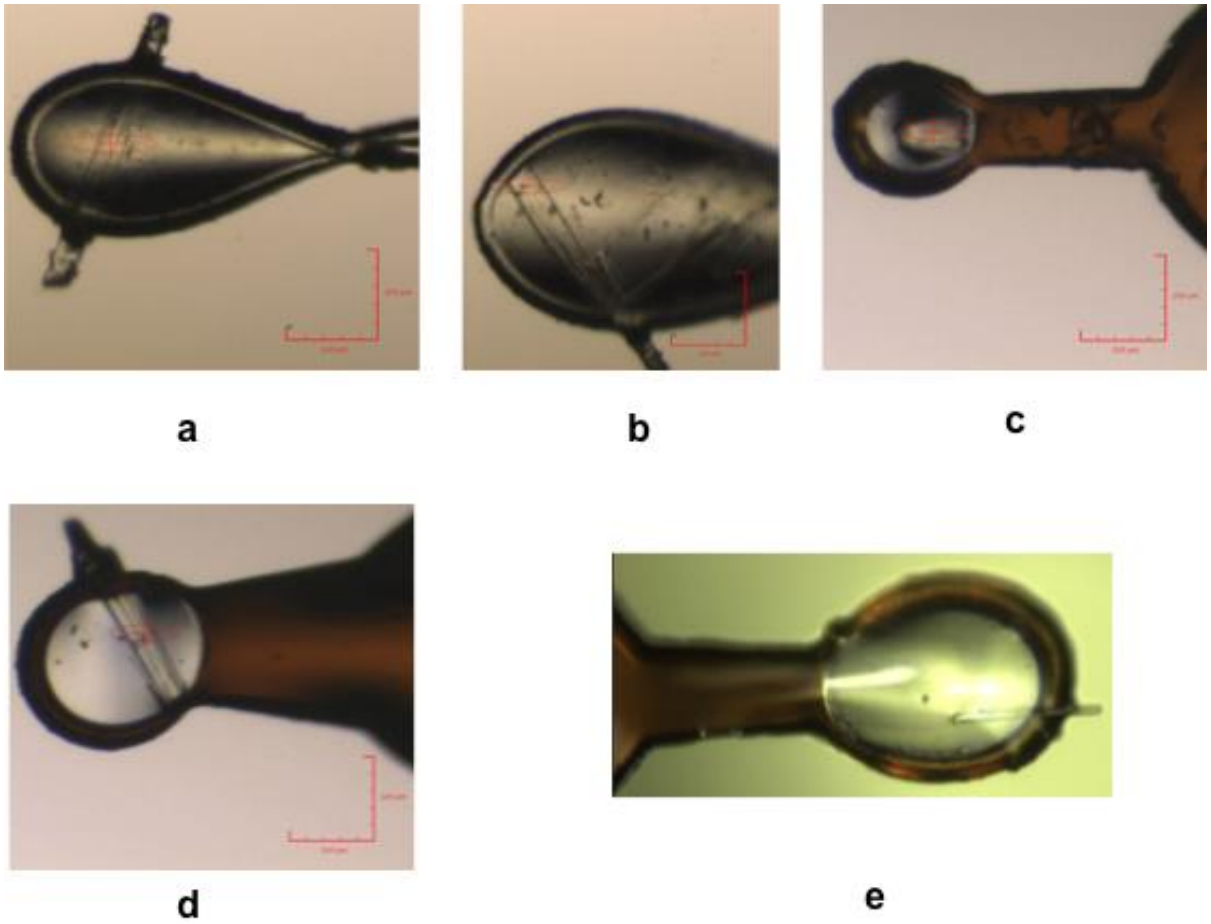

Figure 14- The beam shape x is marked as red elliptical circle and beam size (μm) is marked at lower right and values of the beam size is listed in Table 2. (a) Crystal obtained for full-length *Pv*p43 was cryo-soaked in 200 mM $CoCl_2$ salt for 30 s (Form 1 SG $P4_12_12$). (b) Native crystal of NTD of *Pv*p43 (Form 2 SG $P2_1$) and (c) NTD of *Pv*p43 in complex with GSH (Form 3 SG $P2_12_12_1$). (d) Form 1 (SG $P4_3$) and (e) Form 2 (SG $P2_12_12_1$) crystals of *Pv*p43 CTD.

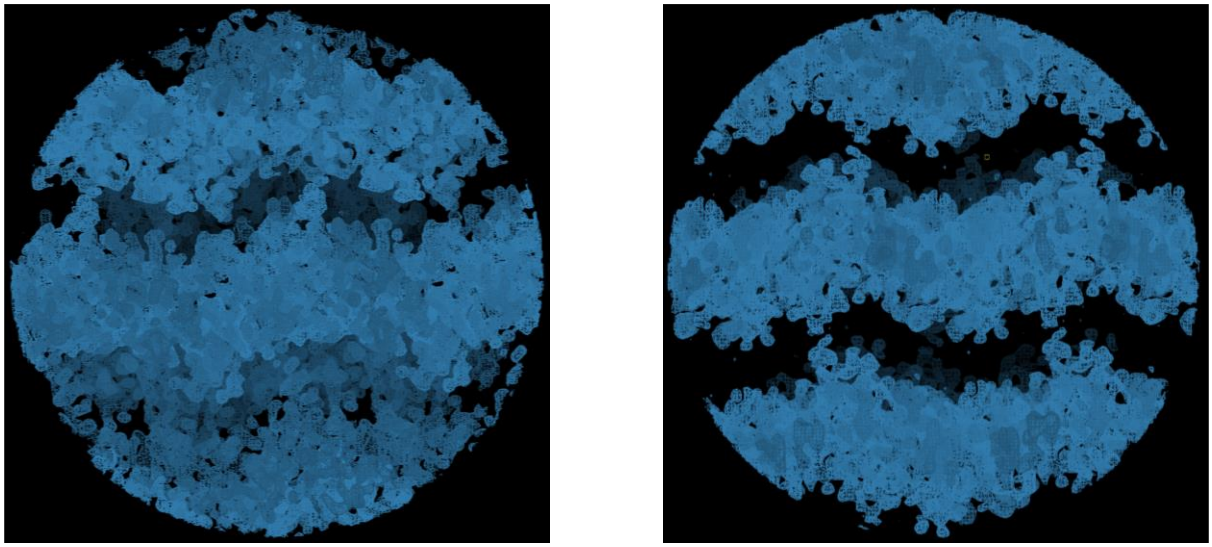

a b

Figure 15- Map contrast after phasing and density modification for (a) Co-SAD data set x10_3 and (b) merged Co-SAD data set. The map was contoured at 1 σ level.

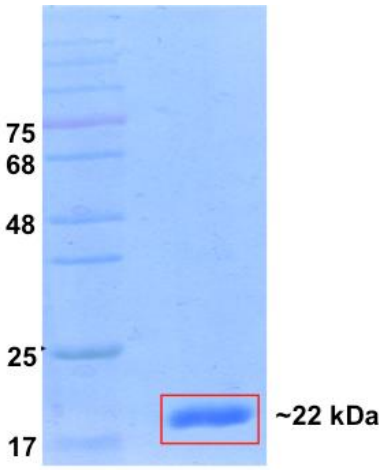

Figure 26- SDS PAGE analysis of the crystallized fragment size of *Pv*p43 full-length protein.

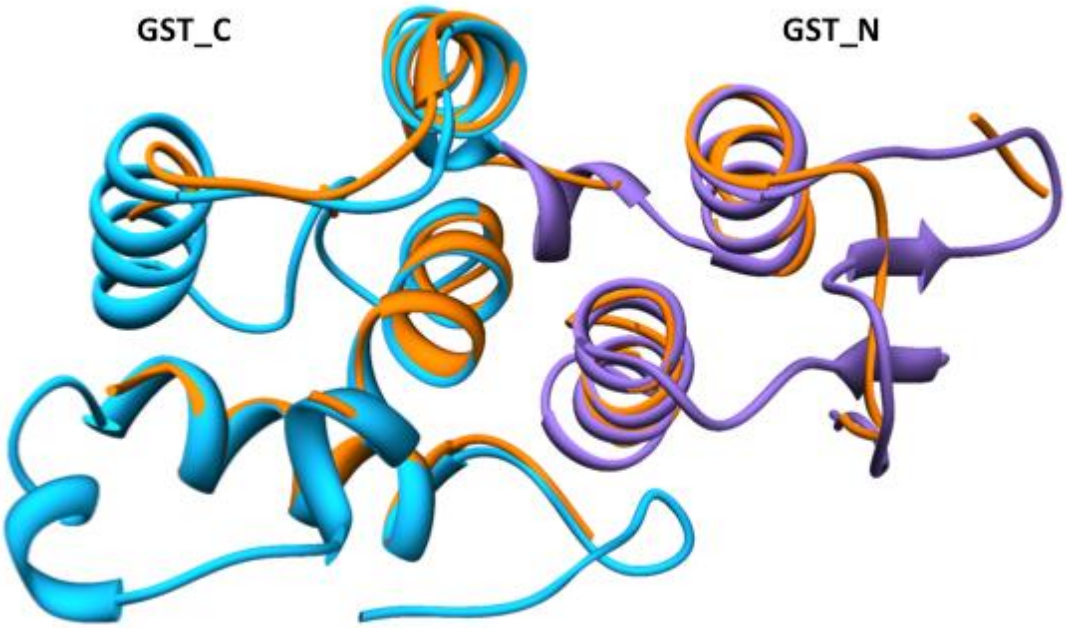

Figure 37-The partially built model (orange) from Co-SAD data was overlapped with the final refined model of *Pv*p43 NTD. The N-terminal thioredoxin fold (GST-N, purple) and C-terminal all α-helical domain (GST-C, blue) are labeled.

Table 3a- Summary of anomalous data collection and anomalous signal analysis[##]

Data Set[##]	Co-x3_2	Co-x3_4	Co-x5_2	Co-x7_2
Beam line	DLS I02	DLS I02	DLS I02	DLS I02
Wavelength (λ) (Å)	1.59	1.59	1.59	1.59
Detector type	DECTRIS PILATUS 6MF	DECTRIS PILATUS 6MF	DECTRIS PILATUS 6MF	DECTRIS PILATUS 6MF
Crystal-to-detector distance (mm)	625	625	625	625
Oscillation (°)	0.1	0.1	0.1	0.1
Exposure (s)	0.050	0.050	0.050	0.050
Beam size (μm) (elliptical)	100 x 20	100 x 20	100 x 20	100 x 20
Flux (photons s^{-1})	1.16×10^{11}	1.16×10^{11}	1.16×10^{11}	1.16×10^{11}
Transmission (%)	4.94	4.94	4.94	4.94
Number of images	7200	7200	7200	9900
Cell dimensions *a*, *b*, *c* (Å)	86.99, 86.99, 53.29	86.93, 86.93. 53.34	86.72, 86.72. 53.24	86.81, 86.81. 53.48
Space group	$P4_12_12$	$P4_12_12$	$P4_12_12$	$P4_12_12$
Resolution (Å)	86.99-2.67 (2.72-2.67)	61.47-2.71 (2.76-2.71)	61.32-3.11 (3.16-3.11)	61.39-2.75 (2.80-2.75)
R_{meas} (%)	0.111 (4.468)	0.110 (3.625)	0.266 (3.004)	0.134 (3.404)
$\langle I/\sigma(I)\rangle$	19.2 (1.0)	20.8 (1.1)	10.3 (0.7)	20.4 (1.3)
Completeness (%)	96.0 (71.1)	96.9 (73.3)	100.0 (96.2)	92.2 (47.9)
Average redundancy	44.4 (27.3)	44.9 (29.6)	42.1 (20.5)	65.4 (63.8)
$CC_{1/2}$	1.0 (0.5)	1.0 (0.5)	1.0 (0.2)	1.0 (0.6)
Number of observations	263434 (5778)	257492 (6327)	166795 (3661)	343056 (8670)
Number of unique reflections	5929 (212)	5734 (214)	3963 (179)	5245 (136)
$[\Delta F/\sigma(\Delta F)]$	1.22	1.30	1.01	1.25
$(\langle\Delta F\rangle/\langle F\rangle)$	0.065	0.067	0.131	0.065

Practical resolution limit of anomalous signal (Å)	4.9	4.6	8.4	4.9

Table 3b- Summary of anomalous data collection and anomalous signal analysis[#]

Data Set[#]	Co-x7_4	Co-x9_2	Co-x10_3	Co-x10_6
Beam line	DLS I02	DLS I02	DLS I02	DLS I02
Wavelength (λ) (Å)	1.59	1.59	1.59	1.59
Detector type	DECTRIS PILATUS 6MF	DECTRIS PILATUS 6MF	DECTRIS PILATUS 6MF	DECTRIS PILATUS 6MF
Crystal-to-detector distance (mm)	625	625	625	625
Oscillation (°)	0.1	0.1	0.1	0.1
Exposure (s)	0.050	0.050	0.050	0.050
Beam size (μm) (elliptical)	100 x 20	100 x 20	100 x 20	100 x 20
Flux (photons s^{-1})	1.12×10^{11}	9.62×10^{10}	6.54×10^{10}	5.57×10^{10}
Transmission (%)	4.94	4.94	3.0	3.0
Number of images	9900	7200	9900	9900
Cell dimensions *a*, *b*, *c* (Å)	87.00, 87.00. 53.29	86.66, 86.66. 53.33	87.40, 87.40. 53.41	86.97, 86.97. 53.283
Space group	$P4_12_12$	$P4_12_12$	$P4_12_12$	$P4_22_12$
Resolution (Å)	61.52-2.67 (2.72-2.67)	86.66-2.75 (2.80-2.75)	61.80-2.59 (2.63-2.59)	61.50-2.81 (2.86-2.810
R_{meas} (%)	0.122 (3.883)	0.188 (3.039)	0.081 (3.353)	0.092 (2.885)
$\langle I/\sigma(I) \rangle$	23.9 (1.5)	14.6 (0.7)	27.1 (1.2)	22.7 (1.1)
Completeness (%)	88.9 (42.9)	100.0 (100.0)	95.8 (71.8)	100.0 (98.8)
Average redundancy	65.3 (61.4)	44.3 (23.4)	58.1 (28.3)	63.3 (43.3)
$CC_{1/2}$	1.0 (0.6)	1.0 (0.5)	1.0 (0.7)	1.0 (0.9)
Number of observations	359633 (7803)	251067 (6671)	379840 (6850)	338184 (10387)
Number of unique reflections	5504 (127)	5664 (285)	6539 (242)	5338 (240)
$[\Delta F/\sigma(\Delta F)]$	1.38	1.22	1.71	1.29

(⟨ΔF⟩/⟨F⟩)	0.056	0.118	0.062	0.052
Practical resolution limit of anomalous signal (Å)	4.5	5.4	4.0	4.5

[#] Several Co-SAD data sets were collected using ten different crystals (x1-x10) and multiple datasets were collected for each crystal at a different spots. The statistics of the selected data sets with (ΔF)/σ(ΔF) >1.0 were listed Supplementary Tables S1a and S1b.

[##] In the data set name, x1 to x10 refer the crystal number and the number after the underscore refer to the number of the dataset that was collected on a particular crystal at different spots.

Table 3c- Statistics of merged Co-SAD data set and anomalous signal analysis

Data Set	Merged data[#]
Beam line	DLS I02
Wavelength (λ) (Å)	1.59
Detector type	DECTRIS PILATUS 6MF
Crystal-to-detector distance (mm)	625
Oscillation (°)	0.1
Exposure (s)	0.050
Beam size (μm) (elliptical)	100 x 20
Flux (photons s^{-1})	1.12×10^{11}
Number of images	44100
Cell dimensions *a*, *b*, *c* (Å)	86.99, 86.99. 53.35
Space group	$P4_12_12$
Resolution (Å)	61.51-2.67 (2.72-2.67)
R_{meas} (%)	0.107 (2.193)
$\langle I/\sigma(I)\rangle$	40.8 (1.1)
Completeness (%)	97.1 (77.9)
Average redundancy	136.0 (19.7)
$CC_{1/2}$	1.0 (0.6)
Number of observations	1521516 (8672)
Number of unique reflections	11188 (441)
$[\Delta F/\sigma(\Delta F)]$	2.01
$(\langle\Delta F\rangle/\langle F\rangle)$	0.043
Practical resolution limit of anomalous signal (Å)	3.7

The merged five different data sets are: x3_2, x3_4, x7_2, x10_3 and x10_6

Table 4-Results of DALI search for *Pv*p43 CTD (residues 241-405) against PDB25 (a subset of Protein Data Bank).

The structure was specified by concatenating string of the PDB identifier (4 characters) and a chain identifier (1 character). The match list is sorted by Z-scores (Z-scores between 8 and 20 means the two are probably homologous). The other listed parameters in the Table S3 are: root-mean-square deviation (RMSD) of C^{α} atoms in superimposition; Lali (number of structurally equivalent positions; and N_{res} - length of the structural neighbor and %id - percentage amino acid identity in aligned positions.

No	PDB_Chain	Z-Score	RMSD	Lali	N_{res}	%	Description
1	1NTG_A	26.5	1.3	162	171	38	Tyrosyl-Trna Synthetase
2	4R1J_A	25.5	1.4	162	174	31	Gu4 Nucleic-Binding Protein 1
3	5H34_B	14.0	1.7	103	112	36	Methionine-Trna Ligase
4	2Q2H_A	12.1	2.3	104	118	23	Secretion Chaperone, Phage-Display Derived
5	3PCO_B	9.7	3.0	102	795	28	Phenylalanyl-Trna Synthetase, Alpha Subunit
6	3BU2_A	9.3	3.4	96	195	28	Putative Trna-Binding Protein

Table 5-Results of DALI search for *Pv*p43 NTD (residues 1-180) against PDB25 (a subset of Protein Data Bank).

The structure was specified by concatenating string of the PDB identifier (4 characters) and a chain identifier (1 character). The match list is sorted by Z-scores (Z-scores between 8 and 20 means the two are probably homologous). The other listed parameters in Table S3 are: root mean square deviation (RMSD) of C^{α} atoms in superimposition; Lali (number of structurally equivalent positions); N_{res} - length of the structural neighbor and %id - percentage amino acid identity in aligned positions.

No.	PDB_Chain	Z-score	RMSD	Lali	N_{res}	% id	Description
1	5A34_C	15.0	2.6	153	170	17	Bifunctional Glutamate/Proline-tRNA Ligase
2	3MDK_B	14.9	2.7	159	206	10	Stringent Starvation Protein A
3	1NHY_A	14.8	2.4	158	219	13	Elongation Factor 1-Gamma 1
4	4ZB7_A	14.8	2.7	152	171	12	Pcure2p6
5	3VK9_B	14.7	2.7	156	213	13	Glutathione S-Transferase Delta
6	5G5A_A	14.6	2.8	157	219	13	Glutathione S-Transferase U25
7	5Y6L_B	14.5	3.2	150	173	14	Methionine--Trna Ligase, Cytoplasmic
8	5NR1_A	14.3	2.5	156	226	10	Ftsz-Binding Protein Fzla
9	4KDU_A	14.0	2.7	155	207	12	Glutathione S-Transferase Domain
10	4GLT_A	13.9	2.6	153	208	8	Glutathione S-Transferase-Like Protein
11	5FT3_B	13.7	2.7	154	221	16	Glutathione S-Transferase Epsilon 2
12	4O92_A	13.7	2.8	147	196	12	Glutathione S-Transferase
13	5U51_C	13.6	2.5	151	195	11	Stringent Starvation Protein A
14	4MPG_B	13.6	2.6	156	252	12	Glutathione S-Transferase Theta-2
15	4XT0_A	13.5	2.3	152	243	14	Protein Ligf
16	6F70_A	13.4	2.6	157	242	12	Glutathione Transferase
17	1OYJ_C	13.4	2.8	157	227	11	Glutathione S-Transferase

18	3RBT_D	13.2	2.6	155	242	14	Glutathione Transferase O1
19	5O84_A	13.1	2.9	153	216	14	Glutathione S-Transferase U23
20	4MDC_B	13.0	2.7	153	233	11	Putative Glutathione S-Transferase
21	4IW9_B	13.0	2.8	159	215	12	Glutathione Transferase
22	3M8N_D	12.9	2.7	149	222	12	Possible Glutathione S-Transferase
23	4AGS_A	12.9	2.9	157	445	8	Thiol-Dependent Reductase 1
24	4EXJ_B	12.9	2.9	153	222	17	Uncharacterized Protein
25	3LXT_D	12.3	3.2	152	205	7	Glutathione S Transferase
26	4JBB_A	12.3	2.5	145	208	10	Putative Glutathione S-Transferase
27	3LG6_A	12.3	2.7	152	229	11	Putative Glutathione Transferase
28	3LXZ_A	12.2	3.2	153	218	10	Glutathione S-Transferase Family Protein
29	5UUN_A	12.1	2.9	161	286	10	Glutathione S-Transferase-Like Protein
30	4BVY_A	12.1	2.6	144	211	10	Methionine--Trna Ligase, Cytoplasmic
31	2YCD_A	12.0	2.6	147	213	13	Glutathione S-Transferase
32	2HQT_J	11.9	2.5	98	121	19	Gu4 Nucleic-Binding Protein 1
33	2HRA_A	11.8	2.9	144	180	9	Glutamyl-Trna Synthetase, Cytoplasmic
34	4KF9_A	11.7	2.6	151	318	10	Glutathione S-Transferase Protein
35	4G10_A	11.7	2.9	154	263	7	Glutathione S-Transferase Homolog
36	4AI6_A	11.7	3.1	150	2650	13	Glutathione S-Transferase Class-Mu 26 Kda Isozyme
37	2WB9_A	11.5	2.8	147	211	12	Glutathione Transferase Sigma Class
38	5LKD_A	11.4	3.0	160	352	9	Glutathione S-Transferase Omega-Like 2
39	4PTS_B	11.3	3.1	158	333	11	Glutathione S-Transferase
40	5A5H_D	11.3	3.3	151	213	7	Bifunctional Glutamate/Proline--Trna Ligase

41	5XFT_A	11.1	2.7	142	215	8	Dehydroascorbate Reductase
42	3H1N_B	11.0	3.4	154	242	11	Probable Glutathione S-Transferase
43	5U51_A	10.7	2.9	142	203	13	Stringent Starvation Protein A
44	4W66_A	10.7	3.0	153	236	8	Glutathione S-Transferase Domain Protein
45	2D2Z_B	10.6	2.9	145	240	12	Chloride Intracellular Channel Protein 4
46	1Z9H_A	10.2	2.8	145	274	10	Membrane-Associated Prostaglandin E Synthase-2
47	4LMV_A	10.0	3.0	148	252	9	Glutathione Transferase
48	2YV9_A	10.0	3.1	154	285	11	Chloride Intracellular Channel Exc-4
49	2FNO_A	9.9	3.5	153	239	6	Agr_Pat_752p
50	3IR4_A	9.2	3.5	141	218	11	Glutaredoxin 2

Chapter-3

Functional and biological characterization of *Plasmodium vivax* p43 protein

Introduction

As evident from the functional point of view, human AIMP1 (ARS-interacting multifunctional protein 1) was primarily stated as a supporting factor in the multisynthetase (ARS) complex consisting of 9 (Glu, Ile, Met, Pro, Leu, Arg, Gln, Asp, and Lys) diverse tRNA synthetases and 2 other auxiliary non-enzyme proteins-AIMP2 and 3 (70). The higher eukaryotes exhibit a substantious categorization of amino acid and tRNA association through the emergence of the multisynathetase complex (MSC). The MSC complex of the eukaryote nematode-*Caenorhabditis elegans* consists of eight of the nine synthetases (7 are common with human) (134).

Lower eukaryotes on the other hand involve a smaller constitution comprising of methyl tRNA synthetase (MRS) and glutamyl tRNA synthetase (ERS) together with the cofactor protein ARC1p which is a counterpart of mammalian AIMP1(56). ARC1p, by virtue of binding to $tRNA^{Glu}$ and $tRNA^{Met}$ surges the local concentration of tRNA for their respective synthetases. ARC1p also involves in maintenance of telomeres, regulation of transcription and ribosomal biogenesis (135). The GST-like domains of the three proteins are involved to form this complex (59).

The mammalian AIMP1 lacks the GST-like domain of ARC1p, though the AIMP3 of 18kDa constitutes a GST-like domain interacting with methionyl (MRS) (136) and glutamyl-prolyl tRNA synthetase (EPRS) (96). Since the AIMP1 binds to both the EPRS and AIMP2 and also to AIMP3 by lieu of its entire tertiary structure ; all the three subordinate non-synthetase proteins

form the central anchoring structure for the nine synthetases in the multisynthetase complex (70). The MSCs outlined from eukaryotes and archaea improve the early translation proficiency, stability of proteins, event synchronization during elongation , tRNA synthesis and its transfer to ribosome (52).

The *Plasmodium* p43 or tRNA import protein (tRIP) hence also might interact with aminoacyl tRNA synthetases in the parasite in a way similar to yeast ARC1p, *Toxoplasma gondii* p43 (53) or human AIMP1 (62). We have reviewed here the complex specific as well as the non-canonical functions of these non-synthetase complex interacting proteins in all the genera and have tried to speculate the biological functions of *Plasmodium* p43 on the basis of our experimental and bioinfomatic characterization.

aaRS complex interacting multifunctional proteins (AIMPs) and their roles in complex formation

In 1990, Quevillion et al found out the sequences of the three non-enzymatic structural subordinate proteins from the CHO cell library (137, 138).

AIMP3/p18 is sturdily affixed to methionyl-tRNA synthetase (MRS) which assigns methionine (Met) to initiator tRNA ($tRNAi^{Met}$). Hence MRS has a major role in initiation of translation. AIMP3 recruits eIF2γ to the MRS–AIMP3 complex. The level of Met-tRNAi Met which is bound to eIF2 complex was also reduced by knocking down of AIMP3. This resulted in diminished translation thus elucidating AIMP3 as a critical player for effective protein synthesis (139). The third subordinate factor p18 shares homology with the N terminal domain of human Valyl tRNA synthetase (VRS) which mediates complex formation with EF-1H (66, 138). The EF-1A also binds to lysyl tRNA synthetase (KRS) thus providing a capable means to transport tRNAs from the multisynthetase complex to ribosomes for efficient protein synthesis (140).

The p38/AIMP2 auxiliary protein has no homologue in archaea, bacteria and yeast. The non-synthetase scaffold protein p38 also mediates protein protein interactions. It harbors a leucine zipper motif. Precisely, p38 dimerizes upon itself and also interacts with p43, class I synthetases-arginyl (RRS) and glutaminyl tRNA synthetases (QRS), class II ones-aspartyl (DRS) and lysyl tRNA synthetases (KRS) and also with the glu-pro (EPRS) (136). The interconnection between the association in the mammalian MSC is elucidated by the static that binding of glutaminyl tRNA sythetase (QRS) to p38 is boosted in the company of arginyl tRNA synthetase as well as p43. This proves that a quaternary complex facilitates the foundation of the multisynthetase complex (52). AIMP1 binds and facilitates the catalytic reaction of arginyl tRNA synthetase also (141). Arginyl tRNA synthetase (RRS) of higher eukaryotes has an extended N terminal domain which promotes translation and cell growth and anchorage into the multisynthetase complex. The crystal structure of the glutaminyl (QRS), arginyl (RRS) and the auxiliary protein AIMP1 displays characteristic features of the MSC. Here the N terminal portion of RRS forms a coiled coil architecture with the N terminal helical domain of AIMP1 and also anchors the C terminal domain of the QRS thus constituting the assemblage of the MSC (142). As per the previous research, the MSC components are divided into 2 subdomains basing on their alliance with AIMP2. One of them consists of RRS, QRS and AIMP1 (p43) which is connected to the N terminus of AIMP2. Another one includes DRS, MRS, KRS and AIMP3.This subdomain is associated with the C terminal GST domain of AIMP2 (143). The knockdown of p38 in cell culture released KRS and DRS from the MSC. Henceforth, the MSC was overall divided into two stable complexes – complex I consisted of EPRS, LRS, IRS, MRS, LRS and p18 whereas subcomplex II constituted p43, QRS and RRS. Knockdown of p18 released MRS and that of p43 resulted in an MSC deprived of RRS and QRS (144). 4 aminoacyl tRNA synthetases consisting of the GST domains- MRS-AIMP3-EPRS-AIMP2 constitute the core of the complex by their protein protein interactions (96). These four together with DRS, LRS and IRS constitute the

subcomplex I whereas AIMP1, QRS and RRS with KRS dimer and AIMP2 form the subcomplex II (145). Thus p38/AIMP2 conclusively forms the core structural protein for mediating protein protein interactions with AIMP1 and other synthetases like DRS, RRS, QRS and KRS (137).

AIMP1 thus conclusively binds to GST-like domains of EPRS and AIMP3 and also interacts with AIMP2, thus behaving as a docking site for tRNA and GST-like domain harboring proteins of the multisynthetase complex (70).

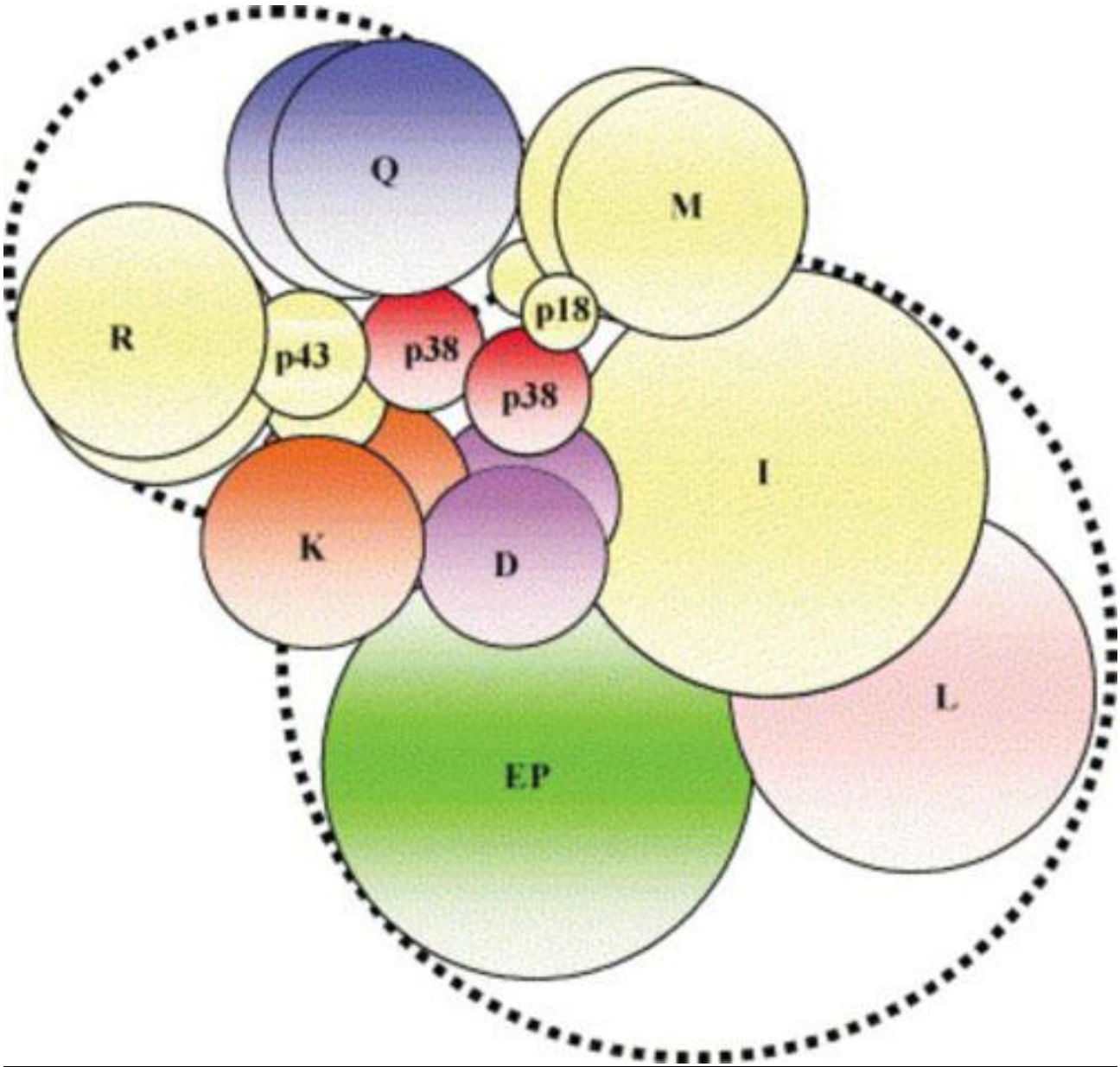

Figure 18- Proposed two-dimensional architecture of the multi synthetase complex in higher eukaryotes (Adapted from Liang et al) (137)

Non canonical functions of AIMPs

AIMP2

As far the non-canonical functions are concerned, the p38/AIMP2 also binds to the FUSE-binding protein (c-myc activator), thus ubiquitinylating it and hence promoting the downregulation of c-myc. P38 also undergoes ubiquitinylation by associating with Parkin (146, 147). FBP1 is a transcriptional regulator of the proto-oncogene c-myc. C- myc is a regulator of cell proliferation, apoptosis and differentiation. FBP1 binds to the central domain of AIMP2 via its C terminal portion. Invivo studies have proved that when AIMP2 is knocked down, the level of FBP1 and hence expression of c-myc rise in fetal lungs. This in turn leads to defects in lung differentiation and respiratory distress syndrome (148). AIMP2 is also involved in the cell fate decision of proliferation vs apoptosis by virtue of signaling pathways which involve p53, FBP1 and TNF-receptor associated factor 2 (TRAF 2) (94).

AIMP1

The C terminal portion of the auxiliary protein p43/AIMP1 houses an endothelial monocyte activating polypeptide II (EMAP-II) like domain that displays tRNA binding (56, 149). This domain shares homology with the ARC1p protein of yeast which aids the association of tRNA to glutamyl and methionyl tRNA synthetases (150). Following its cleavage from the full length p43, it gets involved in mediating endothelial functions as proinflammatory cytokine (52).

The non-canonical functions of mammalian AIMP1 (p43) entail several extracellular functions on various targets. AIMP1 also allows for fractional homology with a few inflammatory cytokines as RANTES (regulated on activation, normal T cell expressed and presumably secreted) as well as MCP-1 (monocyte chemotactic protein-1) and also acts like a cytokine on monocytes, fibroblasts and endothelial cells. CD23 also acts as receptor of AIMP1 and promotes cell migration and TNFα secretion by it (151). It also performs alike a glucagon-like hormone

(141). In native state, p43 might function for channeling of tRNA but after processing in the tumorigenic cells, it imbibes inflammatory properties akin to programmed cell death (149). The p43 also exists in the endoplasmic reticulum holding back the heat-shock protein (hsp) gp96 thus preventing its extracellular exposure which might activate autoimmune reactions (141). Hence the retention of gp96 in endoplasmic reticulum is attributed to its interaction with the central region of mammalian AIMP1 (151). AIMP1 by virtue of is C terminal region also inhibits ubiquitylation of Smurf2 which negatively regulates the TGF-β signaling. Hence, p43 indirectly governs the TGF-β dependent cell growth (152). The secretory form also acts upon endothelial cells, immune cells, fibroblasts etc. The pancreatic α cells also contain the p43 which is secreted into the bloodstream in hypoglycemic condition to maintain the blood sugar level (153).

Many neurologic disorders like pontocerebellar hypoplasias (PCH) and leukodystrophies arise due to pathogenic variants of synthetase genes. Also loss of function mutations (nonsense vaiant and bi-allelic frameshift) in AIMP1 has been linked to hypomyelinating leukodystrophy-3 (MIM 260600)(154). This results in hypomyelination, progressive microcephaly, cerebral atrophy, early neurodegeneration as well as epilepsy (155–157). On the other hand missense variants cause intellectual disability either with or without neurodegeneration(158).

AIMP1 is secreted from a variety of cells like immune cells and prostate cancer cells. It thereby acts upon macrophages/monocytes, fibroblasts and endothelial cells and also activates proinflammatory cytokines like TNF-α, interleukin (IL-8), macrophage chemotactic protein-1 (MCP-1), IL-1b, macrophage inflammatory protein-1a (MIP-1a). AIMP1 also controls angiogenesis and helps for the proliferation of fibroblasts (159).

AIMP3

AIMP3 also plays role in tumorigenesis and aging. AIMP3/p18 controls cellular ageing through ubiquitylation of lamin A and its degradation through E3 ubiquitin ligase Siah1 (160). Also, the AIMP3 binds strongly to MRS. In the MSC, MRS and AIMP3 also interact with the GTPase domain of eukaryotic initiation factor 2γ (eIF2γ) via their GST domains (139). The AIMP3/p18 also triggers the ataxia telangiectasia mutated (ATM) and ATR (ATM and Rad3-related) protein kinases. This in turn promotes the increase of p53 to combat DNA damage (161).

The AIMPS are also expressed in the Schwann cells in case of injured peripheral nerves. The levels of AIMPs decrease during nerve regeneration. Hence another non-canonical function of AIMPS is to act as the morphological intracellular indicator of degenerating peripheral nerves (162).

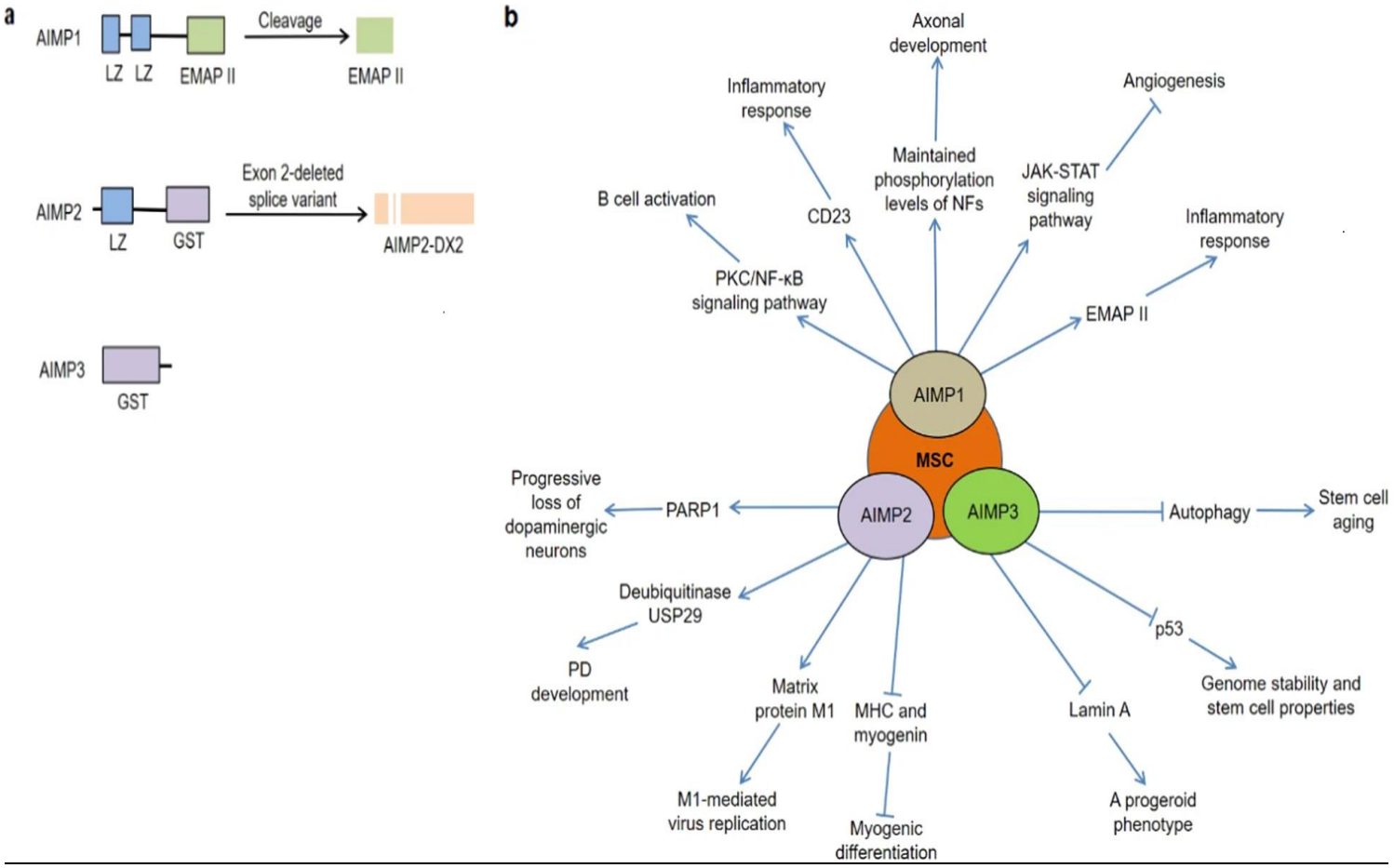

Figure 19-Domain structures and biological non-canonical functions of AIMPs; a. Key domains of AIMPs, b. Different biological functions of AIMP. (Adapted from Zhou et al)(163)

Material and methods

Thermal shift assay with metal ions and reduced glutathione- GSH

*Pv*p43 was diluted in the thermal shift assay buffer (50 mM Tris pH 8, 200 mM NaCl, 5% glycerol, 5mM β-Me) at a final concentration of 2 µM. SYPRO orange dye (Life Technologies, 470/570 nm, 5000X) from Invitrogen was used at a final concentration of 2X for binding the protein. Different metals ligands (2mM of copper, cesium, cadmium, barium, magnesium, manganese, calcium chloride) and reduced glutathione-GSH in varying concentrations from 1 to 20 mM were added to the protein in TSA buffer and incubated at room temperature for ten mins. Then, samples were heated from 25 to 99 C at a rate of 1°C min-1 and fluorescence signals monitored by StepOnePlus quantitative real-time PCR system (Life technologies). Each curve was an average of three measurements and data were analyzed using thermal shift software from Applied biosystems. Assay buffers along with dye only and no protein were used as controls where flat lines were observed for these fluorescence readings at all temperatures. Boltzmann Tm (melting temperature) and derivative Tm were found to have similar values and latter was used for analysis.

Western blotting

Polyclonal antibodies were raised against highly purified recombinant Pvp43 in rabbits cand procured commercially. To check the expression and molecular size of native p43, parasites in asynchronous cultures were released from infected RBCs by 0.05 % w/v saponin lysis and pellets were washed in phosphate buffered saline (PBS). Parasites were lysed by three rounds of freeze-thawing in RIPA buffer (Sigma) that contained protease inhibitors cocktail. Lysates were

centrifuged and supernatants were separated on SDS-PAGE. Proteins were then transferred to PVDF membrane (Bio-Rad) and blots were probed using specific primary antibodies (1:10000) and secondary horseradish peroxide (HRP) conjugated antibodies (1:300000 dilutions). Bands were visualized using an ECL-femto detection kit (Pierce). The recombinant protein was also checked for expression using primary antibodies (1:1000) and secondary horseradish peroxide (HRP) conjugated antibodies (1:5000 dilutions). Western blots were developed with colorimetric substrate DAB. The antibody recognizes the full-length protein also with the N terminal protein.

Immunofluorescence assay

Immunofluorescence assay (IFA) was performed as described earlier (164). Cells were washed in PBS and fixed in solution using 4 % w/v paraformaldehyde and 0.0075 % w/v glutaraldehyde in PBS for 25 min. After a PBS wash, cells were permeabilized by using 0.1 % v/v Triton X-100 in PBS for 10 min. After another PBS wash, cells were treated with 0.1 mg ml-1 sodium borohydride in PBS for 10 min. Cells were washed again with PBS, blocked in 4 % w/v BSA in PBS for 1 h and incubated overnight with purified rabbit anti-protein IgG antibody (1:200 dilution) at 4°C. Cells were then washed three times with PBS for 10 min each and incubated with Alexa Flour 488 tagged anti-rabbit secondary antibody (Life technologies) and Alexa Flour 594 tagged anti-rabbit secondary antibody (Life technologies) for 1 h at room temperature, and cells were allowed to settle onto coverslips coated with poly-L-lysine (100 µg ml-1). Finally, the coverslips were washed three times in PBS, mounted in antifade with DAPI reagent (Life technologies) and sealed. Confocal microscopy was performed on a Nikon A1R-A1 microscope. Pre-immune sera were taken as negative controls.

Glutathione-S-Transferase (GST) assay

Glutathione-S-transferases (GSTs) are enzymes which detoxify xenobiotics in mammals. The enzymes hence exert a protective effect on the cells by conjugation of the thiol group of glutathione to electrophilic xenobiotics. GST activity is also present in bacteria, insects, yeast, plants, and mammalian liver tissues. The Glutathione S-Transferase (GST) Assay Kit employs 1-Chloro-2,4-dinitrobenzene (CDNB). When the thiol group of the glutathione is conjygated to the cDNB substrate, the absorbance at 340 nm increases which is indicative of a cDNB conjugate.Upon conjugation of the thiol group of glutathione to the CDNB substrate, there is an increase in the absorbance at 340 nm. This assay kit measures the total GST activity in lysates, tissue homogenates, proteins etc. The GST assay was done with standardization in UV absorbant 96 well plates. Saturating concentration of GSH at 5mM and cDNB were added to PBS (substrate solution). GST enzyme was used as the positive control and substrate solution as the blank. Proteins were used upto 2uM. Readings were taken at A_{340} at 25 degrees upto 30 minutes at 30 secs intervals (linear reaction). Other synthetases and bovine serum albumin (BSA) were used as negative controls along with the test samples of Pvp43 full length, N terminal and C terminal proteins.

Multisynthetase complex in *Plasmodium* as speculated bioinformatically

We tried to speculate the interacting partners of p43 in the malaria parasite with the help of STRING software which could delineate its protein association networks. We ran it for the synthetases which were part of the MSC in Apicomplexan eukaryote like *Toxoplasma gondii* (53) eukaryotes along with p43. The partners delineated for p43 and those of the synthetases were cross checked for each other's partners by the software. The settings were customized to increase the stringency. The network association chosen in the software was restricted to physical interaction only which denoted that the proteins constitute a physical complex only rather than

being just functionally related. The minimum required interaction score was also fixed to 0.9 (0.7 for MRS) which indicated the highest confidence. Hence the top five hits were chosen as interacting partners for all the synthetase proteins including p43 with an interaction score ranging from 0.7 to 0.9.

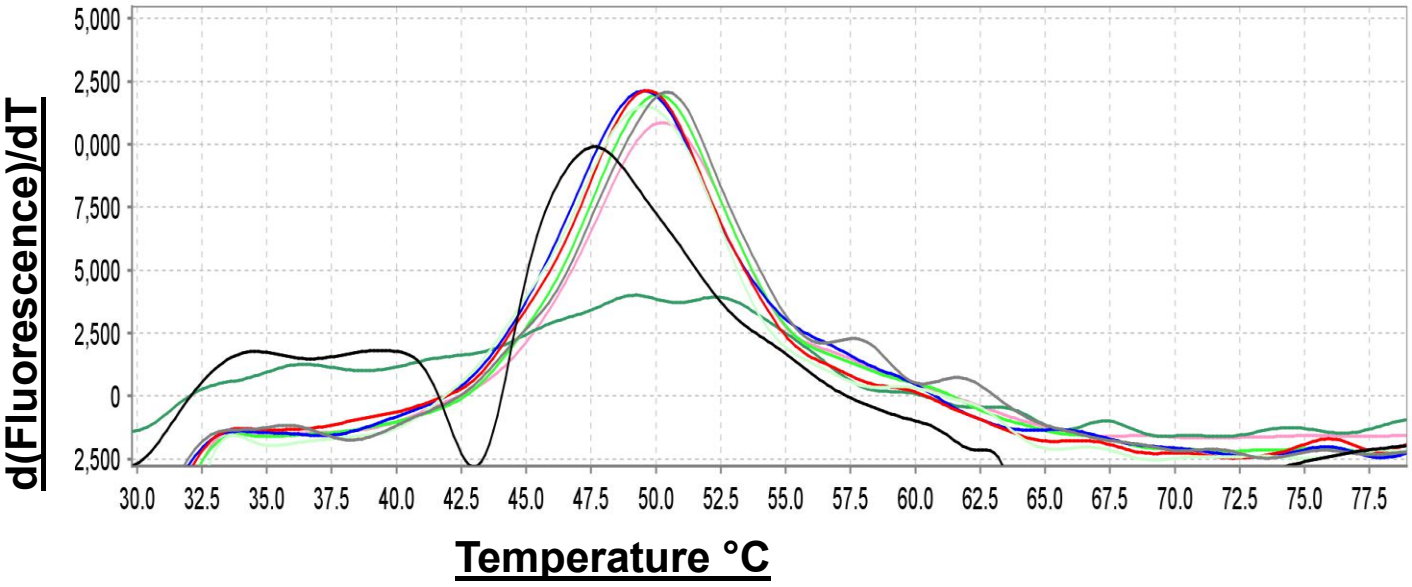

Sl No.	Metal ion	Tm°C	ΔTm (°C)
1.	Apo	50°C	_
2.	Copper chloride	46°C	-4°C
3.	Cesium chloride	50°C	No shift
4.	Barium chloride	50°C	No shift
5.	Cadmium chloride	50°C	No shift
6.	Manganese chloride	50°C	No shift
7.	Magnesium chloride	50°C	No shift
8.	Calcium chloride	50°C	No shift

Figure 20- Thermal shift assay (TSA) of Pvp43 with different metal ions

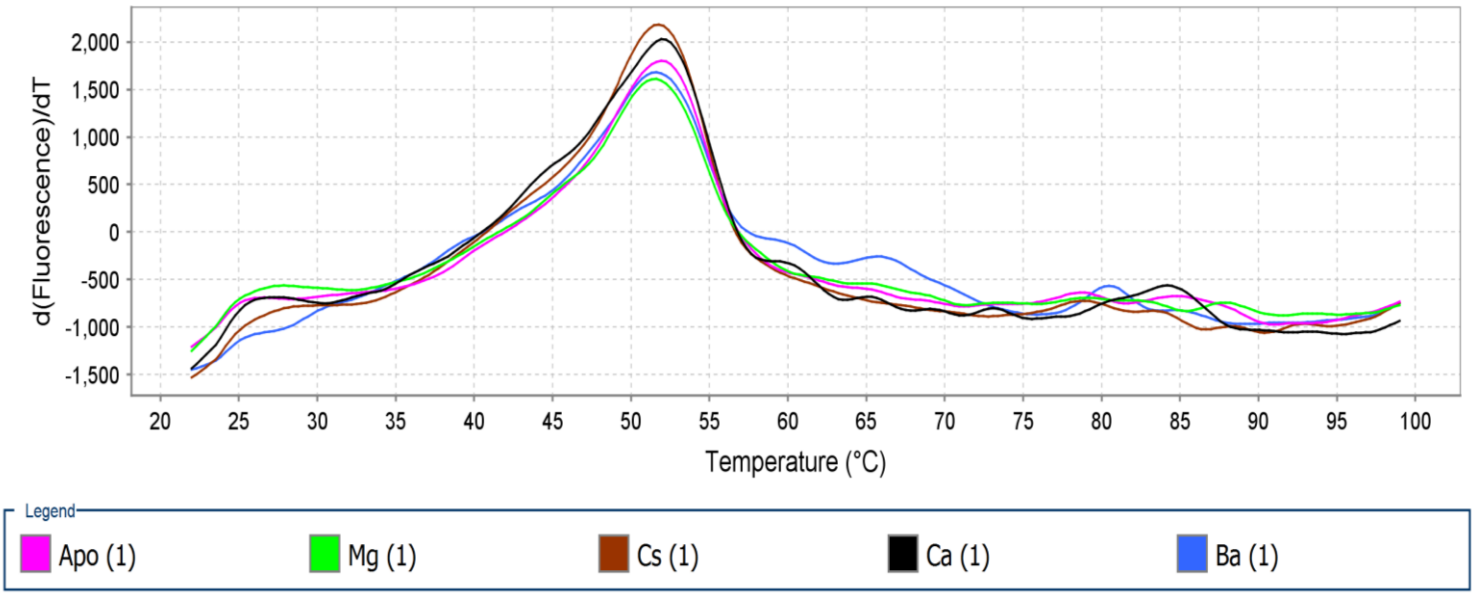

Sl No.	Metal ion	Tm°C	ΔTm (°C)
1.	Apo	51±0.3 °C	_
2.	Barium chloride	51±0.2 °C	No shift
3.	Calcium chloride	51±1 °C	1°C
4.	Cesium chloride	51±0.2 °C	No shift
5.	Magnesium chloride	51±0.3 °C	No shift

Figure 21- Thermal shift assay (TSA) of Pvp43 with different metal ions

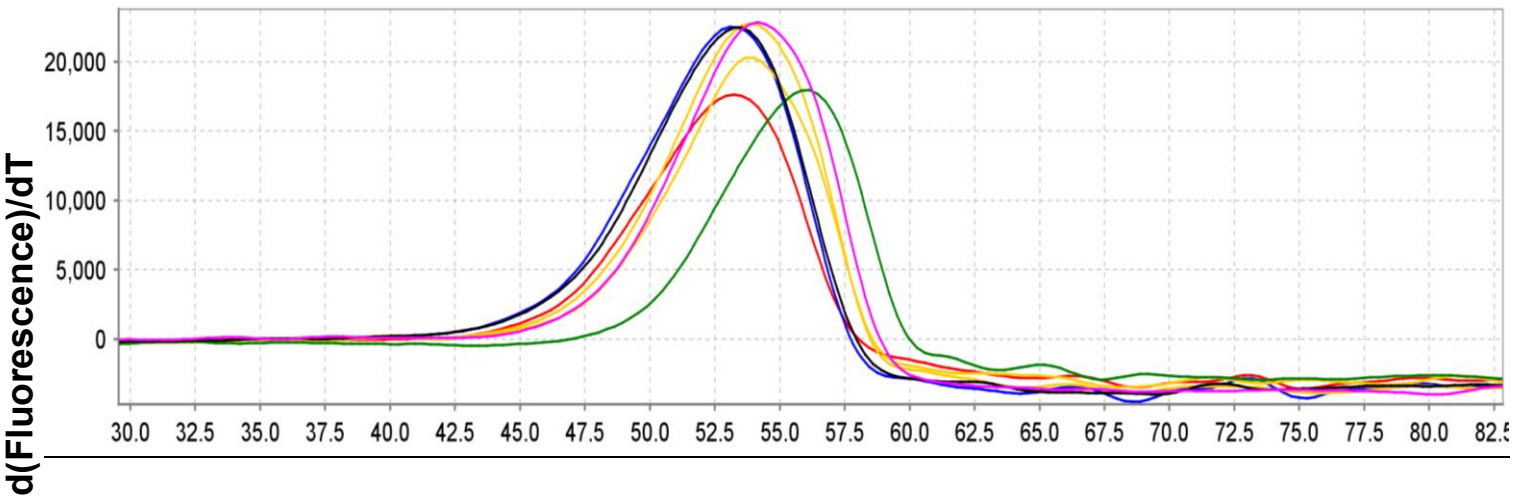

Sl No.	Substrate	Tm°C	ΔTm (°C)
1.	Apo	53.28±0.2 °C	_
2.	GSH 1 mM	53.39±0.3 °C	No shift
3.	GSH 2 mM	53.30±0.2 °C	No shift
4.	GSH 5 mM	53.85±0.2 °C	0.5 °C
5.	GSH 10 mM	54.15±0.2 °C	0.87 °C
6.	GSH 20 mM	55.99±0.2 °C	2.14 °C

Figure 22- Thermal shift assay (TSA) of *Pv*p43 with Glutathione Reductase (GSH)

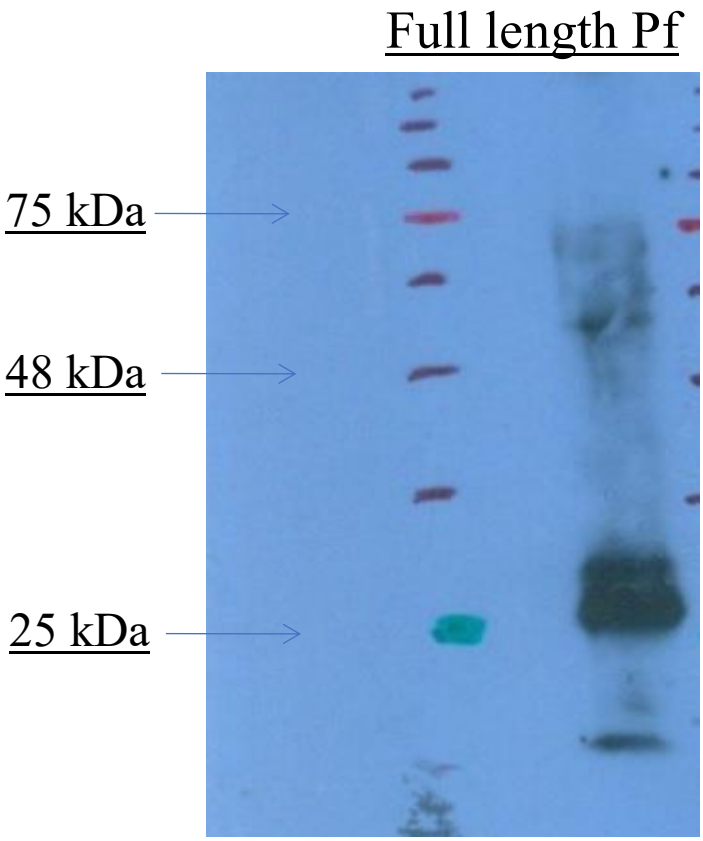

Figure 23-Western blot developed with ECL and imprinted on X ray film using full length antibodies in parasite lysate. There is signal around 48 kDa. There is also a degradation product around 25 kDa recognized by antibodies, which shows that the p43 also got processed invivo in the lysate. This could be either N or C terminal of the p43.

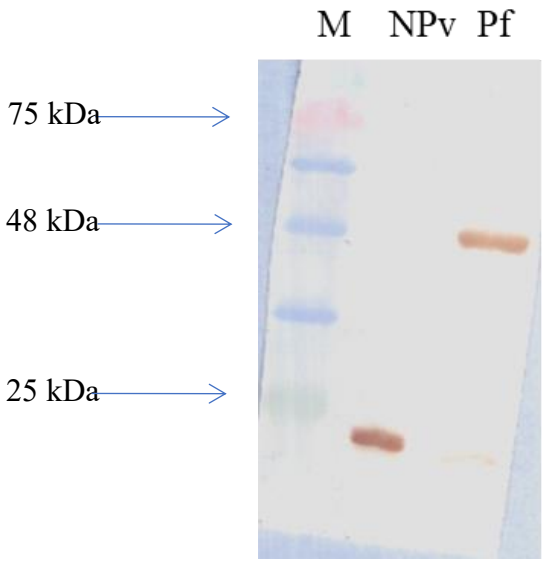

Figure 24-Western blots developed with colorimetric substrate DAB using N term antibodies in recombinantly purified proteins (N term *Pv*p43 and full length *Pv*p43). The antibody recognizes the full-length protein also with the N term protein.

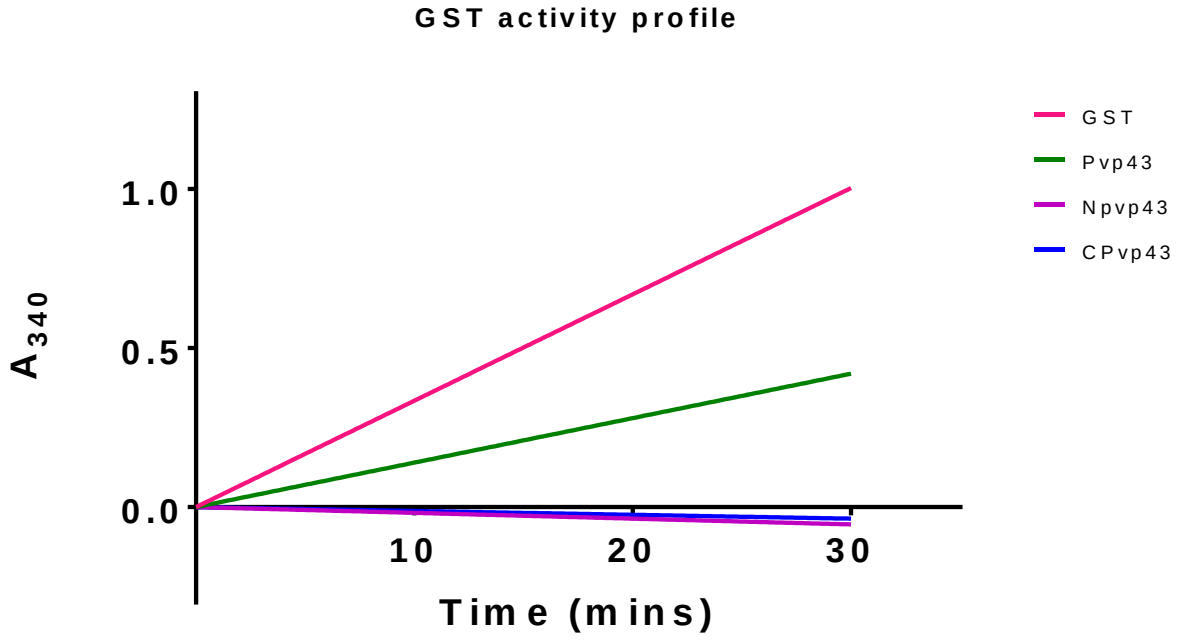

	GST		Pvp43		NPvp43		CPvp43
A340/min	**0.762192**		**0.325973**		**-0.00087**		**0.00115**
Sp.activity=µmol/ml/min	**359.5244**		**38.44025**		**-1.6478**		**0.021698**

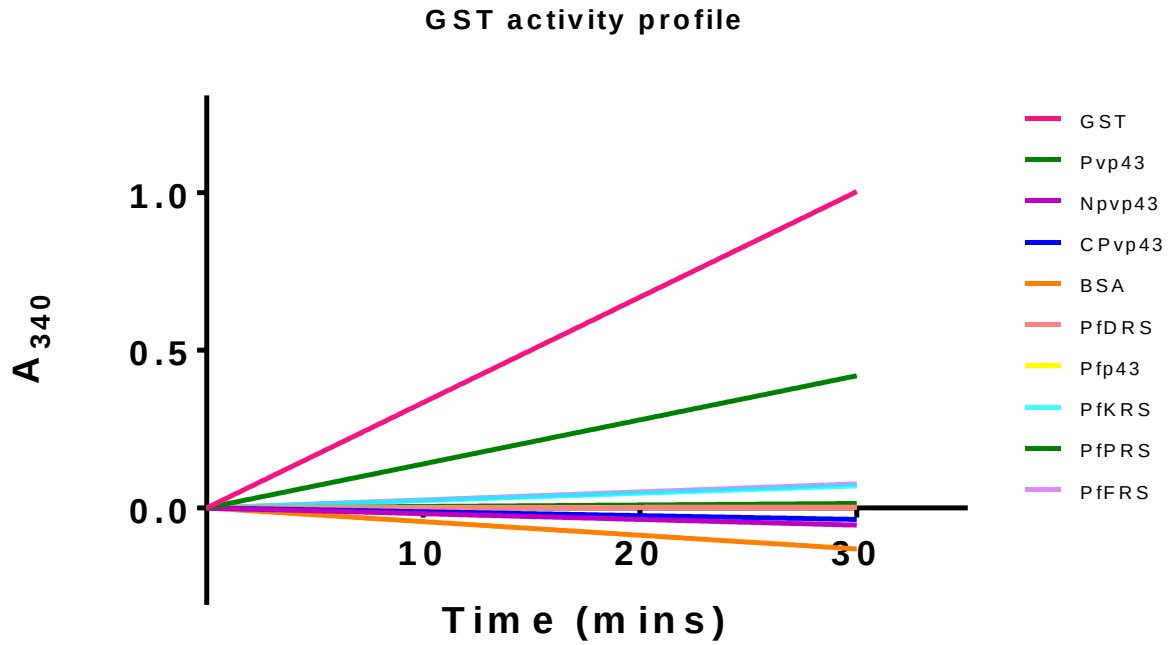

Figure 25- Readings were taken at A_{340} at 25 degrees upto 30 mins at 30 secs intervals. Only the full length p43 protein was active in conjugating cDNB with reduced GSH thus elucidating the GST activity retained in its N terminal GST-like domain. The BSA and rest of the synthetases were inactive for the GST activity. The p43 proteins are showed in a separate panel with their specific activities.

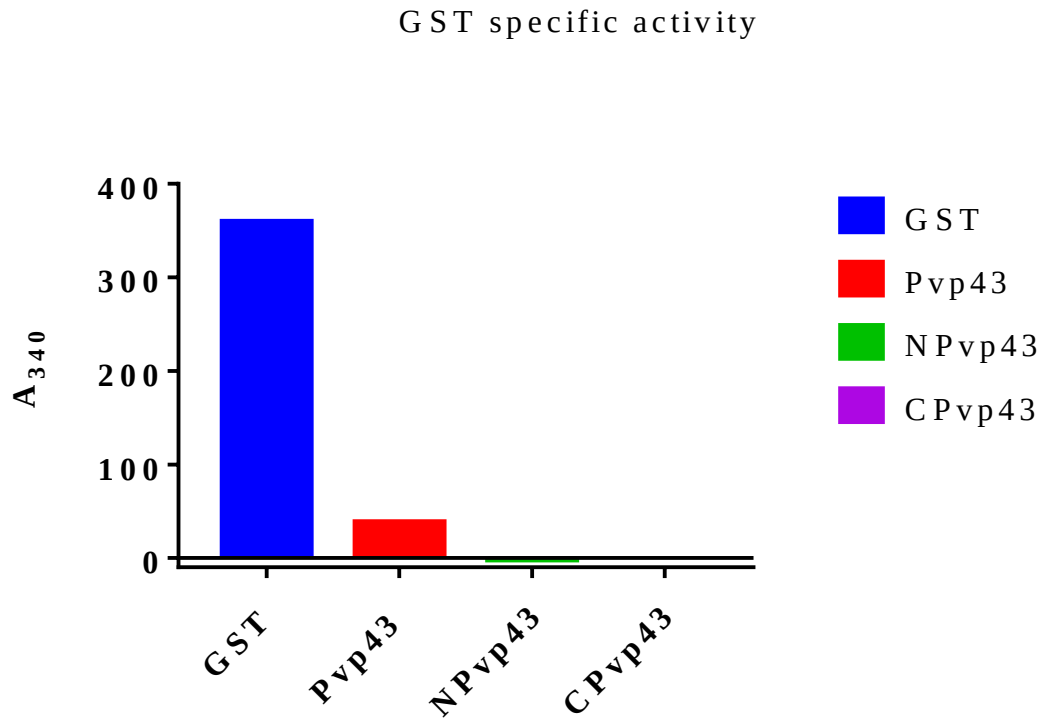

Figure 26- Only the full length p43 protein was active in conjugating cDNB with reduced GSH thus elucidating the GST activity retained in its N terminal GST-like domain. The specific activities of the p43 proteins are plotted. Though less as compared to the positive control of the GST enzyme, the full length *Pv*p43 was significantly active in forming the GS-cDNB conjugate as compared to the shorter constructs. This is evident from the plotted specific activities.

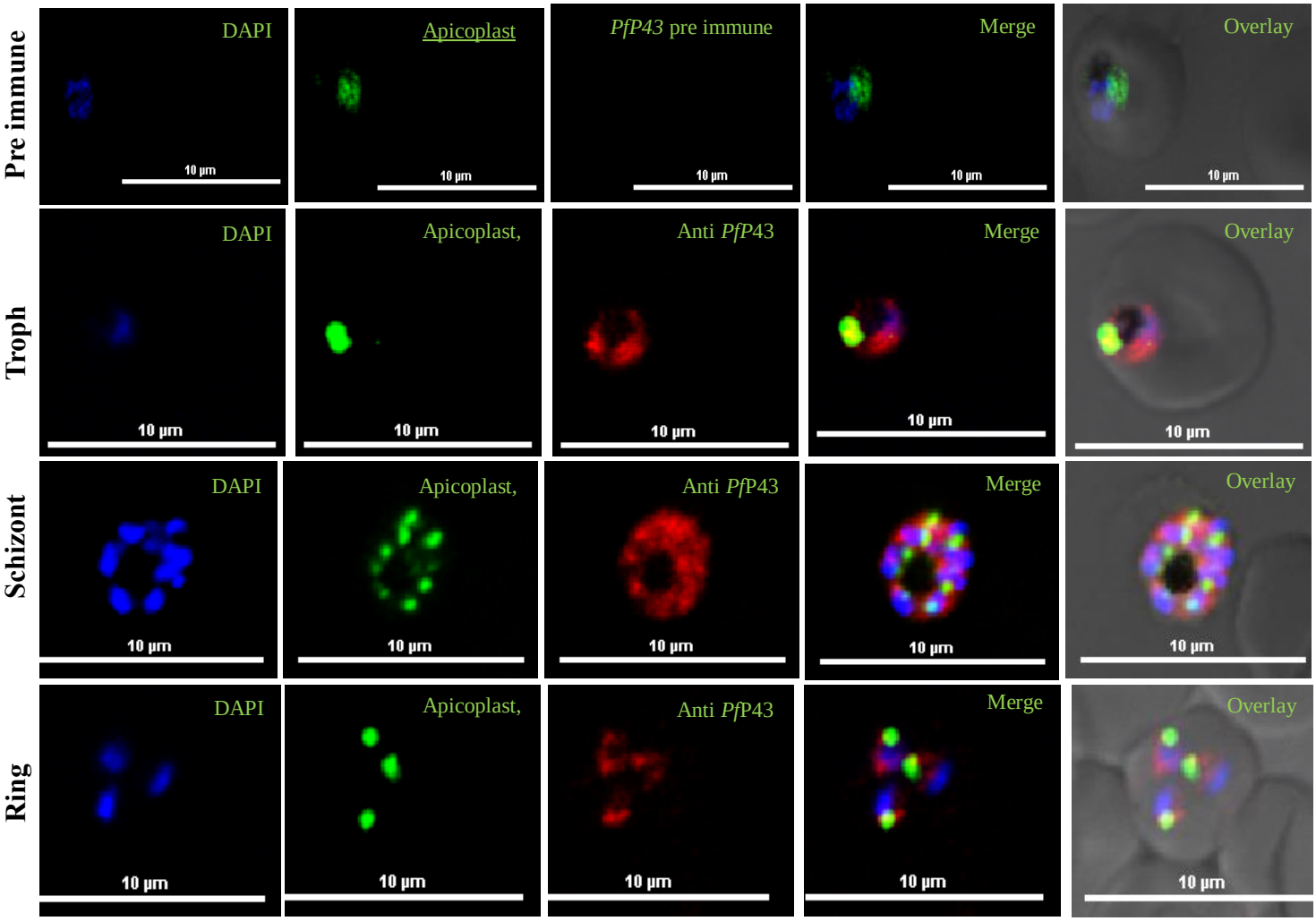

Figure 27- Confocal microscopy-data based spatial distribution of *Pf*p43 antibodies against *P. falciparum* (asexual stage D10-ACP line) in infected RBCs (trophozoites). Shown are DAPI staining of nucleus in blue , *Pf*p43 stained with Alexa 594 in red. The non-apicoplast , non-nuclear, cytoplasmic localization of *Pf*p43 is evident in *P.falciparum* where apicoplast is stained green (D10-ACP-GFP). There is also no background in the pre immune sera.

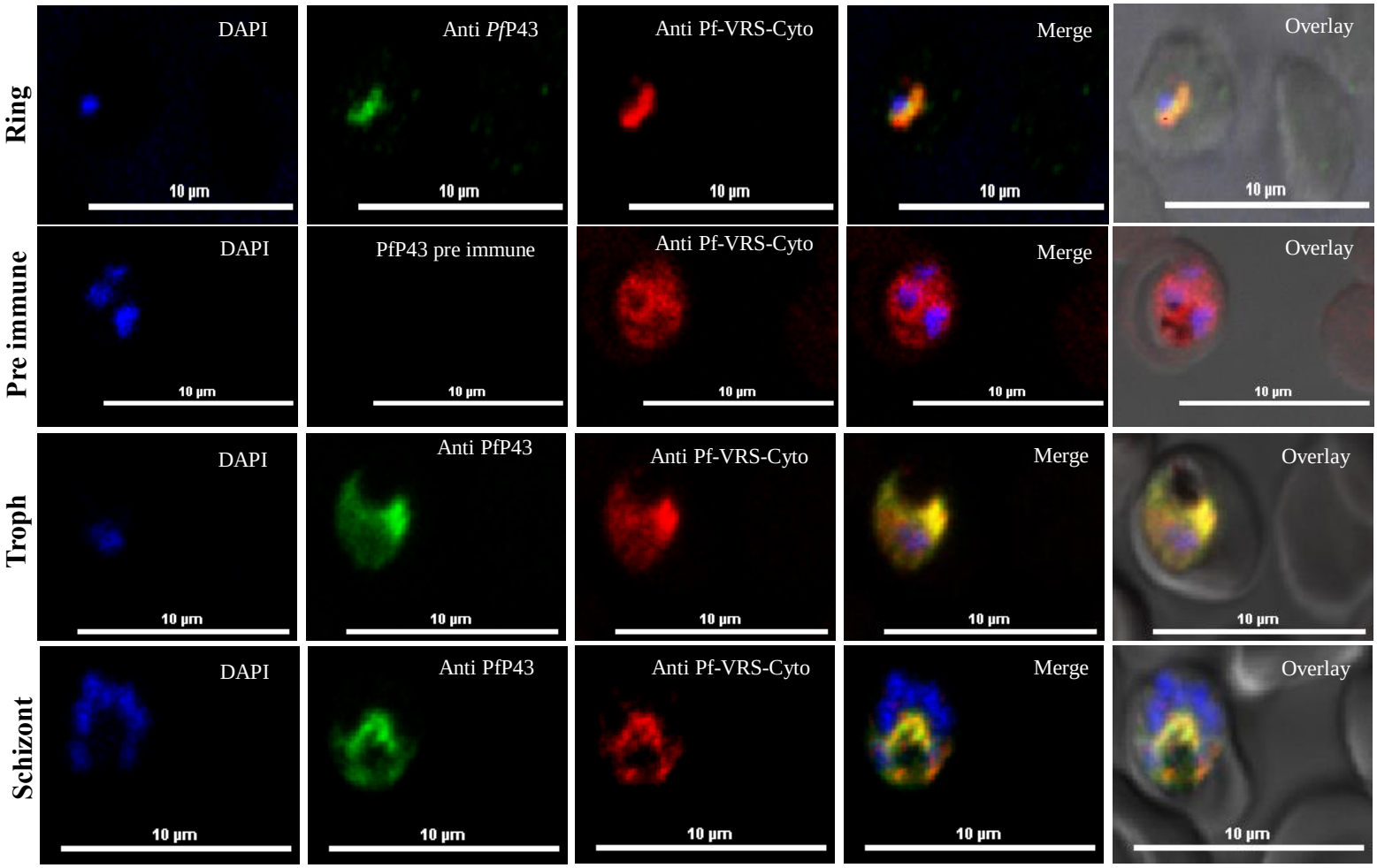

Figure 28-Confocal microscopy-data based spatial distribution of *Pf*P43 (asexual stage-3D7 line) in infected RBCs. Shown are DAPI staining of nucleus in blue, *Pf*P43 stained with Alexa 488 in green and *Pf*VRS stained with Alexa 594 in red. *Pf*P43 is non-nuclear in blood stages of the parasite and resides in its cytoplasm. Non-nuclear localization with control *Pf*VRS is also shown.

Table of protein-interactions: The major interactions of the p43 complex are marked red; the distant interactions are marked green

Proteins	Partner 1	Partner 2	Partner 3	Partner 4	Partner 5
P43	ERS	QRS	IRS (putative)	LRS (putative)	TRS (putative)
ERS	EF1 (uncharacterized)	MRS-β-subunit; tRNA binding protein, putative	IRS (putative)	LRS (uncharacterized)	PRS (putative) (uncharacterized)
QRS	MRS-β-subunit; tRNA binding protein, putative	IRS (putative)	PRS	LRS (uncharacterized)	ARS
YRS	MRS-β-subunit; tRNA binding protein, putative	CRS (putative)	IRS (putative)	TRS (putative)	ARS
MRS	QRS (putative)	LRS (uncharacterized)	TRS (putative)	ERS (putative)	

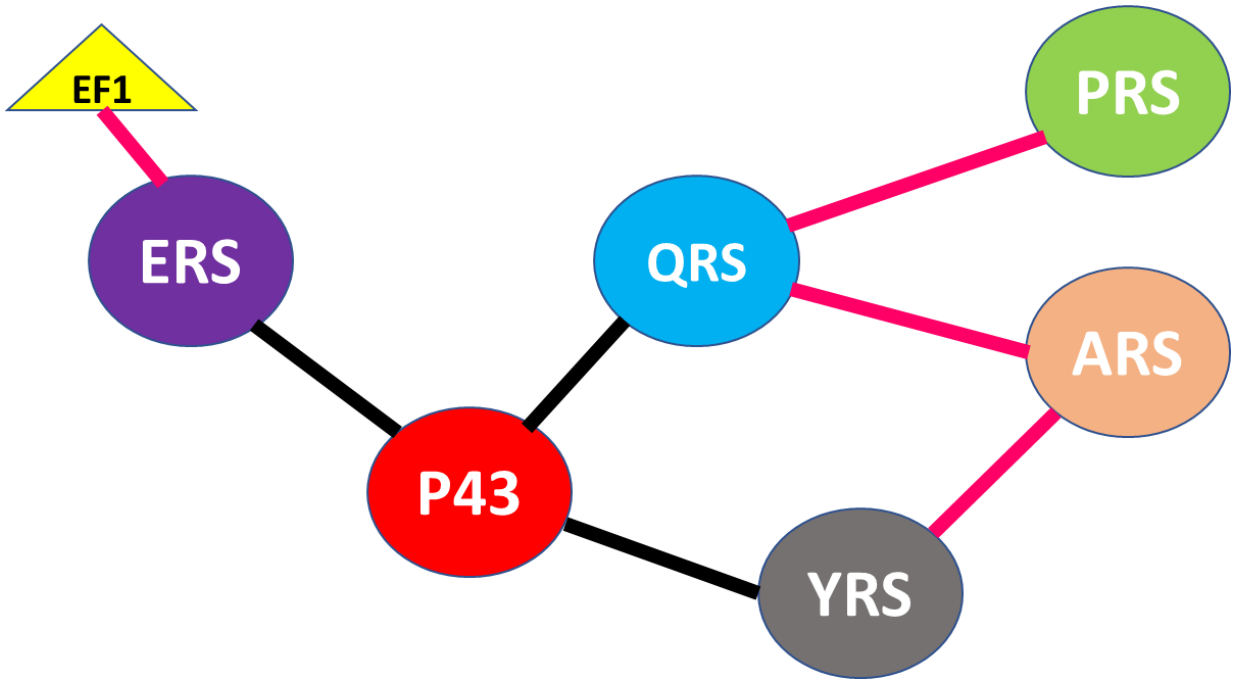

Figure 29- Predicted complex of Plasmodium p43- The black lines denote direct interactions of p43. The pink lines indicate individual interactions of the synthetases. ERS=glutamyl tRNA synthetase, EF1=elongation factor 1, QRS=glutaminyl tRNA synthetase, YRS=tyrosyl tRNA synthetase, ARS=alanyl and PRS=prolyl tRNA synthetase.

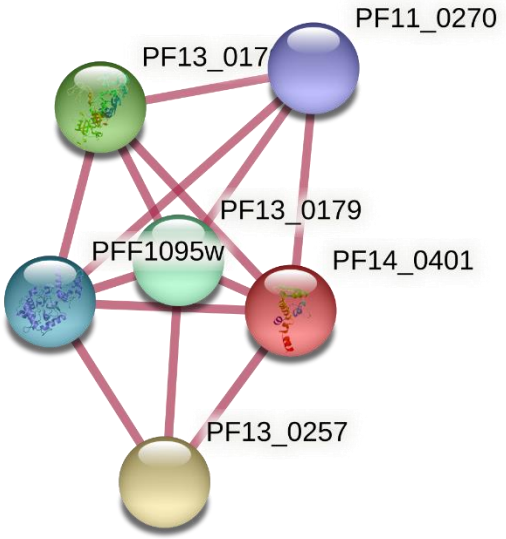

STRING interaction fig. of p43

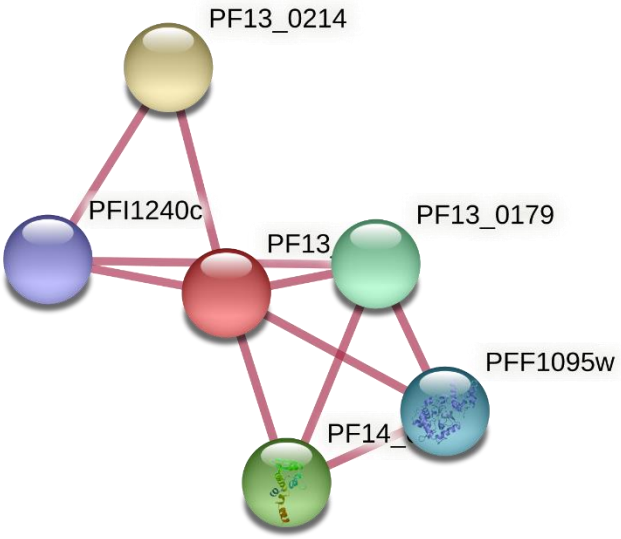

STRING interaction fig. of ERS

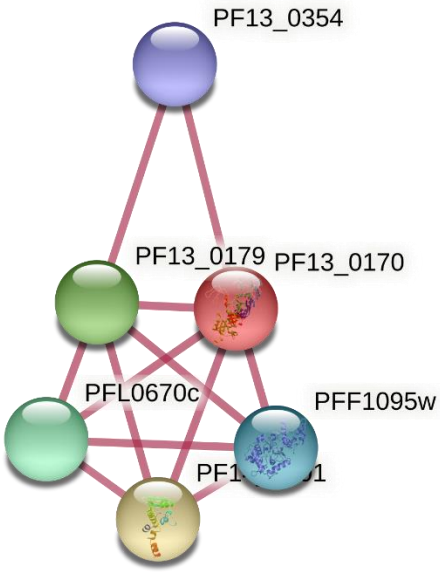

STRING interaction fig. of QRS

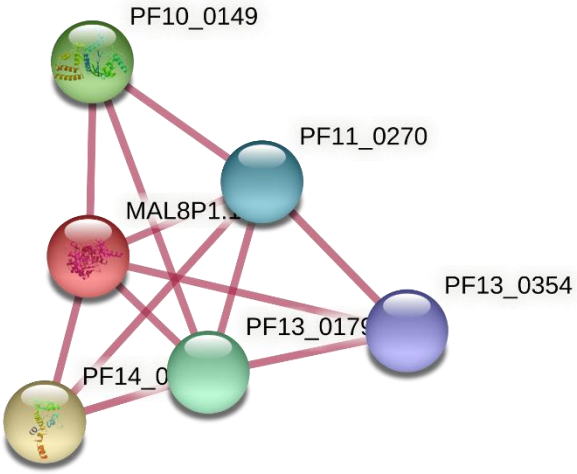

STRING interaction fig. of YRS

Figure 30- STRING interaction network of the proposed complex proteins (Adapted from STRING software (165)**)**

Results and discussion

We did the thermal shift assays with reduced glutathione (GSH) as well as metals to delineate any metal binding or GSH binding properties in p43. But we didn't find any significant shift either of these. Hence no metal binding properties and hence active sites could be deciphered for p43. Only with a very high concentration of GSH as 20 mM, we could have a 2-degree shift which was indicative of a mild form of interaction. GSH being a natural substrate didn't enforce a tight binding leading to strong conformational chnage. Hence the shift indicated little thermal stability only with a milder shift towards the right unlike any strong inhibitor that would cause a shift of atleast 5 degrees indicating enhanced thermal stability and thus major conformational change. This was at consensus with our GST assays where the full length *Pv*p43 was active towards conjugating GSH with cDNB displaying its minor GST activity due to the GST-like fold.

The western blotting against recombinant proteins as well as in lysates confirms the presence of p43. Since *Pv* and *Pf* p43 share almost 80 % identity among themselves and the whole native protein was used to raise antibody, the antibody recognises both the recombinant *Pv*p43 as well as the *Pf*p43 in the culture lysate. Since we experienced autodegradation of p43 during recombinant protein purification, we had to clone two separate domains keeping in view the lysine and asparagine rich linker region in between the N and C terminals. This linker region being disordered, looped and prone to degradation cleaved the protein into two even in the native state. This showed us a degradation product around 25 KDa in the western blot of *Pf* lysate.

The confocal studies of *Pf*p43 showing colocalization with cytosolic *Pf*VRS with a Pearson's correlation coefficient ranging between 0.7-0.9 also proved and supplemented the cytosolic localization of the p43 protein in the *Plasmodium* parasite.

Though it was already shown that the p43 or tRNA import protein is important for the parasite in importing exogenous tRNAs from the extracellular space or host into the parasite, the p43 protein was not essential for the survival of the *Plasmodium* parasite, though integrity of the asexual blood stage growth was compromised (62). The tRIP/p43 also had similar tRNA binding capacity in its C terminal domain like that of Trbp111, ARC1p and AIMP1 (62). The p43 protein has a constitutive expression throughout the sexual and asexual blood stages as well as mosquito stages of the parasite.

We speculated that the multisynthetase complex as delineated in the apicomplexan *Toxoplasma* should be similar to the complex of the apicomplexan *Plasmodium* too. The scaffold proteins p38 and p18 are also absent in the *Plasmodium*. The interactors of *Tg*-p43 included MRS, ERS, QRS and YRS. Hence after analyzing through the STRING software, we found out that- p43 had major interactions with ERS, YRS, QRS and vice versa. Also, the ERS was associated with the elongation factor 1 (EF1). QRS had interactions with PRS and ARS too. YRS, together with associating with p43 also was associated to ARS. Though few of the interactions in these analyses were putative/uncharacterized; keeping in view the high confidence score and literature-based data, we can project that the multisynthetase complex in *Plasmodium* too consists of ERS, QRS and YRS. The MRS-β-subunit; tRNA binding protein, (putative) is a homologue of p43 as delineated through DALI software in the previous chapter. Hence when we got MRS-β-subunit as a putative interactor of ERS/QRS and YRS, we hypothesized that being structurally related, it can be deciphered as none other than the scaffold protein p43. The distant functional interactions can include those of QRS with ARS and PRS and that of YRS too with ARS. The alpha helical GST-C terminal like domains of p43, QRS, YRS and ERS together might interact to contribute to the formation of the multisynthetase complex like that in *Toxoplasma*. Since p43 is not essential for the survival of the parasite as already mentioned, we provide an insight to develop inhibitors which could target these interactions. Any inhibitor like that could hence

prove to be multi-targetting. The hindrance of these interactions could devastate the translational machinery as well as any other non-canonical functions as well thus proving detrimental to the parasite.

Summary

Plasmodium parasites are single celled organisms that are the root cause malaria and resultant morbidity in stricken regions around the world. Although most terrible of human malaria parasites is *P. falciparum*, its variant *P. vivax* is also common in India, South East Asia and Latin America. On global scale, malaria is a grave health concern despite synchronized and active efforts. Amongst the five human malarial species of *Plasmodia*, *P. falciparum* is accountable for maximum ill health and demises.

Due to the present status of evolving resistance to existing anti-malarials, there is a crucial need for the progress of new therapeutic agents and, finding potential drug targets. Over the past few years, several laboratories are fervent regarding the malarial translational apparatus as it can be targeted for inhibitor discovery or might help to elucidate the functional biology of the parasite.

In higher eukaryotes, few *aaRS*s are existing as a larger multi- *aaRS* complex (MSC) composed of nine synthetases (arginyl-, aspartyl-, glutamyl-, glutaminyl-, leucyl-, lysyl-, isoleucyl-, methionyl- and prolyl-tRNA synthetases). The MSC has a combination of class I and class II *aaRS*s with three non- *aaRS* proteins p38, p43 and p18. This is ambiguous why certain *aaRS*s occur as a complex while some exist in free form. MSC might aid in effectual translation by arresting mingling of charged tRNAs with cellular pool and by increasing local concentration of tRNA alongside the site of translation. As in the case of the translational apparatus, few of these aminoacyl-tRNA synthetase-interacting multifunctional proteins (AIMPs) partake regulatory roles as cytokines or precursors thereof . Particularly, p43 is identified to be cleaved into EMAP II, a secreted peptide responsible for angiogenesis and induction of apoptosis. Protein-protein

interaction studies demonstrate that the major roles of the AIMPs are as the primary factors driving the assemblage of MARS complexes.

In case of *Plasmodium*, the parasite may require host tRNAs to sustain its own protein synthesis and/or as regulatory RNAs. Thus, these functions of the complex as well as integrity of the complex might be attributed to the scaffold proteins as p43. *Plasmodium* lacks p38 and p18. Hence our focus was to delineate the structural protein p43 and its implicated biological role in the malaria parasite.

Many conserved domains are recognized in both the non-catalytic extensions of the AIMPs as well as the aaRS . For example, a motif with homology to C-terminal domain of glutathione-S-tranferase (GST-like domain) is present often in proteins related to protein synthesis and initiates protein-protein interactions for these assemblies . The precise molecular basis of these interactions and how they relate to the function of these poorly understood complexes yet awaits additional studies.

Being a part of the multisynthetase complex, these scaffold proteins as p43 thus suggest a tRNA binding capability for probable sustenance of the parasite. Overall, the present work was envisaged to the biochemical and structural characterization of p43 protein of Apicomplexan parasites as *Plasmodium falciparum/vivax* involved in key essential pathways as protein translation, complex formation etc which are essential to the biology of the parasite.

The structure of p43 thereby gave us an insight of its GST-C like domains as well as the oligonucleotide binding (OB) fold. The overall full-length structure delineated was tetrameric assembly and the GST-C like N terminal domain was found to be dimer with the monomeric OB-fold like C terminal domain. Earlier characterizations from Bour et al give us a clear insight of tRNA binding capability of the C terminal domain of *Plasmodium* p43. The GST-like domains discovered structurally might contribute to associations within the multisynthetase complex of

the malarial parasite. The cytosolic localizations were re-asserted for the scaffold protein p43 invivo. The thermal shift assays with metals and GSH did not suggest any conformational stability. Through protein-protein interaction software and based on literature review of Toxoplasma, we delineated similar partner synthetases (ERS, QRS and YRS) for p43 and suggested a model for the MSC in malaria. These interactions could also be targeted. Since p43 is not indispensable for survival of the malarial parasite as already mentioned, we provide an insight to develop inhibitors which could target these interactions. Any inhibitor like that could hence prove to be multi-targeting. The hindrance of these interactions could devastate the translational machinery as well as any other non-canonical functions as well thus proving detrimental to the parasite.

References

1. Carter, R., and Mendis, K. N. (2002) Evolutionary and Historical Aspects of the Burden of Malaria Evolutionary and Historical Aspects of the Burden of Malaria. *Clin. Microbiol. Rev.* **15**, 564–594
2. Bayoumi, R. A., and Saha, N. (1987) Some blood genetic markers of the Nuba and Hawazma tribes of Western Sudan. *Am. J. Phys. Anthropol.* **73**, 379–388
3. Cho (2016) 乳鼠心肌提取 HHS Public Access. *Physiol. Behav.* **176**, 100–106
4. Miller, L., Good, M., and Milon, G. (1994) Malaria pathogenesis. *Science (80-.).* **264**, 1878–1883
5. Bourges, M., and Peigue, H. (1978) Gastro-ent rites aigu s infantiles h Rotavirus
6. Sinden, R. E. (2007) Malaria, mosquitoes and the legacy of Ronald Ross. *Bull. World Health Organ.* **85**, 894–896
7. Bratitsis, T., and Demetriadis, S. (2013) Research approaches in computer-supported collaborative learning. *Int. J. e-Collaboration*. **9**, 1–8
8. Ross, R. (2002) The role of the mosquito in the evolution of the malarial parasite: the recent researches of Surgeon-Major Ronald Ross, I.M.S. 1898. *Yale J. Biol. Med.* **75**, 103–105
9. Willcox, M. L., and Bodeker, G. (2004) Traditional herbal medicines for malaria. *BMJ.* **329**, 1156–9
10. Berard, C. W. (1972) Book Reviews: Book Reviews. *Blood*. **40**, 612
11. Talisuna, A. O., Bloland, P., and D'Alessandro, U. (2004) History, dynamics, and public health importance of malaria parasite resistance. *Clin.Microbiol.Rev.* **17**, 235–254
12. Radloff, P. D., Philipps, J., Hutchinson, D., and Kremsner, P. G. (1996) Atovaquone plus proguanil is an effective treatment for Plasmodium ovale and P. Malariae malaria.

Trans. R. Soc. Trop. Med. Hyg. **90**, 682

13. Gatton, M. L., Martin, L. B., and Cheng, Q. (2004) Evolution of resistance to sulfadoxine-pyrimethamine in Plasmodium falciparum. *Antimicrob. Agents Chemother.* **48**, 2116–2123

14. Rosenthal, P. J. (2003) Antimalarial drug discovery: Old and new approaches. *J. Exp. Biol.* **206**, 3735–3744

15. Woodrow, C. J., Haynes, R. K., and Krishna, S. (2005) Artemisinins. *Postgrad. Med. J.* **81**, 71–78

16. Haynes, R. K. (2001) Artemisinin and derivatives: The future for malaria treatment? *Curr. Opin. Infect. Dis.* **14**, 719–726

17. Imwong, M., Suwannasin, K., Kunasol, C., Sutawong, K., Mayxay, M., Rekol, H., Smithuis, F. M., Hlaing, T. M., Tun, K. M., van der Pluijm, R. W., Tripura, R., Miotto, O., Menard, D., Dhorda, M., Day, N. P. J., White, N. J., and Dondorp, A. M. (2017) The spread of artemisinin-resistant Plasmodium falciparum in the Greater Mekong subregion: a molecular epidemiology observational study. *Lancet Infect. Dis.* **17**, 491–497

18. Gamo, F. J., Sanz, L. M., Vidal, J., De Cozar, C., Alvarez, E., Lavandera, J. L., Vanderwall, D. E., Green, D. V. S., Kumar, V., Hasan, S., Brown, J. R., Peishoff, C. E., Cardon, L. R., and Garcia-Bustos, J. F. (2010) Thousands of chemical starting points for antimalarial lead identification. *Nature*. **465**, 305–310

19. Delves, M. J., Miguel-Blanco, C., Matthews, H., Molina, I., Ruecker, A., Yahiya, S., Straschil, U., Abraham, M., León, M. L., Fischer, O. J., Rueda-Zubiaurre, A., Brandt, J. R., Cortés, Á., Barnard, A., Fuchter, M. J., Calderón, F., Winzeler, E. A., Sinden, R. E., Herreros, E., Gamo, F. J., and Baum, J. (2018) A high throughput screen for next-generation leads targeting malaria parasite transmission. *Nat. Commun.* 10.1038/s41467-

018-05777-2

20. Tren, R. (2002) WORKING PAPERS SERIES Malaria and Climate Change

21. Lal, S., Sonal, G., and Phukan, P. . (2000) Status of malaria in India. *J Indian Acad Clin Med*. **5**, 19–23

22. Baker, D. A. (2010) Malaria gametocytogenesis. *Mol. Biochem. Parasitol.* **172**, 57–65

23. Martinsen, E. S., Waite, J. L., and Schall, J. J. (2007) Morphologically defined subgenera of Plasmodium from avian hosts: Test of monophyly by phylogenetic analysis of two mitochondrial genes. *Parasitology*. **134**, 483–490

24. Tavares, J., Formaglio, P., Thiberge, S., Mordelet, E., Van Rooijen, N., Medvinsky, A., Ménard, R., and Amino, R. (2013) Role of host cell traversal by the malaria sporozoite during liver infection. *J. Exp. Med.* **210**, 905–915

25. White, N. J. (2011) Determinants of relapse periodicity in Plasmodium vivax malaria. *Malar. J.* **10**, 297

26. Siciliano, G., and Alano, P. (2015) Enlightening the malaria parasite life cycle: Bioluminescent Plasmodium in fundamental and applied research. *Front. Microbiol.* **6**, 1–8

27. Joice, R., Nilsson, S. K., Montgomery, J., Dankwa, S., Morahan, B., Seydel, K. B., Bertuccini, L., Alano, P., Kim, C., Duraisingh, M. T., Taylor, T. E., and Milner, D. A. (2014) Levels and changes of HDL cholesterol and apolipoprotein A-I in relation to risk of cardiovascular events among statin-treated patients; a meta-analysis. *Circulation*. **6**, 1–16

28. Sinden, R. E. (2015) The cell biology of malaria infection of mosquito: Advances and opportunities. *Cell. Microbiol.* **17**, 451–466

29. Baker, D. A. (2010) Malaria gametocytogenesis. *Mol. Biochem. Parasitol.* **172**, 57–65

30. Kappe, S. H. I., Vaughan, A. M., Boddey, J. A., and Cowman, A. F. (2010) That was

then but this is now: Malaria research in the time of an eradication agenda. *Science (80-.).* **328**, 862–866

31. Parroche, P., Lauw, F. N., Goutagny, N., Latz, E., Monks, B. G., Visintin, A., Halmen, K. A., Lamphier, M., Olivier, M., Bartholomeu, D. C., Gazzinelli, R. T., and Golenbock, D. T. (2007) Malaria hemozoin is immunologically inert but radically enhances innate responses by presenting malaria DNA to Toll-like receptor 9. *Proc. Natl. Acad. Sci. U. S. A.* **104**, 1919–1924

32. Tangpukdee, N., Duangdee, C., Wilairatana, P., and Krudsood, S. (2009) Malaria diagnosis: A brief review. *Korean J. Parasitol.* **47**, 93–102

33. Ngasala, B., Mubi, M., Warsame, M., Petzold, M. G., Massele, A. Y., Gustafsson, L. L., Tomson, G., Premji, Z., and Bjorkman, A. (2008) Impact of training in clinical and microscopy diagnosis of childhood malaria on antimalarial drug prescription and health outcome at primary health care level in Tanzania: A randomized controlled trial. *Malar. J.* **7**, 1–11

34. Bates, I., Bekoe, V., and Asamoa-Adu, A. (2004) Improving the accuracy of malaria-related laboratory tests in Ghana. *Malar. J.* **3**, 1–5

35. Reyburn, H., Mbakilwa, H., Mwangi, R., Mwerinde, O., Olomi, R., Drakeley, C., and Whitty, C. J. M. (2007) Rapid diagnostic tests compared with malaria microscopy for guiding outpatient treatment of febrile illness in Tanzania: Randomised trial. *Br. Med. J.* **334**, 403–406

36. Sei, W. L., Jeon, K., Byung, R. J., and Park, I. (2008) Rapid diagnosis of vivax malaria by the SD bioline malaria antigen test when thrombocytopenia is present. *J. Clin. Microbiol.* **46**, 939–942

37. Vo, T. K. D., Bigot, P., Gazin, P., Sinou, V., De Pina, J. J., Huynh, D. C., Fumoux, F., and Parzy, D. (2007) Evaluation of a real-time PCR assay for malaria diagnosis in

patients from Vietnam and in returned travellers. *Trans. R. Soc. Trop. Med. Hyg.* **101**, 422–428

38. Pappas, G., Kiriaze, I. J., and Falagas, M. E. (2008) Insights into infectious disease in the era of Hippocrates. *Int. J. Infect. Dis.* **12**, 347–350

39. Price, R. N. (2000) Artemisinin drugs: Novel antimalarial agents. *Expert Opin. Investig. Drugs*. **9**, 1815–1827

40. Dondorp, A. M., Nosten, F., Yi, P., Das, D., Hanpithakpong, W., Ph, D., Lee, S. J., Ringwald, P., Imwong, M., Chotivanich, K., and Lim, P. (2012) Europe PMC Funders Group Artemisinin Resistance in Plasmodium falciparum Malaria. *N Engl J Med.* **361**, 455–467

41. Witkowski, B., Lelièvre, J., Barragán, M. J. L., Laurent, V., Su, X. Z., Berry, A., and Benoit-Vical, F. (2010) Increased tolerance to artemisinin in plasmodium falciparum is mediated by a quiescence mechanism. *Antimicrob. Agents Chemother.* **54**, 1872–1877

42. NIMR, N. (2009) Malaria India Guidelines

43. Pollack, Y., Katzen, A. L., Spira, D. T., and Golenser, J. (1982) The genome of plasmodium falciparum. I: DNA base composition. *Nucleic Acids Res.* **10**, 539–546

44. Gardner, M. J., Hall, N., Fung, E., White, O., Berriman, M., Hyman, R. W., Carlton, J. M., Pain, A., Nelson, K. E., Bowman, S., Paulsen, I. T., James, K., Eisen, J. A., Rutherford, K., Salzberg, S. L., Craig, A., Kyes, S., Chan, M. S., Nene, V., Shallom, S. J., Suh, B., Peterson, J., Angiuoli, S., Pertea, M., Allen, J., Selengut, J., Haft, D., Mather, M. W., Vaidya, A. B., Martin, D. M. A., Fairlamb, A. H., Fraunholz, M. J., Roos, D. S., Ralph, S. A., McFadden, G. I., Cummings, L. M., Subramanian, G. M., Mungall, C., Venter, J. C., Carucci, D. J., Hoffman, S. L., Davis, R. W., Fraser, C. M., and Barrell, B. (2002) Genome sequence of the human malaria parasite Plasmodium falciparum. *Nature*. **419**, 498–511

45. FEAGIN, J. E., GARDNER, M. J., WILLIAMSON, D. H., and WILSON, R. J. M. (1991) The Putative Mitochondrial Genome of Plasmodium falciparum. *J. Protozool.* **38**, 243–245

46. Wilson, R. J. M. (Iain., Denny, P. W., Preiser, P. R., Rangachari, K., Roberts, K., Roy, A., Whyte, A., Strath, M., Moore, D. J., Moore, P. W., and Williamson, D. H. (1996) Complete gene map of the plastid-like DNA of the malaria parasite Plasmodium falciparum. *J. Mol. Biol.* **261**, 155–172

47. Caro, F., Ahyong, V., Betegon, M., and DeRisi, J. L. (2014) Genome-wide regulatory dynamics of translation in the Plasmodium falciparum asexual blood stages. *Elife*. **3**, 1–24

48. Preston, M. D., Campino, S., Assefa, S. A., Echeverry, D. F., Ocholla, H., Amambua-Ngwa, A., Stewart, L. B., Conway, D. J., Borrmann, S., Michon, P., Zongo, I., Ouédraogo, J. B., Djimde, A. A., Doumbo, O. K., Nosten, F., Pain, A., Bousema, T., Drakeley, C. J., Fairhurst, R. M., Sutherland, C. J., Roper, C., and Clark, T. G. (2014) A barcode of organellar genome polymorphisms identifies the geographic origin of Plasmodium falciparum strains. *Nat. Commun.* 10.1038/ncomms5052

49. Eriani, G., Delarue, M., Poch, O., Gangloff, J., and Moras, D. (1990) Partition of tRNA synthetases into two classes based on mutually exclusive sets of sequence motifs. *Nature*. **347**, 203–206

50. Burbaum, J. J., and Schimmel, P. (1991) Structural relationships and the classification of aminoacyl-tRNA synthetases. *J. Biol. Chem.* **266**, 16965–16968

51. Bhatt, T., Kapil, C., Khan, S., Jairajpuri, M., Sharma, V., Santoni, D., Silvestrini, F., Pizzi, E., and Sharma, A. (2009) A genomic glimpse of aminoacyl-tRNA synthetases in malaria parasite Plasmodium falciparum. *BMC Genomics*. **10**, 644

52. Hausmann, C. D., and Ibba, M. (2008) Aminoacyl-tRNA synthetase complexes:

molecular multitasking revealed. *FEMS Microbiol. Rev.* **32**, 705–21

53. van Rooyen, J. M., Murat, J.-B., Hammoudi, P.-M., Kieffer-Jaquinod, S., Coute, Y., Sharma, A., Pelloux, H., Belrhali, H., and Hakimi, M.-A. (2014) Assembly of the novel five-component apicomplexan multi-aminoacyl-tRNA synthetase complex is driven by the hybrid scaffold protein Tg-p43. *PLoS One*. **9**, e89487

54. Lee, S. W. (2004) Aminoacyl-tRNA synthetase complexes: beyond translation. *J. Cell Sci.* **117**, 3725–3734

55. Cahuzac, B., Berthonneau, E., Birlirakis, N., Guittet, E., and Mirande, M. (2000) A recurrent RNA-binding domain is appended to eukaryotic aminoacyl-tRNA synthetases. *EMBO J.* **19**, 445–52

56. Simos, G., Segref, A., Fasiolo, F., Hellmuth, K., Shevchenko, A., Mann, M., and Hurt, E. C. (1996) The yeast protein Arc1p binds to tRNA and functions as a cofactor for the methionyl- and glutamyl-tRNA synthetases. *EMBO J.* **15**, 5437–48

57. Morales, A. J., Swairjo, M. A., and Schimmel, P. (1999) Structure-specific tRNA-binding protein from the extreme thermophile Aquifex aeolicus. *EMBO J.* **18**, 3475–3483

58. Kaminska, M., Havrylenko, S., Decottignies, P., Gillet, S., Le Maréchal, P., Negrutskii, B., and Mirande, M. (2009) Dissection of the structural organization of the aminoacyl-tRNA synthetase complex. *J. Biol. Chem.* **284**, 6053–6060

59. Koehler, C., Round, A., Simader, H., Suck, D., and Svergun, D. (2013) Quaternary structure of the yeast Arc1p-aminoacyl-tRNA synthetase complex in solution and its compaction upon binding of tRNAs. *Nucleic Acids Res.* **41**, 667–676

60. Karanasios, E., Simader, H., Panayotou, G., Suck, D., and Simos, G. (2007) Molecular Determinants of the Yeast Arc1p-Aminoacyl-tRNA Synthetase Complex Assembly. *J. Mol. Biol.* **374**, 1077–1090

61. Swairjo, M. A., Morales, A. J., Wang, C. C., Ortiz, A. R., and Schimmel, P. (2000) Crystal structure of trbp111: a structure-specific tRNA-binding protein. *EMBO J.* **19**, 6287–98

62. Bour, T., Mahmoudi, N., Kapps, D., Thiberge, S., Bargieri, D., Ménard, R., and Frugier, M. (2016) *Apicomplexa* -specific tRip facilitates import of exogenous tRNAs into malaria parasites. *Proc. Natl. Acad. Sci.* **113**, 4717–4722

63. Park, S. G., Kang, Y.-S., Ahn, Y. H., Lee, S. H., Kim, K.-R., Kim, K.-W., Koh, G. Y., Ko, Y.-G., and Kim, S. (2002) Dose-dependent biphasic activity of tRNA synthetase-associating factor, p43, in angiogenesis. *J. Biol. Chem.* **277**, 45243–8

64. Park, H., Park, S. G., Kim, J., Ko, Y.-G., and Kim, S. (2002) Signaling pathways for TNF production induced by human aminoacyl-tRNA synthetase-associating factor, p43. *Cytokine*. **20**, 148–53

65. Matschurat, S., Knies, U. E., Person, V., Fink, L., Stoelcker, B., Ebenebe, C., Behrensdorf, H. A., Schaper, J., and Clauss, M. (2003) Regulation of EMAP II by hypoxia. *Am. J. Pathol.* **162**, 93–103

66. Sang Lee, J., Gyu Park, S., Park, H., Seol, W., Lee, S., and Kim, S. (2002) Interaction network of human aminoacyl-tRNA synthetases and subunits of elongation factor 1 complex. *Biochem. Biophys. Res. Commun.* **291**, 158–164

67. Kim, J. Y., Kang, Y.-S., Lee, J.-W., Kim, H. J., Ahn, Y. H., Park, H., Ko, Y.-G., and Kim, S. (2002) p38 is essential for the assembly and stability of macromolecular tRNA synthetase complex: implications for its physiological significance. *Proc. Natl. Acad. Sci. U. S. A.* **99**, 7912–6

68. Guigou, L., Shalak, V., and Mirande, M. (2004) The tRNA-Interacting Factor p43 Associates with Mammalian Arginyl-tRNA Synthetase but Does Not Modify Its tRNA Aminoacylation Properties †. *Biochemistry*. **43**, 4592–4600

69. Wolfe, C. L., Warrington, J. A., Treadwell, L., and Norcum, M. T. (2005) A three-dimensional working model of the multienzyme complex of aminoacyl-tRNA synthetases based on electron microscopic placements of tRNA and proteins. *J. Biol. Chem.* **280**, 38870–38878

70. Schwarz, M. A., Lee, D. D., and Bartlett, S. (2018) Aminoacyl tRNA synthetase complex interacting multifunctional protein 1 simultaneously binds Glutamyl-Prolyl-tRNA synthetase and scaffold protein aminoacyl tRNA synthetase complex interacting multifunctional protein 3 of the multi-tRNA synthetase complex. *Int. J. Biochem. Cell Biol.* **99**, 197–202

71. Renault, L., Kerjan, P., Pasqualato, S., Ménétrey, J., Robinson, J. C., Kawaguchi, S. I., Vassylyev, D. G., Yokoyama, S., Mirande, M., and Cherfils, J. (2001) Structure of the EMAPII domain of human aminoacyl-tRNA synthetase complex reveals evolutionary dimer mimicry. *EMBO J.* **20**, 570–578

72. Bour, T., Mahmoudi, N., Kapps, D., Thiberge, S., Bargieri, D., Ménard, R., and Frugier, M. (2016) *Apicomplexa* -specific tRip facilitates import of exogenous tRNAs into malaria parasites. *Proc. Natl. Acad. Sci.* **113**, 4717–4722

73. Manickam, Y., Chaturvedi, R., Babbar, P., Malhotra, N., Jain, V., and Sharma, A. (2018) Drug targeting of one or more aminoacyl-tRNA synthetase in the malaria parasite Plasmodium falciparum. *Drug Discov. Today*. **23**, 1233–1240

74. Jain, V., and Sharma, A. (2017) Repurposing of Potent Drug Candidates for Multiparasite Targeting. *Trends Parasitol.* **33**, 158–161

75. Ibba, M., and Soll, D. (2000) Aminoacyl-tRNA Synthesis. *Annu. Rev. Biochem.* **69**, 617–150

76. Schimmel, P., and Ribas De Pouplana, L. (2000) Footprints of aminoacyl-tRNA synthetases are everywhere. *Trends Biochem. Sci.* **25**, 207–209

77. Pang, L., Weeks, S. D., and Van Aerschot, A. (2021) Aminoacyl-trna synthetases as valuable targets for antimicrobial drug discovery. *Int. J. Mol. Sci.* **22**, 1–34

78. Das, P., Babbar, P., Malhotra, N., Sharma, M., Jachak, G. R., Gonnade, R. G., Shanmugam, D., Harlos, K., Yogavel, M., Sharma, A., and Reddy, D. S. (2018) Specific Stereoisomeric Conformations Determine the Drug Potency of Cladosporin Scaffold against Malarial Parasite. *J. Med. Chem.* **61**, 5664–5678

79. Jain, V., Yogavel, M., Kikuchi, H., Oshima, Y., Hariguchi, N., Matsumoto, M., Goel, P., Touquet, B., Jumani, R. S., Tacchini-Cottier, F., Harlos, K., Huston, C. D., Hakimi, M. A., and Sharma, A. (2017) Targeting Prolyl-tRNA Synthetase to Accelerate Drug Discovery against Malaria, Leishmaniasis, Toxoplasmosis, Cryptosporidiosis, and Coccidiosis. *Structure*. **25**, 1495-1505.e6

80. Sharma, M., Malhotra, N., Yogavel, M., Harlos, K., Melillo, B., Comer, E., Gonse, A., Parvez, S., Mitasev, B., Fang, F. G., Schreiber, S. L., and Sharma, A. (2021) Structural basis of malaria parasite phenylalanine tRNA-synthetase inhibition by bicyclic azetidines. *Nat. Commun.* 10.1038/s41467-020-20478-5

81. Khan, S., Garg, A., Camacho, N., Van Rooyen, J., Kumar Pole, A., Belrhali, H., Ribas de Pouplana, L., Sharma, V., and Sharma, A. (2013) Structural analysis of malaria-parasite lysyl-tRNA synthetase provides a platform for drug development. *Acta Crystallogr. Sect. D Biol. Crystallogr.* **69**, 785–795

82. Baragaña, B., Forte, B., Choi, R., Hewitt, S. N., Bueren-Calabuig, J. A., Pisco, J. P., Peet, C., Dranow, D. M., Robinson, D. A., Jansen, C., Norcross, N. R., Vinayak, S., Anderson, M., Brooks, C. F., Cooper, C. A., Damerow, S., Delves, M., Dowers, K., Duffy, J., Edwards, T. E., Hallyburton, I., Horst, B. G., Hulverson, M. A., Ferguson, L., Jiménez-Díaz, M. B., Jumani, R. S., Lorimer, D. D., Love, M. S., Maher, S., Matthews, H., McNamara, C. W., Miller, P., O'Neill, S., Ojo, K. K., Osuna-Cabello, M., Pinto, E.,

Post, J., Riley, J., Rottmann, M., Sanz, L. M., Scullion, P., Sharma, A., Shepherd, S. M., Shishikura, Y., Simeons, F. R. C., Stebbins, E. E., Stojanovski, L., Straschil, U., Tamaki, F. K., Tamjar, J., Torrie, L. S., Vantaux, A., Witkowski, B., Wittlin, S., Yogavel, M., Zuccotto, F., Angulo-Barturen, I., Sinden, R., Baum, J., Gamo, F. J., Mäser, P., Kyle, D. E., Winzeler, E. A., Myler, P. J., Wyatt, P. G., Floyd, D., Matthews, D., Sharma, A., Striepen, B., Huston, C. D., Gray, D. W., Fairlamb, A. H., Pisliakov, A. V., Walpole, C., Read, K. D., Van Voorhis, W. C., and Gilbert, I. H. (2019) Lysyl-tRNA synthetase as a drug target in malaria and cryptosporidiosis. *Proc. Natl. Acad. Sci. U. S. A.* **116**, 7015–7020

83. Luth, M. R., Gupta, P., Ottilie, S., and Winzeler, E. A. (2018) Using in Vitro Evolution and Whole Genome Analysis to Discover Next Generation Targets for Antimalarial Drug Discovery. *ACS Infect. Dis.* **4**, 301–314

84. Hoepfner, D., McNamara, C. W., Lim, C. S., Studer, C., Riedl, R., Aust, T., McCormack, S. L., Plouffe, D. M., Meister, S., Schuierer, S., Plikat, U., Hartmann, N., Staedtler, F., Cotesta, S., Schmitt, E. K., Petersen, F., Supek, F., Glynne, R. J., Tallarico, J. A., Porter, J. A., Fishman, M. C., Bodenreider, C., Diagana, T. T., Movva, N. R., and Winzeler, E. A. (2012) Selective and specific inhibition of the plasmodium falciparum lysyl-tRNA synthetase by the fungal secondary metabolite cladosporin. *Cell Host Microbe*. **11**, 654–663

85. Pham, J. S., Dawson, K. L., Jackson, K. E., Lim, E. E., Pasaje, C. F. A., Turner, K. E. C., and Ralph, S. A. (2014) Aminoacyl-tRNA synthetases as drug targets in eukaryotic parasites. *Int. J. Parasitol. Drugs Drug Resist.* **4**, 1–13

86. Singh, U. P., Bhat, H. R., Gahtori, P., and Singh, R. K. (2013) Hybrid phenylthiazole and 1,3,5-triazine target cytosolic leucyl-tRNA synthetase for antifungal action as revealed by molecular docking studies. *Silico Pharmacol.* 10.1186/2193-9616-1-3

87. Kim, Y., Shin, J., Li, R., Cheong, C., Kim, K., and Kim, S. (2000) A novel anti-tumor cytokine contains an RNA binding motif present in aminoacyl-tRNA synthetases. *J. Biol. Chem.* **275**, 27062–27068

88. Simader, H., Hothorn, M., and Suck, D. (2006) Structures of the interacting domains from yeast glutamyl-tRNA synthetase and tRNA-aminoacylation and nuclear-export cofactor Arc1p reveal a novel function for an old fold. *Acta Crystallogr. Sect. D Biol. Crystallogr.* **62**, 1510–1519

89. Ivakhno, S. S., and Kornelyuk, A. I. (2004) Cytokine-like activities of some aminoacyl-tRNA synthetases and auxiliary p43 cofactor of aminoacylation reaction and their role in oncogenesis. *Exp. Oncol.* **26**, 250–5

90. Ko, Y. G., Park, H., Kim, T., Lee, J. W., Park, S. G., Seol, W., Kim, J. E., Lee, W. H., Kim, S. H., Park, J. E., and Kim, S. (2001) A cofactor of tRNA synthetase, p43, is secreted to up-regulate proinflammatory genes. *J. Biol. Chem.* **276**, 23028–33

91. Park, S. G., Shin, H., Shin, Y. K., Lee, Y., Choi, E.-C., Park, B.-J., and Kim, S. (2005) The novel cytokine p43 stimulates dermal fibroblast proliferation and wound repair. *Am. J. Pathol.* **166**, 387–398

92. Park, B. J., Oh, Y. S., Park, S. Y., Choi, S. J., Rudolph, C., Schlegelberger, B., and Kim, S. (2006) AIMP3 haploinsufficiency disrupts oncogene-induced p53 activation and genomic stability. *Cancer Res.* **66**, 6913–6918

93. Kim, M. J., Park, B. J., Kang, Y. S., Kim, H. J., Park, J. H., Kang, J. W., Lee, S. W., Han, J. M., Lee, H. W., and Kim, S. (2003) Downregulation of FUSE-binding protein and c-myc by tRNA synthetase cofactor p38 is required for lung cell differentiation. *Nat. Genet.* **34**, 330–336

94. Choi, J. W., Kim, D. G., Park, M. C., Um, J. Y., Han, J. M., Park, S. G., Choi, E.-C., and Kim, S. (2009) AIMP2 promotes TNF -dependent apoptosis via ubiquitin-mediated

degradation of TRAF2. *J. Cell Sci.* **122**, 2710–2715

95. Feng, L., Tumbula-Hansen, D., Toogood, H., and Söll, D. (2003) Expanding tRNA recognition of a tRNA synthetase by a single amino acid change. *Proc. Natl. Acad. Sci. U. S. A.* **100**, 5676–5681

96. Cho, H. Y., Maeng, S. J., Cho, H. J., Choi, Y. S., Chung, J. M., Lee, S., Kim, H. K., Kim, J. H., Eom, C. Y., Kim, Y. G., Guo, M., Jung, H. S., Kang, B. S., and Kim, S. (2015) Assembly of multi-tRNA synthetase complex via heterotetrameric glutathione transferase-homology domains. *J. Biol. Chem.* **290**, 29313–29328

97. Nomanbhoy, T., Morales, A. J., Abraham, A. T., Vörtler, C. S., Giegé, R., and Schimmel, P. (2001) Simultaneous binding of two proteins to opposite sides of a single transfer RNA. *Nat. Struct. Biol.* **8**, 344–348

98. Kaminska, M., Deniziak, M., Kerjan, P., Barciszewski, J., and Mirande, M. (2000) A recurrent general RNA binding domain appended to plant methionyl-tRNA synthetase acts as a cis-acting cofactor for aminoacylation. *EMBO J.* **19**, 6908–6917

99. Winter, G., Lobley, C. M. C., and Prince, S. M. (2013) Decision making in xia2. *Acta Crystallogr. Sect. D Biol. Crystallogr.* **69**, 1260–1273

100. Winter, G., Waterman, D. G., Parkhurst, J. M., Aaron, S., Gildea, R. J., Gerstel, M., Fuentes-montero, L., Michels-clark, T., Young, I. D., and Sauter, K. (2018) DIALS : implementation and evaluation of a new integration package. 10.1107/S2059798317017235

101. Kabsch, W. (2010) Integration, scaling, space-group assignment and post-refinement. *Acta Crystallogr. Sect. D Biol. Crystallogr.* **66**, 133–144

102. Winn, M. D., Ballard, C. C., Cowtan, K. D., Dodson, E. J., Emsley, P., Evans, P. R., Keegan, R. M., Krissinel, E. B., Leslie, A. G. W., McCoy, A., McNicholas, S. J., Murshudov, G. N., Pannu, N. S., Potterton, E. A., Powell, H. R., Read, R. J., Vagin, A.,

and Wilson, K. S. (2011) Overview of the CCP4 suite and current developments. *Acta Crystallogr. Sect. D Biol. Crystallogr.* **67**, 235–242

103. Sheldrick, G. M. (2007) A short history of SHELX. *Acta Crystallogr. Sect. A Found. Crystallogr.* **64**, 112–122

104. Zwart, P. H., Grosse-Kunstleve, R. W., Adams, P. D., and Zwart, P. H., Grosse-Kunstleve, R. W., Adams, P. D. (2005) Xtriage and Fest: automatic assessment of X-ray data and substructure structure factor estimation. *CCP4 Newsl.* LBNL-60875

105. McCoy, A. J., Grosse-Kunstleve, R. W., Adams, P. D., Winn, M. D., Storoni, L. C., and Read, R. J. (2007) Phaser crystallographic software. *J. Appl. Crystallogr.* **40**, 658–674

106. Terwilliger, T. C., Adams, P. D., Read, R. J., McCoy, A. J., Moriarty, N. W., Grosse-Kunstleve, R. W., Afonine, P. V., Zwart, P. H., and Hung, L. W. (2009) Decision-making in structure solution using Bayesian estimates of map quality: The PHENIX AutoSol wizard. *Acta Crystallogr. Sect. D Biol. Crystallogr.* **65**, 582–601

107. Adams, P. D., Afonine, P. V., Bunkóczi, G., Chen, V. B., Davis, I. W., Echols, N., Headd, J. J., Hung, L. W., Kapral, G. J., Grosse-Kunstleve, R. W., McCoy, A. J., Moriarty, N. W., Oeffner, R., Read, R. J., Richardson, D. C., Richardson, J. S., Terwilliger, T. C., and Zwart, P. H. (2010) PHENIX: A comprehensive Python-based system for macromolecular structure solution. *Acta Crystallogr. Sect. D Biol. Crystallogr.* **66**, 213–221

108. Liebschner, D., Afonine, P. V., Baker, M. L., Bunkoczi, G., Chen, V. B., Croll, T. I., Hintze, B., Hung, L. W., Jain, S., McCoy, A. J., Moriarty, N. W., Oeffner, R. D., Poon, B. K., Prisant, M. G., Read, R. J., Richardson, J. S., Richardson, D. C., Sammito, M. D., Sobolev, O. V., Stockwell, D. H., Terwilliger, T. C., Urzhumtsev, A. G., Videau, L. L., Williams, C. J., and Adams, P. D. (2019) Macromolecular structure determination using X-rays, neutrons and electrons: Recent developments in Phenix. *Acta Crystallogr. Sect.*

D Struct. Biol. **75**, 861–877

109. Langer, G. G., Wiegels, T., and Lamzin, V. S. (2013) research papers Visual automated macromolecular model building research papers. 10.1107/S0907444913000565

110. Panjikar, S., Parthasarathy, V., Lamzin, V. S., Weiss, M. S., and Tucker, P. A. (2005) Auto-Rickshaw: An automated crystal structure determination platform as an efficient tool for the validation of an X-ray diffraction experiment. *Acta Crystallogr. Sect. D Biol. Crystallogr.* **61**, 449–457

111. Murshudov, G. N., Skubák, P., Lebedev, A. A., Pannu, N. S., Steiner, R. A., Nicholls, R. A., Winn, M. D., Long, F., and Vagin, A. A. (2011) REFMAC5 for the refinement of macromolecular crystal structures. *Acta Crystallogr. Sect. D Biol. Crystallogr.* **67**, 355–367

112. Adams, P. D., Grosse-Kunstleve, R. W., Hung, L. W., Ioerger, T. R., McCoy, A. J., Moriarty, N. W., Read, R. J., Sacchettini, J. C., Sauter, N. K., and Terwilliger, T. C. (2002) PHENIX: Building new software for automated crystallographic structure determination. *Acta Crystallogr. Sect. D Biol. Crystallogr.* **58**, 1948–1954

113. Adams, P. D., Pavel, V., Chen, V. B., Ian, W., Echols, N., Moriarty, N. W., Read, R. J., Richardson, D. C., Jane, S., and Thomas, C. (2010) research papers PHENIX : a comprehensive Python-based system for macromolecular structure solution research papers. 10.1107/S0907444909052925

114. Emsley, P., Lohkamp, B., Scott, W. G., and Cowtan, K. (2010) Features and development of Coot. *Acta Crystallogr. Sect. D Biol. Crystallogr.* **66**, 486–501

115. Yang, X., Liu, J., Skene, R. J., Mcree, D. E., and Schimmel, P. (2003) Crystal Structure of an EMAP-II-Like Cytokine Released from a Human tRNA Synthetase. **86**, 1246–1257

116. Chen, V. B., Arendall, W. B., Headd, J. J., Keedy, D. A., Immormino, R. M., Kapral, G.

J., Murray, L. W., Richardson, J. S., and Richardson, D. C. (2010) MolProbity: All-atom structure validation for macromolecular crystallography. *Acta Crystallogr. Sect. D Biol. Crystallogr.* **66**, 12–21

117. Joosten, R. P., Long, F., Murshudov, G. N., and Perrakis, A. (2014) The PDB_REDO server for macromolecular structure model optimization. 10.1107/S2052252514009324

118. Pettersen, E. F., Goddard, T. D., Huang, C. C., Couch, G. S., Greenblatt, D. M., Meng, E. C., and Ferrin, T. E. (2004) UCSF Chimera-a visualization system for exploratory research and analysis. *J. Comput. Chem.* **25**, 1605–12

119. Hunter, S., Apweiler, R., Attwood, T. K., Bairoch, A., Bateman, A., Binns, D., Bork, P., Das, U., Daugherty, L., Duquenne, L., Finn, R. D., Gough, J., Haft, D., Hulo, N., Kahn, D., Kelly, E., Laugraud, A., Letunic, I., Lonsdale, D., Lopez, R., Madera, M., Maslen, J., Mcanulla, C., McDowall, J., Mistry, J., Mitchell, A., Mulder, N., Natale, D., Orengo, C., Quinn, A. F., Selengut, J. D., Sigrist, C. J. A., Thimma, M., Thomas, P. D., Valentin, F., Wilson, D., Wu, C. H., and Yeats, C. (2009) InterPro: The integrative protein signature database. *Nucleic Acids Res.* **37**, 211–215

120. Letunic, I., Doerks, T., and Bork, P. (2012) SMART 7: Recent updates to the protein domain annotation resource. *Nucleic Acids Res.* **40**, 302–305

121. Sigrist, C. J. A., Cerutti, L., De Castro, E., Langendijk-Genevaux, P. S., Bulliard, V., Bairoch, A., and Hulo, N. (2009) PROSITE, a protein domain database for functional characterization and annotation. *Nucleic Acids Res.* **38**, 161–166

122. Marchler-Bauer, A., Bo, Y., Han, L., He, J., Lanczycki, C. J., Lu, S., Chitsaz, F., Derbyshire, M. K., Geer, R. C., Gonzales, N. R., Gwadz, M., Hurwitz, D. I., Lu, F., Marchler, G. H., Song, J. S., Thanki, N., Wang, Z., Yamashita, R. A., Zhang, D., Zheng, C., Geer, L. Y., and Bryant, S. H. (2017) CDD/SPARCLE: Functional classification of proteins via subfamily domain architectures. *Nucleic Acids Res.* **45**, D200–D203

123. Finn, R. D., Bateman, A., Clements, J., Coggill, P., Eberhardt, R. Y., Eddy, S. R., Heger, A., Hetherington, K., Holm, L., Mistry, J., Sonnhammer, E. L. L., Tate, J., and Punta, M. (2014) Pfam: The protein families database. *Nucleic Acids Res.* **42**, 222–230

124. Sheldrick, G. M. (2010) Experimental phasing with SHELXC / D / E : combining chain tracing with density modification . *Acta Crystallogr. Sect. D Biol. Crystallogr.* **66**, 479–485

125. Rogers, L. K., Leinweber, B. L., and Smith, C. V. (2006) Detection of reversible protein thiol modifications in tissues. *Anal. Biochem.* 10.1016/j.ab.2006.08.020

126. Weerapana, E., Wang, C., Simon, G. M., Richter, F., Khare, S., Dillon, M. B. D., Bachovchin, D. A., Mowen, K., Baker, D., and Cravatt, B. F. (2010) Quantitative reactivity profiling predicts functional cysteines in proteomes. *Nature*. 10.1038/nature09472

127. Kim, H. J., Ha, S., Lee, H. Y., and Lee, K. J. (2015) Rosics: Chemistry and proteomics of cysteine modifications in redox biology. *Mass Spectrom. Rev.* 10.1002/mas.21430

128. Mathieu, Y., Prosper, P., Buée, M., Dumarçay, S., Favier, F., Gelhaye, E., Gérardin, P., Harvengt, L., Jacquot, J. P., Lamant, T., Meux, E., Mathiot, S., Didierjean, C., and Morel, M. (2012) Characterization of a Phanerochaete chrysosporium glutathione transferase reveals a novel structural and functional class with ligandin properties. *J. Biol. Chem.* 10.1074/jbc.M112.402776

129. Helmich, K. E., Pereira, J. H., Gall, D. L., Heins, R. A., McAndrew, R. P., Bingman, C., Deng, K., Holland, K. C., Noguera, D. R., Simmons, B. A., Sale, K. L., Ralph, J., Donohue, T. J., Adams, P. D., and Phillips, G. N. (2016) Structural basis of stereospecificity in the bacterial enzymatic cleavage of β-aryl ether bonds in lignin. *J. Biol. Chem.* 10.1074/jbc.M115.694307

130. Draper, D. E., and Reynaldo, L. P. (1999) SURVEY AND SUMMARY RNA binding

strategies of ribosomal proteins. *Nucleic Acids Res.* **27**, 381–388

131. Murzin, A. G. (1993) OB (oligonucleotide/oligosaccharide binding)-fold: common structural and functional solution for non-homologous sequences. *EMBO J.* **12**, 861–867

132. Holm, L., and Sander, C. (1993) Protein structure comparison by alignment of distance matrices. *J. Mol. Biol.* **233**, 123–138

133. Simos, G., Segref, A., Fasiolo, F., Hellmuth, K., Shevchenko, A., Mann, M., and Hurt, E. C. (1996) The yeast protein Arc1p binds to tRNA and functions as a cofactor for the methionyl- and glutamyl-tRNA synthetases. *EMBO J.* **15**, 5437–48

134. Havrylenko, S., Legouis, R., Negrutskiis, B., and Mirande, M. (2011) Caenorhabditis elegans evolves a new architecture for the multi-aminoacyl-tRNA synthetase complex. *J. Biol. Chem.* **286**, 28476–28487

135. Scriptie, B. (2010) Multi-functionality of aminoacyl-tRNA synthetases An example of biological complexity

136. Quevillon, S., Robinson, J. C., Berthonneau, E., Siatecka, M., and Mirande, M. (1999) Macromolecular assemblage of aminoacyl-tRNA synthetases: Identification of protein-protein interactions and characterization of a core protein. *J. Mol. Biol.* **285**, 183–195

137. Liang, D., Halpert, M. M., Konduri, V., and Decker, W. K. (2015) Stepping out of the Cytosol: AIMp1/p43 Potentiates the Link between Innate and Adaptive Immunity. *Int. Rev. Immunol.* **34**, 367–381

138. Quevillon, S., and Mirande, M. (1996) The p18 component of the multisynthetase complex shares a protein motif with the beta and gamma subunits of eukaryotic elongation factor 1. *FEBS Lett.* **395**, 63–7

139. Kang, T., Kwon, N. H., Lee, J. Y., Park, M. C., Kang, E., Kim, H. H., Kang, T. J., and Kim, S. (2012) AIMP3/p18 controls translational initiation by mediating the delivery of charged initiator tRNA to initiation complex. *J. Mol. Biol.* **423**, 475–481

140. Guzzo, C. M., and Yang, D. C. H. (2008) Lysyl-tRNA synthetase interacts with EF1α, aspartyl-tRNA synthetase and p38 in vitro. *Biochem. Biophys. Res. Commun.* **365**, 718–723

141. Jung, M. H., Sang, G. P., Liu, B., Park, B. J., Jin, Y. K., Cheng, H. J., Yeong, W. S., Li, Z., and Kim, S. (2007) Aminoacyl-tRNA synthetase-interacting multifunctional protein 1/p43 controls endoplasmic reticulum retention of heat shock protein gp96: Its pathological implications in lupus-like autoimmune diseases. *Am. J. Pathol.* **170**, 2042–2054

142. Fu, Y., Kim, Y., Jin, K. S., Kim, H. S., Kim, J. H., Wang, D., Park, M., Jo, C. H., Kwon, N. H., Kim, D., Kim, M. H., Jeon, Y. H., Hwang, K. Y., Kim, S., and Cho, Y. (2014) Structure of the ArgRS-GlnRS-AIMP1 complex and its implications for mammalian translation. *Proc. Natl. Acad. Sci. U. S. A.* **111**, 15084–9

143. Cheng, J., and Deming, T. J. (2011) synthesis of polypeptides by ROP of NCAs. *Pept. Mater.* **310**, 1–26

144. Mirande, M. (2017) The aminoacyl-tRNA synthetase complex. *Subcell. Biochem.* **83**, 505–522

145. Khan, K., Baleanu-Gogonea, C., Willard, B., Gogonea, V., and Fox, P. L. (2020) 3-Dimensional architecture of the human multi-tRNA synthetase complex. *Nucleic Acids Res.* **48**, 8740–8754

146. Corti, O., Hampe, C., Koutnikova, H., Darios, F., Jacquier, S., Prigent, A., Robinson, J. C., Pradier, L., Ruberg, M., Mirande, M., Hirsch, E., Rooney, T., Fournier, A., and Brice, A. (2003) The p38 subunit of the aminoacyl-tRNA synthetase complex is a Parkin substrate: Linking protein biosynthesis and neurodegeneration. *Hum. Mol. Genet.* **12**, 1427–1437

147. Ko, H. S., Von Coelln, R., Sriram, S. R., Kim, S. W., Chung, K. K. K., Pletnikova, O.,

Troncoso, J., Johnson, B., Saffary, R., Goh, E. L., Song, H., Park, B. J., Kim, M. J., Kim, S., Dawson, V. L., and Dawson, T. M. (2005) Accumulation of the authentic parkin substrate aminoacyl-tRNA synthetase cofactor, p38/JTV-1, leads to catecholaminergic cell death. *J. Neurosci.* **25**, 7968–7978

148. Blair, R. (2017) 乳鼠心肌提取 HHS Public Access. *Physiol. Behav.* **176**, 139–148

149. Quevillon, S., Agou, F., Robinson, J. C., and Mirande, M. (1997) The p43 component of the mammalian multi-synthetase complex is likely to be the precursor of the endothelial monocyte-activating polypeptide II cytokine. *J. Biol. Chem.* **272**, 32573–32579

150. Golinelli-Cohen, M. P., and Mirande, M. (2007) Arc1p is required for cytoplasmic confinement of synthetases and tRNA. *Mol. Cell. Biochem.* **300**, 47–59

151. Oommen, E., Hummel, A., Allmannsberger, L., Cuthbertson, D., Carette, S., Pagnoux, C., Hoffman, G. S., Jenne, D. E., Khalidi, N. A., Koening, C. L., Langford, C. A., McAlear, C. A., Moreland, L., Seo, P., Sreih, A., Ytterberg, S. R., Merkel, P. A., Specks, U., and Monach, P. A. (2017) IgA antibodies to myeloperoxidase in patients with eosinophilic granulomatosis with polyangiitis (Churg-Strauss). *Clin. Exp. Rheumatol.* **35**, 98–101

152. Lee, Y. S., Han, J. M., Son, S. H., Choi, J. W., Jeon, E. J., Bae, S. C., Park, Y. I., and Kim, S. (2008) AIMP1/p43 downregulates TGF-β signaling via stabilization of smurf2. *Biochem. Biophys. Res. Commun.* **371**, 395–400

153. Lee, S. W., Kim, G., and Kim, S. (2008) Aminoacyl-tRNA synthetase-interacting multi-functional protein 1/p43: An emerging therapeutic protein working at systems level. *Expert Opin. Drug Discov.* **3**, 945–957

154. Accogli, A., Russell, L., Sébire, G., Rivière, J. B., St-Onge, J., Addour-Boudrahem, N., Laporte, A. D., Rouleau, G. A., Saint-Martin, C., and Srour, M. (2019) Pathogenic variants in AIMP1 cause pontocerebellar hypoplasia. *Neurogenetics*. 10.1007/s10048-

019-00572-7

155. Accogli, A., Guerrero, K., D'Agostino, M. D., Tran, L., Cieuta-Walti, C., Thiffault, I., Chénier, S., Schwartzentruber, J., Majewski, J., and Bernard, G. (2019) Biallelic Loss-of-Function Variants in AIMP1 Cause a Rare Neurodegenerative Disease. *J. Child Neurol.* **34**, 74–80

156. Armstrong, L., Biancheri, R., Shyr, C., Rossi, A., Sinclair, G., Ross, C. J., Tarailo-Graovac, M., Wasserman, W. W., and Van Karnebeek, C. D. M. (2014) AIMP1 deficiency presents as a cortical neurodegenerative disease with infantile onset. *Neurogenetics*. **15**, 157–159

157. Feinstein, M., Markus, B., Noyman, I., Shalev, H., Flusser, H., Shelef, I., Liani-Leibson, K., Shorer, Z., Cohen, I., Khateeb, S., Sivan, S., and Birk, O. S. (2010) Pelizaeus-merzbacher-like disease caused by AIMP1/p43 homozygous mutation. *Am. J. Hum. Genet.* **87**, 820–828

158. BoAli, A., Tlili-Graiess, K., AlHashem, A., AlShahwan, S., Zuccoli, G., and Tabarki, B. (2019) Novel Homozygous Mutation of the AIMP1 Gene: A Milder Neuroimaging Phenotype With Preservation of the Deep White Matter. *Pediatr. Neurol.* **91**, 57–61

159. Min, J., Gyu, S., Lee, Y., and Kim, S. (2006) Structural separation of different extracellular activities in aminoacyl-tRNA synthetase-interacting multi-functional protein, p43/AIMP1. **342**, 113–118

160. Oh, Y. S., Kim, D. G., Kim, G., Choi, E. C., Kennedy, B. K., Suh, Y., Park, B. J., and Kim, S. (2010) Downregulation of lamin A by tumor suppressor AIMP3/p18 leads to a progeroid phenotype in mice. *Aging Cell*. **9**, 810–822

161. Guo, M., and Schimmel, P. (2013) Essential nontranslational functions of tRNA synthetases. 10.1038/nchembio.1158

162. Kim, M., Kim, H., Kim, D., Park, C., Huh, Y., Jung, J., Chung, H. J., and Jeong, N. Y.

(2019) Fluorescence-based analysis of noncanonical functions of aminoacyl-tRNA synthetase-interacting multifunctional proteins (AIMPs) in peripheral nerves. *Materials (Basel).* **12**, 1–12

163. Zhou, Z., Sun, B., Huang, S., Yu, D., and Zhang, X. (2020) Roles of aminoacyl-tRNA synthetase-interacting multi-functional proteins in physiology and cancer. *Cell Death Dis.* 10.1038/s41419-020-02794-2

164. Tonkin, C. J., van Dooren, G. G., Spurck, T. P., Struck, N. S., Good, R. T., Handman, E., Cowman, A. F., and McFadden, G. I. (2004) Localization of organellar proteins in Plasmodium falciparum using a novel set of transfection vectors and a new immunofluorescence fixation method. *Mol. Biochem. Parasitol.* **137**, 13–21

165. Mering, C. Von, Huynen, M., Jaeggi, D., Schmidt, S., Bork, P., and Snel, B. (2003) STRING : a database of predicted functional associations between proteins. **31**, 258–261

research paper

STRUCTURAL BIOLOGY

ISSN 2059-7983

Crystal structures of the two domains that constitute the *Plasmodium vivax* p43 protein

Swati Gupta,[a]‡ Jyoti Chhibber-Goel,[a]‡ Manmohan Sharma,[a,b]‡ Suhel Parvez,[b] Karl Harlos,[c] Amit Sharma[a] and Manickam Yogavel[a]*

[a]Molecular Medicine – Structural Parasitology Group, International Centre for Genetic Engineering and Biotechnology (ICGEB), Aruna Asaf Ali Road, New Delhi 110 067, India, [b]Department of Medical Elementology and Toxicology, Jamia Hamdard University, New Delhi, India, and [c]Division of Structural Biology, Wellcome Centre for Human Genetics, University of Oxford, Oxford OX3 7BN, England. *Correspondence e-mail: myogavel@gmail.com

Received 12 November 2018
Accepted 5 December 2019

Edited by K. Diederichs, University of Konstanz, Germany

‡ These authors made equal contributions.

Keywords: aminoacyl-tRNA synthetase interacting multifunctional proteins; AIMPs; crystal structure; p43; *Plasmodium vivax*; glutathione S-transferase; GST; tRNA.

PDB references: p43, N-terminal domain, 5zke; 5zkf; 6jre; C-terminal domain, 5zkg; 6ipa

Supporting information: this article has supporting information at journals.iucr.org/d

Scaffold modules known as aminoacyl-tRNA synthetase (aaRS)-interacting multifunctional proteins (AIMPs), such as AIMP1/p43, AIMP2/p38 and AIMP3/p18, are important in driving the assembly of multi-aaRS (MARS) complexes in eukaryotes. Often, AIMPs contain an N-terminal glutathione S-transferase (GST)-like domain and a C-terminal OB-fold tRNA-binding domain. Recently, the apicomplexan-specific *Plasmodium falciparum* p43 protein (*Pf*p43) has been annotated as an AIMP and its tRNA binding, tRNA import and membrane association have been characterized. The crystal structures of both the N- and C-terminal domains of the *Plasmodium vivax* p43 protein (*Pv*p43), which is an ortholog of *Pf*p43, have been resolved. Analyses reveal the overall oligomeric structure of *Pv*p43 and highlight several notable features that show *Pv*p43 to be a soluble, cytosolic protein. The dimeric assembly of the N-terminal GST-like domain of *Pv*p43 differs significantly from canonical GST dimers, and it is tied to the C-terminal tRNA-binding domain via a linker region. This work therefore establishes a framework for dissecting the additional roles of p43 orthologs in eukaryotic multi-protein MARS complexes.

1. Introduction

Aminoacyl-tRNA synthetases (aaRSs) are ubiquitous enzymes that are key players in protein translation (Ibba & Söll, 2000). In eukaryotes, several aaRSs form larger multi-aaRS (MARS) complexes composed of a mixture of class I and class II aaRSs along with three non-aaRS scaffold proteins known as aaRS-interacting multifunctional proteins (AIMPs): AIMP1/p43, AIMP2/p38 and AIMP3/p18 (Lee *et al.*, 2004).

In addition to driving the assembly of MARS complexes, the AIMPs are involved in various biological functions and signalling pathways (Ko *et al.*, 2001; Park *et al.*, 2002, 2005, 2006; Kim *et al.*, 2003; Choi *et al.*, 2009; Wolfe *et al.*, 2005). The AIMPs contain an N-terminal glutathione S-transferase (GST)-like module and a C-terminal oligonucleotide/oligosaccharide-binding (OB) fold containing a tRNA-binding domain (TRBD) (van Rooyen *et al.*, 2014). Structural and biochemical studies have suggested that the N-terminal GST-like domain of the AIMPs is responsible for their association with the MARS complex (Simos *et al.*, 1996; Cho *et al.*, 2015; Simader *et al.*, 2006). For instance, the interaction and complex formation of AIMP2/p38 and AIMP3/p18 with glutamyl-prolyl-tRNA synthetase (EPRS; PDB entries 5a34 and 5bmu, respectively; Cho *et al.*, 2015) and that of AIMP3/p18 with methionyl-tRNA synthetase (MRS; PDB entry 4bvx) *via* the AIMP2/p38 GST-like domain have been reported (Schwarz *et al.*, 2018; van Rooyen *et al.*, 2014; Simos *et al.*, 1996). Furthermore, in yeast, a smaller aaRS complex consisting of

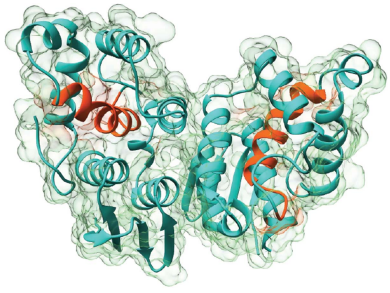

frontiers in Molecular Biosciences

MINI REVIEW
published: 27 August 2018
doi: 10.3389/fmolb.2018.00078

Engagement Rules That Underpin DBL-DARC Interactions for Ingress of *Plasmodium knowlesi* and *Plasmodium vivax* Into Human Erythrocytes

*Manickam Yogavel, Jyoti Chhibber-Goel, Abhishek Jamwal, Swati Gupta and Amit Sharma**

Molecular Medicine - Structural Parasitology Group, International Centre for Genetic Engineering and Biotechnology, New Delhi, India

Malaria parasite erythrocytic stages comprise of repeated bursts of parasites via cyclical invasion of host erythrocytes using dedicated receptor-ligand interactions. A family of erythrocyte-binding proteins from *Plasmodium knowlesi* (*Pk*) and *Plasmodium vivax* (*Pv*) attach to human Duffy antigen receptor for chemokines (DARC) via their Duffy binding-like domains (DBLs) for invasion. Here we provide a novel, testable and overarching interaction model that rationalizes even contradictory pieces of evidence that have so far existed in the literature on *Pk*/*Pv*-DBL/DARC binding determinants. We further address the conundrum of how parasite-encoded *Pk*/*Pv*-DBLs recognize human DARC and collate evidence for two distinct DARC integration sites on *Pk*/*Pv*-DBLs.

Keywords: Duffy antigen receptor for chemokines (DARC), Duffy binding-like domains (DBLs), malaria, *Plasmodium*, Structure

OPEN ACCESS

Edited by:
Luis G. Brieba, Centro de Investigación y de Estudios Avanzados del Instituto Politécnico Nacional, Mexico

Reviewed by:
Rogerio R. Sotelo-Mundo, Center for Research in Food and Development (CIAD), Mexico
Renato Augusto DaMatta, State University of Norte Fluminense, Brazil

****Correspondence:***
Amit Sharma
amitpsharma68@gmail.com

Specialty section:
This article was submitted to Structural Biology, a section of the journal Frontiers in Molecular Biosciences

Received: *22 June 2018*
Accepted: *03 August 2018*
Published: *27 August 2018*

Citation:
Yogavel M, Chhibber-Goel J, Jamwal A, Gupta S and Sharma A (2018) Engagement Rules That Underpin DBL-DARC Interactions for Ingress of Plasmodium knowlesi and Plasmodium vivax Into Human Erythrocytes. Front. Mol. Biosci. 5:78. doi: 10.3389/fmolb.2018.00078

INTRODUCTION

Engagements of specific host receptors with parasite-encoded ligands between human erythrocytes and malaria parasite surface proteins are key events in invasion of merozoites into erythrocytes (Cowman et al., 2017). The signature Duffy binding-like domain (DBL) is present in parasite-encoded erythrocyte binding proteins (EBPs) and in protein families like *Plasmodium falciparum* (*Pf*) erythrocyte membrane protein 1 (EMP1; Cowman et al., 2017). The latter are part of the *var* gene family where they assist in cytoadherence—these contain several copies of DBLs in each protein, whereas the *Pf*-EBP named EBA-175 harbors two copies (F1 and F2) of DBLs (Mayor et al., 2005; Tolia et al., 2005). In contrast EBPs of *Plasmodium knowlesi* (*Pk*) and *Plasmodium vivax* (*Pv*) contain only single copy of DBL each. There are multiple EBPs present in the malaria parasite *Pk* (α, β, and γ), and it is the *Pk*α-DBL and *Pv*-DBL that mediate Duffy antigen receptor for chemokines (DARC)-dependent invasion of erythrocytes in humans (Choe et al., 2005; Hans et al., 2005; Chitnis and Sharma, 2008). Other DBL variants of *Pk*-EBPs: β and γ likely use alternate receptors on rhesus/human erythrocytes and may mediate invasion by Duffy antigen-independent pathways (Chitnis and Miller, 1994; Cowman et al., 2017). The *Pk*/*Pv*-DBLs (as part of their EBPs) are present on merozoite surface and are responsible for binding to the DARC receptor on reticulocytes (**Figure 1**) and thence mediating junction formation that is vital for the parasite invasion process (Adams et al., 1990, 1992; Cowman and Crabb, 2006; Cowman et al., 2017).

ChemBioChem

Combining Chemistry and Biology

Chemistry Europe

European Chemical Societies Publishing

Accepted Article

Title: Inhibition of Plasmodium falciparum Lysyl-tRNA synthetase via a piperidine-ring scaffold inspired Cladosporin analogues

Authors: Palak Babbar, Mizuki Sato, Yogavel Manickam, Siddhartha Mishra, Karl Harlos, Swati Gupta, Suhel Parvez, Haruhisa Kikuchi, and Amit Sharma

To be cited as: *ChemBioChem* 10.1002/cbic.202100212

Link to VoR: https://doi.org/10.1002/cbic.202100212

WILEY-VCH